DESIGN OF A TEST SETUP FOR ALTITUDE SIMULATION

A THESIS SUBMITTED TO
THE GRADUATE SCHOOL OF NATURAL AND APPLIED SCIENCES
OF
MIDDLE EAST TECHNICAL UNIVERSITY

BY

ATAMAN AYDOĞDU

IN PARTIAL FULFILLMENT OF THE REQUIREMENTS
FOR
THE DEGREE OF MASTER OF SCIENCE
IN
MECHANICAL ENGINEERING

SEPTEMBER 2019

Approval of the thesis:

DESIGN OF A TEST SETUP FOR ALTITUDE SIMULATION

submitted by **ATAMAN AYDOĞDU** in partial fulfillment of the requirements for the degree of **Master of Science in Mechanical Engineering Department, Middle East Technical University** by,

Prof. Dr. Halil Kalıpçılar
Dean, Graduate School of **Natural and Applied Sciences** ________________

Prof. Dr. M. A. Sahir Arıkan
Head of Department, **Mechanical Engineering** ________________

Prof. Dr. Abdullah Ulaş
Supervisor, **Mechanical Engineering, METU** ________________

Examining Committee Members:

Assoc. Prof. Dr. Cüneyt Sert
Mechanical Engineering, METU ________________

Prof. Dr. Abdullah Ulaş
Mechanical Engineering, METU ________________

Prof. Dr. Kahraman Albayrak
Mechanical Engineering, METU ________________

Assoc. Prof. Dr. Metin Yavuz
Mechanical Engineering, METU ________________

Assist. Prof. Dr. Onur Baş
Mechanical Engineering, TEDU ________________

Date: 03.09.2019

I hereby declare that all information in this document has been obtained and presented in accordance with academic rules and ethical conduct. I also declare that, as required by these rules and conduct, I have fully cited and referenced all material and results that are not original to this work.

Name, Surname: Ataman Aydoğdu

Signature :

ABSTRACT

DESIGN OF A TEST SETUP FOR ALTITUDE SIMULATION

Aydoğdu, Ataman
Master of Science, Mechanical Engineering
Supervisor: Prof. Dr. Abdullah ULAŞ

September 2019, 117 pages

Altitude simulation testing is an important concept in missile systems, especially in terms of aerothermal ground testing and high speed air breathing engine free-jet testing. Those tests of the missile systems at supersonic speeds need High Altitude Test System (HATS) which simulates Mach number, total pressure and total temperature of the flow on the test article mounted in the test chamber by using free-jet nozzle. To start the free-jet nozzle operation which simulates high altitude conditions, test chamber pressure should be lowered. One of the mostly used methods to reduce the static pressure in the test chamber is ejector systems.

In this thesis, performance of an ejector system is investigated together with the free jet nozzle and test chamber by using numerical and experimental methods. Primarily, ejector system and test section design are performed separately by 'Design by Analysis' method based on Computational Fluid Dynamics (CFD) analyses and optimization algorithms. Nondimensional ejector system and test section geometry are determined. Then, numerical results of ejector system and test section analyses are compared with the numerical results of combined HATS analysis model with 2, 2.5 and 3 Mach free-jet nozzles. Good aggrement between the results is indicated. After that, by using the nondimensional ejector system and test section geometry, experimental setup is designed, manufactured and established in TÜBİTAK-SAGE.

Then, an experimental study is performed to assess the numerical solutions. The effect of the length to diameter ratio (L/D) of ejector diffuser, ejector nozzle exit plane (NXP) location and entrainment ratio (ER) on the pressure distribution along experimental setup and free-jet nozzle starting condition are investigated in detail. At design condition, vacuum pressure value is calculated as 26754 Pa in numerical solution and measured as 30794 Pa in experiment, test chamber pressure value is calculated as 7563 Pa in numerical solution and measured as 7437 Pa in experiment. Comparisons of numerical data with experimental data show a good fit in vacuum pressure and test chamber pressure (within 13% for vacuum pressure and 2% for test chamber pressure).

Keywords: Ejector, High Altitude Test System, Supersonic Diffuser, Altitude Simulation Testing, Entrainment Ratio

ÖZ

İRTİFA BENZETİMİ İÇİN TEST DÜZENEĞİ TASARIMI

Aydoğdu, Ataman
Yüksek Lisans, Makina Mühendisliği
Tez Danışmanı: Prof. Dr. Abdullah ULAŞ

Eylül 2019, 117 sayfa

Füze sistemleri için irtifa benzetim testi, özellikle aerotermal yer testleri ve yüksek hızlı hava solumalı motorların serbest akış testlerinin gerçekleştirilmesi noktasında önemli bir kavramdır. Sesüstü hızlardaki füze sistemlerinin bu testleri için, test odasına konumlandırılmış test kalemi üzerindeki akışın Mach sayısını, toplam basıncını ve toplam sıcaklığını serbest akış lülesi yardımıyla modelleyecek yüksek irtifa test düzeneğine ihtiyaç duyulmaktadır. Serbest akış lülesinin çalışabilmesi için, test odası basıncının düşürülmesi gerekmektedir. Test odası basıncını düşürmek için kullanılan yöntemlerin en yaygın olanlarından biri Ejektör sistemidir.

Bu tez kapsamında, Ejektör sisteminin performansı sayısal ve deneysel yöntemler kullanılarak serbest akış lülesi ve test odası ile birlikte incelenecektir. Öncelikle Ejektör sistemi ve test odası boyutlandırması birbirlerinden ayrı olarak 'Çözümleme ile Tasarım' yöntemi ile eniyileme algoritmaları ve Hesaplamalı Akışkanlar Dinamiği (HAD) çözümlemeleri kullanılarak gerçekleştirilecek, boyutsuz ejektör ve test odası tasarımı yapılacaktır. Sayısal sonuçları doğrulamak adına 2, 2.5 ve 3 Mach lüleleri ile yüksek irtifa test düzeneğinin bütüncül analizleri gerçekleştirilecek, sonuçlar ejektör ve test odası sonuçları karşılaştırılacaktır. Ek olarak, sayısal çözümlemelerden elde edilen boyutsal veriler kullanılarak test düzeneği tasarımı ve üretimi gerçekleştirilmiş, sonrasında sayısal çözümlemeleri doğrulamak adına deneysel çalışma yürütülmüştür.

Böylece ejektor difüzörünün boy-çap oranının, ejektör lüle çıkış düzleminin konumunun ve ejektör sürükleme oranının, test düzeneği boyunca basınç dağılımı ve serbest akış lülesi başlama koşulu üzerindeki etkileri incelenmiştir. Test düzeneği tasarım koşulunda, vakum basıncı değeri analizde 26754 Pa hesaplanmış, testte 30794 Pa olarak ölçülmüş, test odası basıncı değeri analizde 7563 Pa hesaplanmış, testte 7437 Pa olarak ölçülmüştür. Bu durum analiz sonuçları ile deneysel veriler arasında iyi bir uyum olduğunu göstermektedir.

Anahtar Kelimeler: Ejektör, Yüksek İrtifa Test Sistemi, Sesüstü Difüzör, İrtifa Benzetim Testi, Sürükleme Oranı

To my family…

ACKNOWLEDGMENTS

Firstly, I would like to express my deepest thanks and gratitude to Prof. Dr. Abdullah ULAŞ, for his supervision, understanding and guidance through this study.

Also, I'd like to thank to Chief of the Propulsion Systems Division in TÜBİTAK-SAGE, Dr. Bülent SÜMER, for sharing his experience and providing all kinds of convenience.

And a special thanks to Mr. Bora YAZICI for his great contributions, invaluable efforts during the experimental process and discussion on the subject during the preparation of this thesis.

I would like to thank TÜBİTAK-SAGE for their contribution to the manufacturing of experimental setup under HSFSGA Project and TÜBİTAK-SAGE employees who helped me throughout my study.

My gratitude is endless for my love Selen for her unfailing support and encouragement during this difficult period. Without whom this thesis would not have been possible.

Lastly, special thanks goes to my family for always being there for me and giving me the motivation. It would be impossible without their patience and understanding.

TABLE OF CONTENTS

LIST OF TABLES

TABLES

LIST OF FIGURES

FIGURES

LIST OF ABBREVIATIONS

BSP	British Standart Pipe
CAD	Computer Aided Drawing
CFD	Computational Fluid Dynamics
DOE	Design of Experiment
ER	Entrainment Ratio
HATS	High Altitude Test System
L/D	Length to Diameter Ratio
MOGA-2	Multiobjective Genetic Algorithm-2
NPT	National Pipe Thread
NXP	Nozzle Exit Plane
PR	Pressure Ratio
TI	Turbulence Intensity
TÜBİTAK SAGE	The Scientific and Technological Research Council of Turkey Defense Industries Research and Development Institute

LIST OF SYMBOLS

A_{th1}	Ejector Nozzle Throat Area
D_1	Ejector Diffuser Diameter
D_2	Test Section Diffuser Diameter
D_{ex1}	Ejector Nozzle Exit Diameter
D_{ex2}	Free-jet Nozzle Exit Diameter
D_{th1}	Ejector Nozzle Throat Diameter
D_{th2}	Free-jet Nozzle Throat Diameter
L_1	Ejector Diffuser Length
L_2	Test Section Diffuser Length
L_3	Transition Cone Length
L_4	NXP Length
$\dot{m}_s$	Secondary Mass Flow Rate
$\dot{m}_p$	Primary Mass Flow Rate
P_{amb}	Ambient Pressure
P_{ex1}	Ejector Nozzle Exit Pressure
P_{ex2}	Free-jet Nozzle Exit Pressure
P_{tc}	Test Chamber Pressure
P_{t1}	Primary Flow Total Pressure
P_{t2}	Secondary Flow Total Pressure
P_v	Vacuum Pressure

R_u	Universal Gas Constant
T_{amb}	Ambient Temperature
T_{t1}	Primary Flow Total Temperature
T_{t2}	Secondary Flow Total Temperature
α_1	Transition Cone Angle
α_2	Ejector Nozzle Diverging Half Angle
γ	Specific Heat Ratio

CHAPTER 1

INTRODUCTION

1.1. Motivation

In modern missile systems, successful ground testing requires an accurate simulation of flight conditions that the system would be confronted during normal operations. Altitude simulation is an important concept in ground level testing and qualification of missile systems, particularly in terms of aerothermal ground testing and high speed air breathing engine free-jet testing. Those tests of the tactical missile systems at supersonic speeds need High Altitude Test system (HATS) which simulates the airstream flow conditions, pressures, temperatures and airspeed as well as the airstream flow patterns representative of the test article shape and flight altitude.

1.1.1. High Altitude Test System

The fundamental objective of performing the high altitude testing is to test the article under the conditions of nozzle full-flow without any flow separation by creating the test chamber pressure equal or less than the free-jet nozzle exit pressure [1]. Therefore, HATS should create this sufficient low-pressure environment corresponding to the high altitude flight situation [2]. Testing facilities of this type comprises an air storage system, air heater system, a free-jet nozzle, a test chamber that isolates the article from the outside atmosphere, a diffuser and a vacuum system [3], which is shown schematically in Figure 1-1 and Figure 1-2. Mostly used vacuum systems to reduce the static pressure in the test chamber to a value required to start free-jet nozzle operation are Vacuum Sphere and Ejector Diffuser System. In a typical high altitude test system stored a large quantity of high-pressurized air in tanks. Then, this air is fed into the air heater where air is heated up to the correct temperature. After that, the high temperature, high pressure air flows through a free-jet nozzle that accelerates the air to a desired Mach number [4].

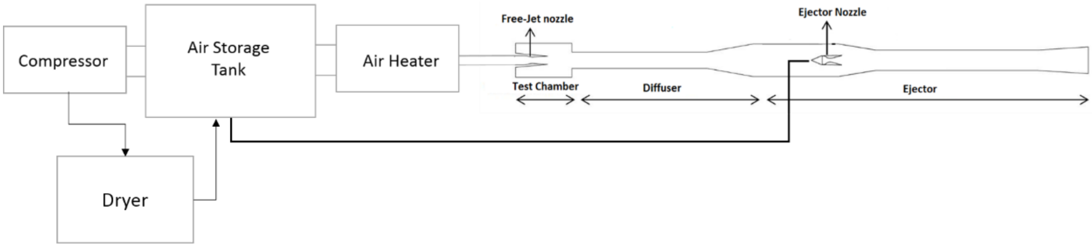

Figure 1-1. High Altitude Test System with Ejector Diffuser System Schematic.

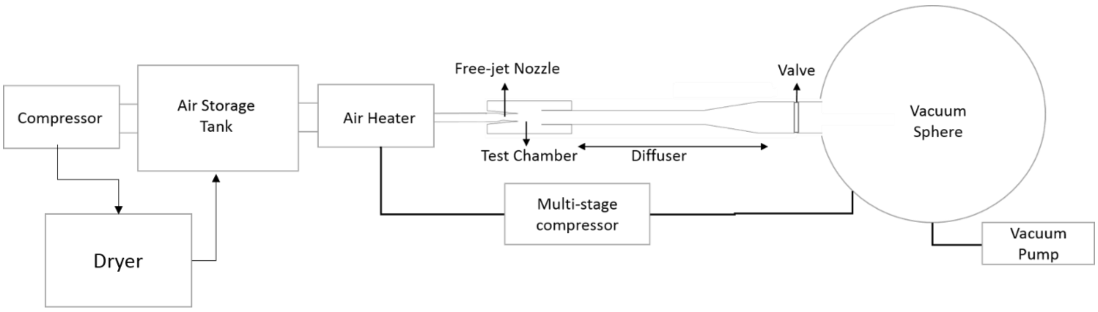

Figure 1-2. High Altitude Test System with Vacuum Sphere System Schematic [5].

1.1.1.1. Air Storage System

Air storage system includes high-pressurized air tanks, dryers, compressors and valves. The capacity of the air tanks determines the duration of the test. During the test, the decrease of the air mass in the air tank causes the pressure and temperature to decrease. This situation might lower the temperature to a value that could damage the system. Moisture creation in a compressor is unavoidable, but if properly treated, it will forestall damage to the mechanical components. To prevent the icing in the system, the tanks should be filled with dry air by using dryer. Control valves are used to control fluid flow by changing the size of the flow passage to supply required pressure or mass flow rate as guided by a controller. Check valve is a closing member which allows fluid to flow through it in only one direction. In the open position it allows forward flow and in closed position it blocks the reverse flow.

1.1.1.2. Air Heater System

To simulate the flow conditions correctly for the total temperature simulation, it is necessary to heat up the test air. An air heater is used to increase the temperature of the air supplied from the air storage system to the desired temperature. There are several methods such as vitiation-type combustion air heater, electric heater and pebble bed heaters for achieving the required high air supply temperature. Vitiation-type combustion air heater uses a combustor upstream of the free-jet nozzle. Vitiator is a combustion chamber. By controlling the fuel mass flow rate, the temperature can be controlled easily. However, combustion products contaminate air. Due to this, additional oxygen is given to fulfill the consumed oxygen in the combustion process. Electric heaters are useful in the way of not polluting the air and easy to control however, power requirements are very high. So, generally for high air mass flow rates an electric heater is not chosen. The pebble heater is a regenerative heat exchanger. Pebble bed storage unit uses the heat capacity of a bed loosely packed with bulk material to store energy. An air is circulated through the bed to add energy [6].

1.1.1.3. Vacuum Sphere

In general, vacuum sphere is used in supersonic wind tunnels as a vacuum system shown schematically in Figure 1-3 and picture of Vacuum Sphere given in Figure 1-4 as an example. Vacuum sphere is lowering the test section pressure to a value that free-jet nozzle operates. However, in true temperature altitude simulation testing, the total temperature of the free-jet nozzle flow is extremely high and vacuum sphere could not work under this condition. The air enters the vacuum sphere should be cold enough for system operation and safety. That’s why, there should be a cooling system between the test section diffuser and the vacuum sphere to cooldown the flow [7]. Due to this complexity, although the ejector system has a lower performance efficiency than the vacuum sphere, it has no moving parts, cheaply operates and simple in design.

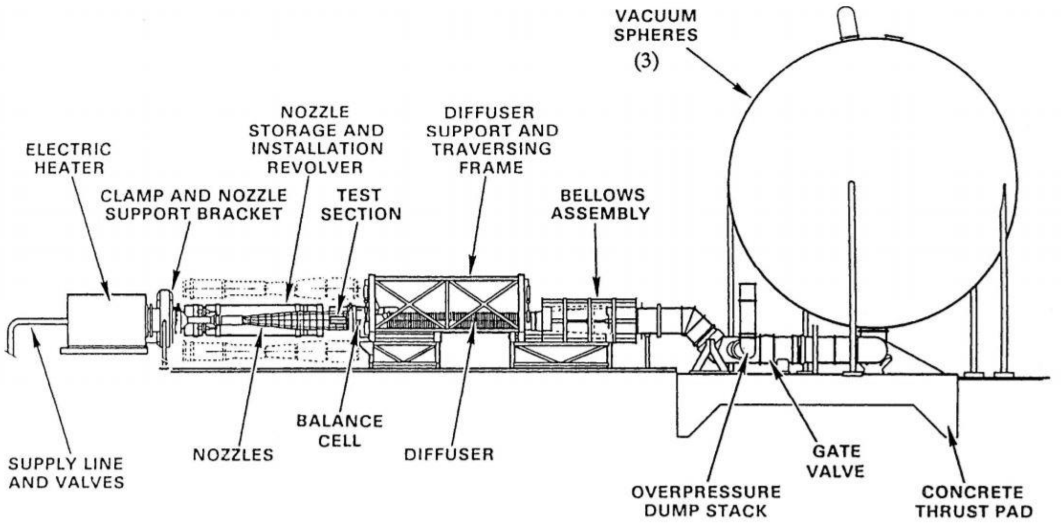

Figure 1-3. Wind Tunnel Schematic with Vacuum Sphere [8].

Figure 1-4. Vacuum Spheres at NASA Langley Research Center [9].

1.1.1.4. Ejector System

Ejectors for compressible fluids are not new and have been known for a long time. An ejector is a simple mechanical device, kind of a vacuum pump, in which the momentum of the primary flow is transferred to the secondary flow. The momentum transfer takes place as the primary flow is injected into the secondary flow that is stagnant or moving [10]. The ejector system is used to get low test cell pressure to help the free-jet nozzle start. Ejector has no moving parts, and requires no power input. Because of this, it can be designed, built and maintained easily compared to turbomachinery devices. A typical ejector schematic given in Figure 1-5. The primary flow is the motive fluid, which has high-pressure, high-energy and the secondary flow is the entrained fluid, which has the low-energy, low-pressure. When the primary flow enters the diffuser, entrains the secondary flow, which is either stationary or moving relative to the ejector. The entrainment of the secondary flow is caused by the reduction of the static pressure of station 1 to a value less than the ambient pressure. The two flows are completely mixed at the end of the mixing tube in an ideal ejector [11]. Ejector study is, however, still challenging due to the complex flow process taking place within them, as a result of their internal geometry, several interacting phenomena such as supersonic conditions, shock wave formation and turbulent mixing of two streams in dynamic and thermal non-equilibrium in a very short time and restricted space [12].

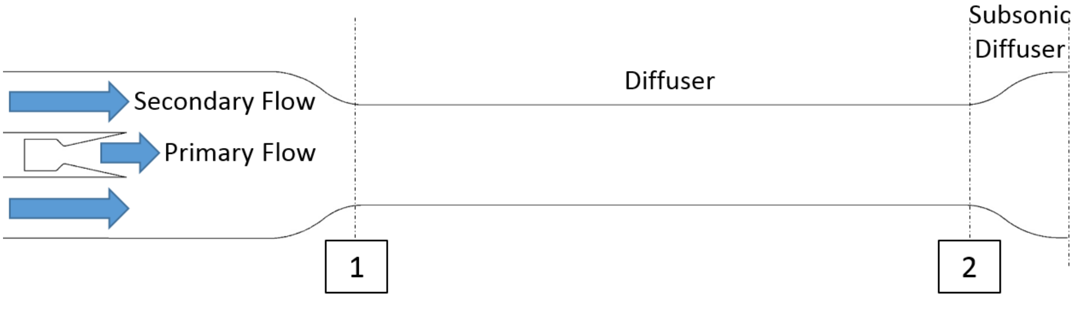

Figure 1-5. Central Injection Type of Ejector Schematic.

Ejectors are classified with respect to the internal flow conditions and inlet configuration shown in Figure 1-6. If the ejector nozzle is convergent and the mach number at the exit of the ejector nozzle smaller than 1, ejector is subsonic. If the ejector nozzle is convergent-divergent, ejector is supersonic.

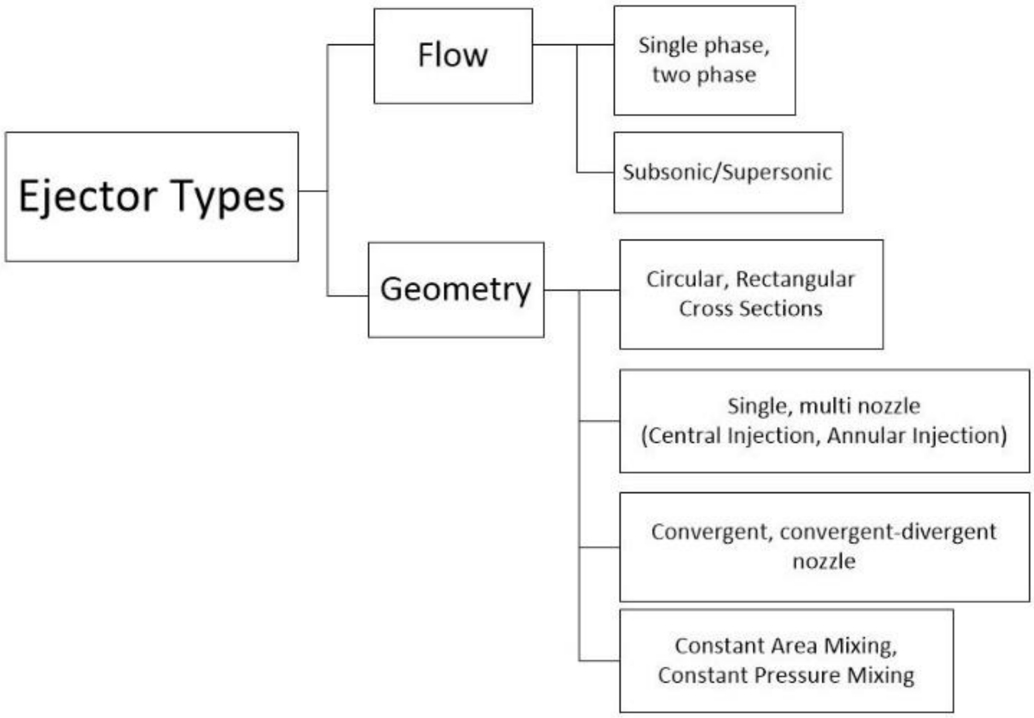

Figure 1-6. Main Ejector Types.

The location of the primary flow can be either central or annular assuming the circular cross sections. In central injection type of ejector, the ejector system is axisymmetric and the primary flow is injected along the centerline of the system as shown in Figure 1-5. This type of ejector is easy to manufacture. Most practical applications of ejectors have used central injection. However, in high altitude test facilities, ejector feed manifold exposures to the hot gas, due to the high free-jet nozzle total temperature [13]. On the other side, in annular injection type of ejector, the ejector system is periodically symmetric and primary flow is annularly injected from multi-nozzle given in Figure 1-7. This type of ejector has better performance [10] however, it is hard to manufacture and has a complicated structure.

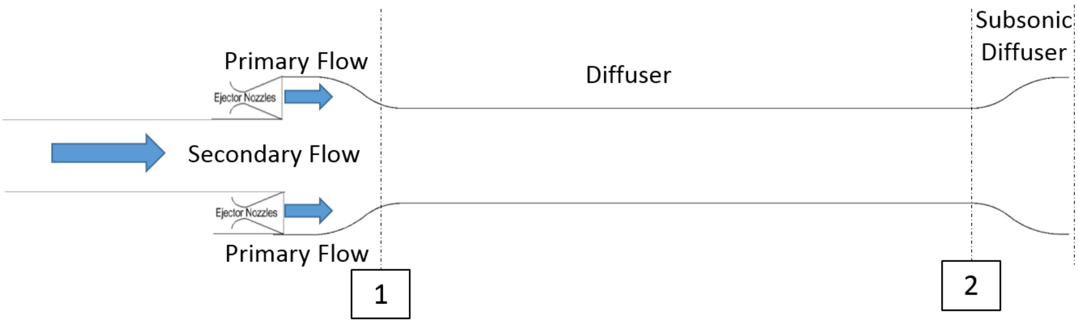

Figure 1-7. Annular Injection Type of Ejector Schematic.

Due to the geometry, ejector may have Constant Pressure or Constant Area Diffuser. The constant area ejector has the simplest geometry, the diffuser is a uniform pipe with constant cross section as shown in Figure 1-8, however, the oblique shock waves sourced from the jet impingement location recur downstream and finally cease with a normal shock wave. The shock trains in this type of ejector are strongly dissipative, and total pressure of nozzle should be high to start ejector system [14]. Although the constant area diffuser ejector can supply higher mass flow rate, constant pressure diffuser ejectors have more stable performance at a broad range of diffuser exit pressure [15]. The constant pressure or second throat diffuser shown in Figure 1-8 has been commonly used in ejector applications. This looks like constant area diffuser in its geometry, except the presence of second throat. The strong shock waves are dispersed into the oblique shock waves of lower intensity.

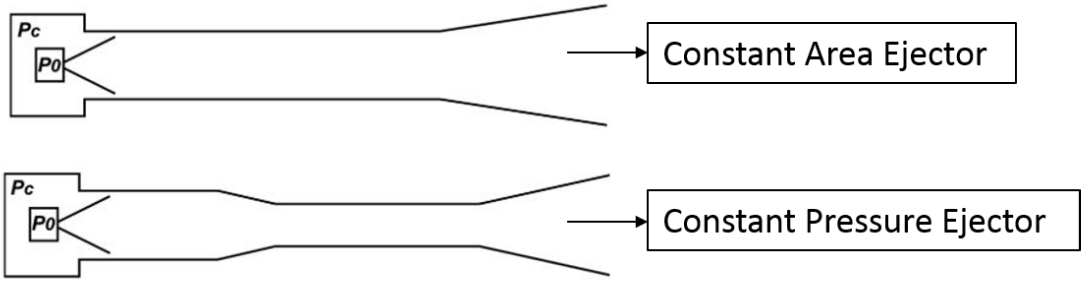

Figure 1-8.Constant Area and Constant Pressure Ejector Schematic [16].

Diffuser is one of the important parts of HATS. The main goal of the diffuser is while increasing the static pressure before opening to atmosphere, slowing the mixed airflow with as a small loss of total pressure as possible. Subsonic diffusers are easy to model by changing the cross section area. However, supersonic exhaust diffusers, which are typically used in altitude simulation testing, are more complicated. They capture supersonic flow and accomplish diffusion through a process of turbulent mixing and multiple shock systems including a combination of normal and oblique shocks. Cross sectional area change is not necessary for supersonic diffusers because the shock trains accomplish to increase static pressure [17]. The supersonic diffusers used in this study is a cylindrical, constant area diffuser.

Ejector system has two main modes of operation, started and unstarted. A sequence of starting operation is given in Figure 1-9. The plot begins when nozzle total pressure, nozzle exit pressure and secondary flow static pressure are equal to ambient pressure. When the nozzle total pressure increases, the secondary flow accelerates from a stagnant ambient state and its static pressure decreases shown in zone (1) in Figure 1-9. In this area, nozzle and ejector are un-started. Only the flow in the nozzle is supersonic and the flow field outside the nozzle is subsonic. While the nozzle total pressure further increases, the shock wave moves out of the nozzle- nozzle is started- to form an oblique shock in diffuser shown in zone (2) in Figure 1-9. When the nozzle total pressure increases more, the diffuser suddenly swallows the oblique shock wave and the whole flow field inside the ejector becomes supersonic; that means ejector and nozzle are started and static pressure of the secondary flow drops suddenly shown in zone (3). Once the ejector is started, further increase in nozzle total pressure will increase secondary flow pressure [18]. Furthermore, in Figure 1-9 there is a region called a hysteresis. The ejector starting pressure is higher than the minimum ejector total pressure necessary for ejector operation. That means there is a hysteresis exists in the supersonic ejector starting process. Also, Bauer et al [19] who worked on the high altitude test facility characteristics and estimating the diffuser performance and starting conditions with/without test article show the hysteresis phenomena by experimental data.

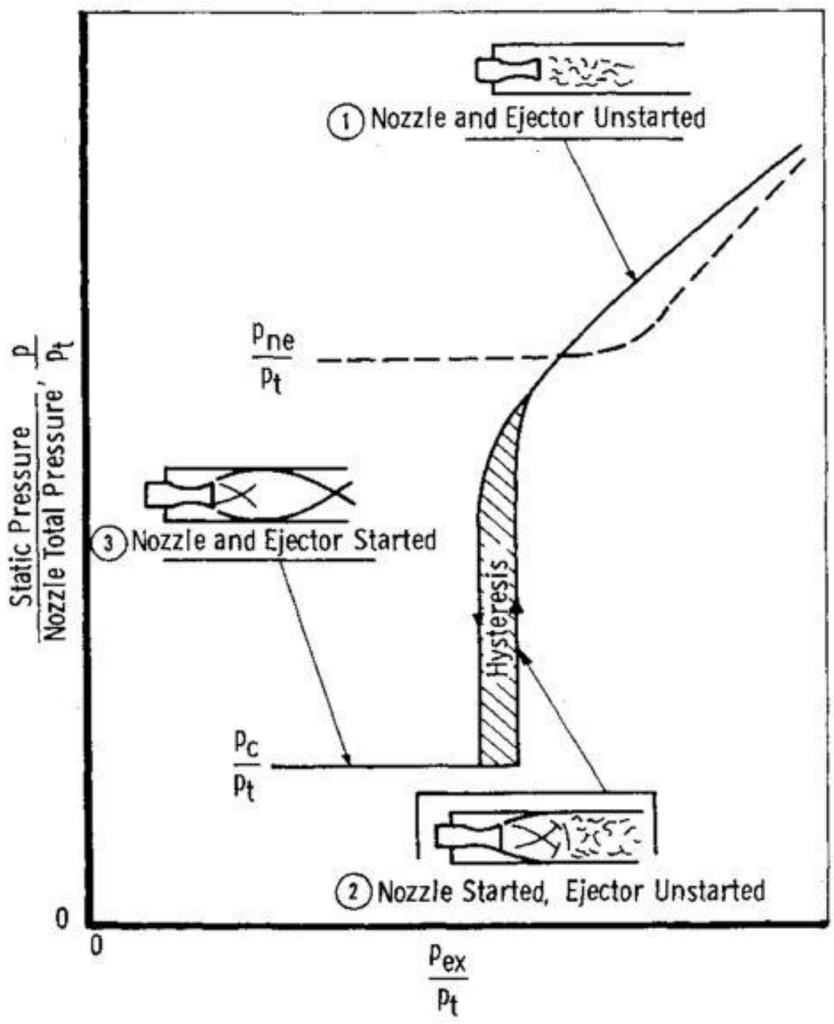

Figure 1-9. Typical Ejector System Starting Phenomena [20].

The performance of an ejector, which is used within a vacuum application, is typically categorized by pressure ratio (PR) at a specific entrainment ratio (ER). The entrainment ratio is the ratio of secondary mass flow rate ($\dot{m}_2$) to primary mass flow rate ($\dot{m}_1$). The pressure ratio is the ratio of vacuum pressure (P_v) to ambient pressure (P_{amb}). Efficient ejector means getting a lower pressure ratio at a specific entrainment ratio.

$$ER = \dot{m}_2/\dot{m}_1 \tag{1-1}$$

$$PR = P_v/P_{amb} \tag{1-2}$$

1.2. Literature Survey

Even though the ejector is physically simplistic, complex flow processes take place within them such as supersonic conditions, shock wave formation, the turbulent mixing and multiple shock systems [21]. Minor variations in ejector geometry or operating conditions seriously effect operational performance [22]. Ejectors have been studied and analyzed for improvements in design and performance in many years. Different methods for calculating ejector-diffuser system performance have been used. Ejectors are mainly designed with one-dimensional analysis, two-dimensional analysis and numerical analysis.

In 1-Dimensional models, the ejector system is divided into parts and locations shown in Figure 1-10. Huang et al. [23] used 1-D approach to simulate ejector performance. Several assumptions were made that contains ideal gas, steady and one dimensional ejector flow, isentropic flow, adiabatic wall, secondary and primary flow starts mixing at y-y section shown in Figure 1-10 with a uniform pressure and sufficient diffuser length for complete mixing before the shock shown in s-s section. Analysis was performed with the developed 1-D model and results are compared with experimental data. It was stated that, developed model can predict the performance of the ejectors. But, there are empirical coefficients determined after the experiments.

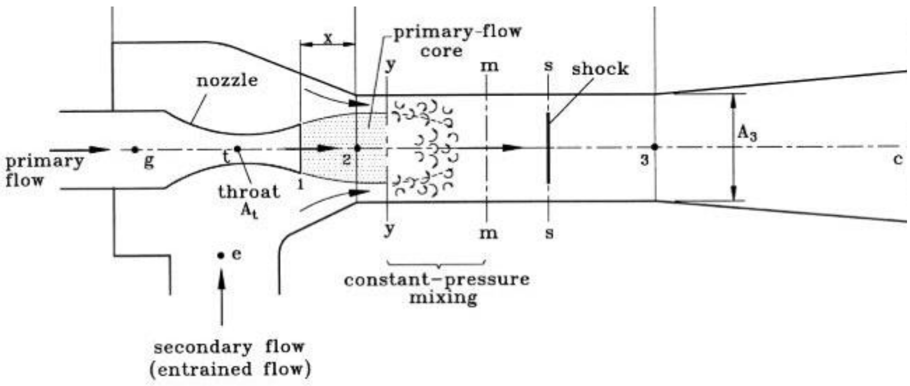

Figure 1-10. Schematic Ejector Diagram [23].

Dutton and Carroll [24] worked on 1-D ejector optimization with respect to ER, Compression Ratio (primary and secondary inlet total pressure ratio) and PR value for gas properties and total temperature of both inlets. The model can optimize one of the given performance variables by taking constant the other two by changing specific heat constants, molecular weights and total temperatures of primary and secondary flows.

German and Bauer [25] worked on the effect of diffuser length on ejector performance by using different ejector nozzles and difffusers. An optimum length of the diffuser is determined at maximum starting pressure of the ejector. Optimum length means, starting pressure of the ejector remained constant for lengths greater than optimum. It was stated that length to diameter ratio of diffuser (L/D) should be higher than 8 for 85% of the normal shock pressure recovery shown in Figure 1-11. In addition, German, Panesci and Clark [26] worked on the performance of ejector-diffuser systems with annular ejector nozzle. It is stated that, for length to diameter ratio of diffuser (L/D) higher than 9, ejector nozzle starting pressure ratio can be calculated within ±8% in the experiment by using 90% of the normal shock pressure ratio. Furthermore, the PR (P_v/P_{amb}) value increases while the diffuser L/D value decreases below nearly L/D=9. For smaller diffuser length than this value, an instability zone might occur when the ejector is unstarted.

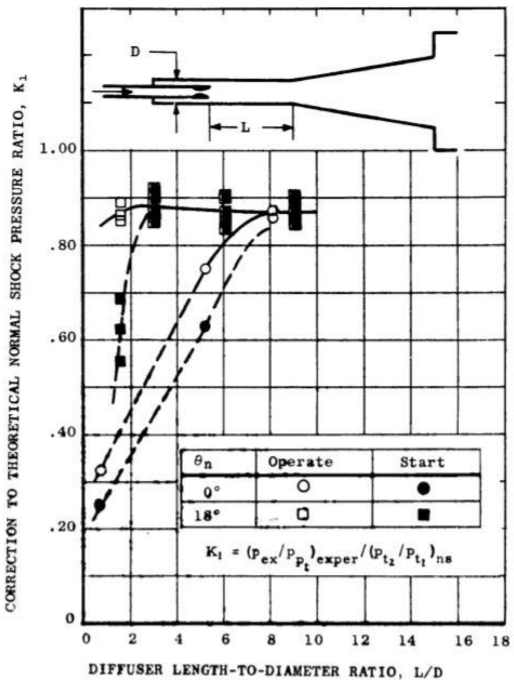

Figure 1-11. Normal Shock Pressure Recovery for Different L/D Ratio [25].

Derick [17] improved the ejector-diffuser system model for annular ejector which includes real gas effects, test article blockage effects and normal shock pressure ratio correction in ejector-diffuser. Model schematic is given in Figure 1-12.

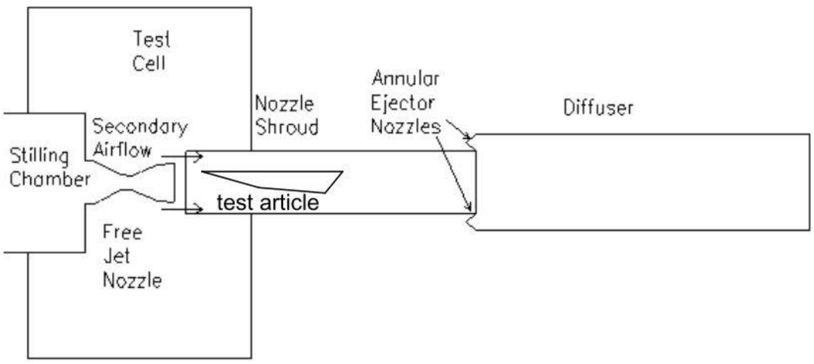

Figure 1-12. Analysis model schematic [17].

In this study both ejector flow and free-jet flow are solved together in transient with and without test article. Due to the high pressure and low temperature inlet condition of ejector nozzle real gas effects has been considered. Also, normal shock pressure recovery factor and test article blockage effect has been included in Matlab-Simulink model. It is seen that including real gas effects change the transient phenomena however, in steady state test cell pressure is calculated same in both real gas modeled and ideal gas modeled ejectors. Moreover, test article drag and blockage effect are modeled and results are compared with the experiments. As it is seen from the comparisons of the model data with experimental data, it accurately simulates both the un-started and started modes of ejector-diffuser system.

Shi et al. [27], developed a new 1-D model which also uses the real gas property in calculations. Although most of the studies focused on the critical mode of ejector, this study mainly focused on the entire operation of ejector which means both sub-critical and critical mode.

Jian-Jun et al. [28] worked on supersonic annular ejector experimentally and used Schlieren device to display internal flow field of ejector system. Ejector starting process is investigated, the pressure distribution along the ejector diffuser is measured and pressure-time history curves are given, however, the dimensions of the experimental setup are not mentioned. Moreover, hysteresis phenomena mentioned in Figure 1-9 is shown experimentally. As seen in Figure 1-13, after the ejector system starts, the nozzle total pressure can be lower than the starting pressure.

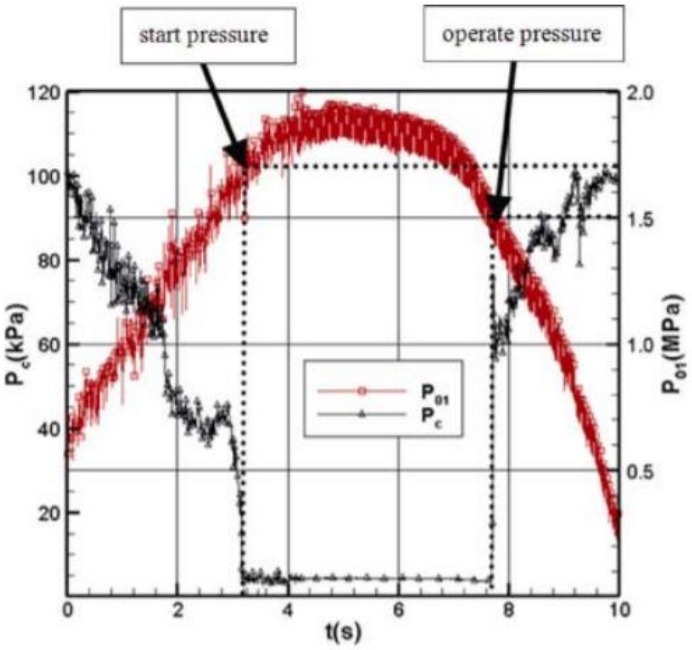

Figure 1-13. Time history of Nozzle Total Pressure and Vacuum Pressure [28].

1-D methods assume constant profiles for each section so; the turbulent mixing and boundary layer effects are not accurately represented. To solve this issue, 2-D methods have been used for axi-symmetric ejector systems by German, Bauer and Panesci [20]. In this work, ejector systems are modeled as an axisymmetric with long diffusers to estimate the required starting pressure of the ejector system. It is stated that developed 2-D model gives good agreement with the experimental results. However, the model which uses method of characteristics, is computationally more intensive than 1-D models.

The application of numerical methods to the study of ejectors is not a new concept. It is believed that computational fluid dynamics might provide a solution to mixing problem of two stream by modeling the geometry of the system in detail. Commercial flow solvers are broadly applicable to the resolution of many flow problems and can be used to accurately foresee the ejector behavior.

Chen et al. [29] studied on the effect of transition cone angle and nozzle exit plane location effect on the flow structure in second throat ejector diffuser system given in Figure 1-14.

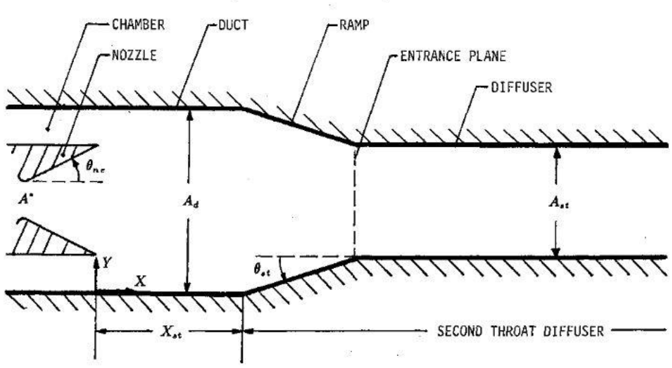

Figure 1-14. Analysis model schematic [29].

Computational analyses are done for supersonic inviscid flowfield. It is stated that, the Mach number distribution on the second throat diffuser inlet plane is the suitable criterion for evaluation of the performance of the system because the larger flow velocity leads to a better pressure recovery and larger exhaust pressure at the diffuser exit. For different transition cone angle and nozzle exit plane location average mach number values at the entrance plane of diffuser are given in Figure 1-15. As it is seen from the results, increase in the transition cone angle increases the mach number value, however for different transition cone angle values, optimum nozzle exit plane length changes. So, the effect of these parameters should be analyzed together.

	θ_{st}, deg		
X_{st}	6	8	10
0.8	3.435	3.581	3.645
1.0	3.508	3.680	3.766
1.2	3.541	3.739	3.802
1.4	3.538	3.701	3.810
1.6	3.535	3.663	3.774
1.8	—	3.642	3.722
2.0	—	—	3.694

Figure 1-15. Mach number values at the entrance plane [29].

Also, Kracik and Dvorak [30] numerically and experimentally investigated the ejector nozzle exit plane location effect on constant-area diffuser ejector performance. k-ω SST turbulence model was used in CFD analysis. For different nozzle exit plane locations, by changing the back pressure, entrainment ratios are calculated in CFD and measured in experiments. Comparison of the numerical simulations and experiments are given. It is stated that, the error remains below 10% for most of the data points and largest error is lower than 20%.

Manikanda et al. [2] worked on the effect of change in back pressure on ejector system by using numerical methods. FLUENT software has been used in numerical analysis and results are compared with experiments. It is shown that when the back pressure is lowered, the shock system moves away from the free-jet nozzle.

Park et al. [16] studied on the constant pressure ejector system by using 1-D, experimental and numerical methods with nitrogen as a gas to model the rocket engines with a high expansion-ratio nozzle. Diffusers are designed by using a normal shock theory. Than, with no induced secondary flow experimental and numerical analysis have been carried out. Rocket nozzle is used as an ejector nozzle in this work. Effect of diffuser geometry, effect of diffuser inlet to second-throat area ratio, effect of nozzle contour and ejector starting and terminating transient have been focused on. Ashokkumar et al. [31] also studied on ejector diffuser design both numerically and experimentally with a high expansion-ratio ejector nozzle.

Desevaux and Lanzetta [21] worked on the shock-train region and mixing region to determine the optimum diffuser length with secondary flow assumption. For the given geometry, laser tomography image and contour plot of shock train and mixing region were given in Figure 1-16. Both numerical and experimental pressure data along the centerline were compared by changing the total pressure of the ejector nozzle.

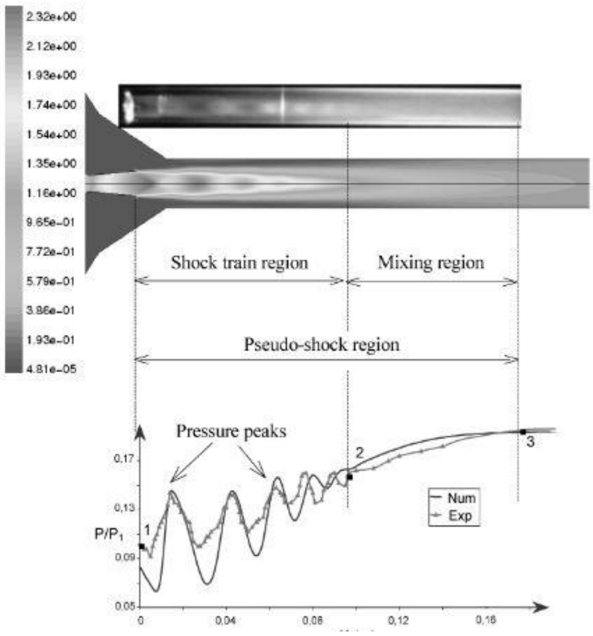

Figure 1-16. Pressure data along the centerline of diffuser in shock train and mixing region [21].

By using the length of shock train and mixing region, L/D ratio of the ejector diffuser was determined for different Mach numbered nozzles given in Figure 1-17. As a result, the pseudo-shock region length to the duct diameter ratio is between 5.1 and 8.8 in numerical data and between 5.2 and 9.7 for experimental data. There are nearly 8% difference between the experimental results and numerical results.

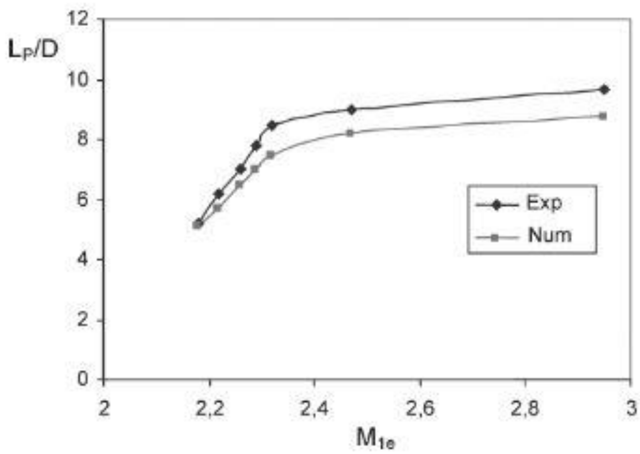

Figure 1-17. L/D ratio of pseudo-shock region in the ejector diffuser for different Mach numbered nozzles [21].

Rose, Jinu and Brindha [3] studied on the high altitude test facility to perform wind tunnel experiments. As a design methodology, they respectively worked on free-jet nozzle design, test section design, test article holding mechanisms and ejector-diffuser system design. 2-D axiymmetic and 3-D numerical analysis are done using ANSYS FLUENT 14.5. Designed experimental setup is given schematically in Figure 1-18. In this work, nozzle-diffuser starting characteristics, turbulence parameters measurements, high altitude test facility and wind tunnel comparison are done. CFD results are given for each parameter. However, the experimental results and system dimensions are not given clearly.

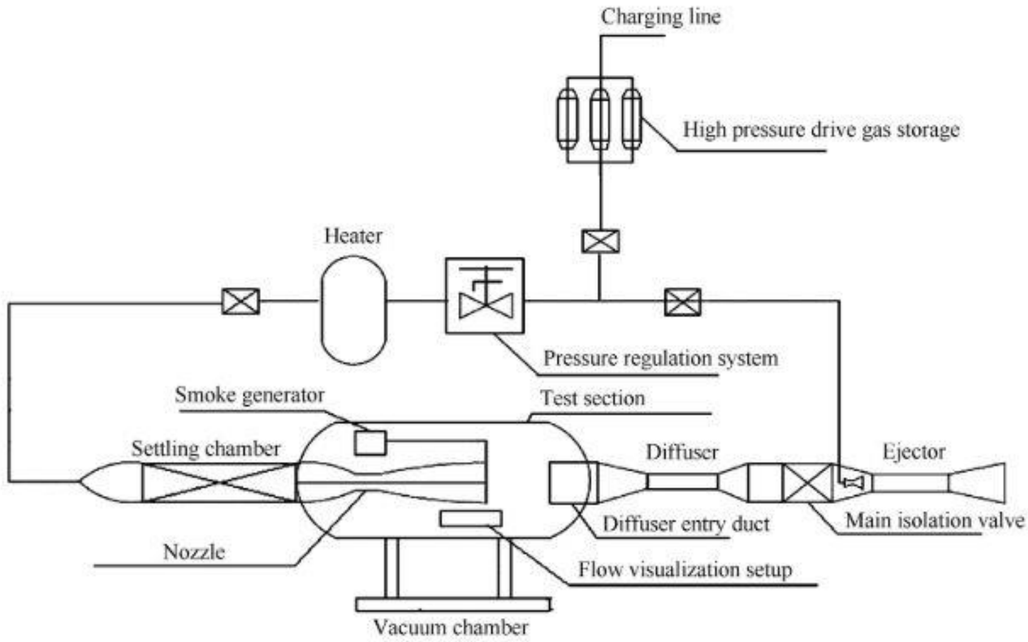

Figure 1-18. High Altitude Test Facility experimental setup used in [3].

1.3. TÜBİTAK-SAGE Test Facility

A simplified sketch of the facility is given in Figure 1-19. The working fluid in the test facility is an air. Compressors are used to fill the air storage tank. Pressure transducers and temperature sensors measure pressure and temperature in the tanks. During the test, the decrease of the air mass in the tank causes the pressure and temperature to decrease. This situation might lower the temperature to a value that could damage the system. To prevent the icing in the system, the tanks are filled with dry air by using dryer. There are two feeding lines in the system, one of them connected to ejector nozzle feed manifold and the other one connected to free-jet nozzle.

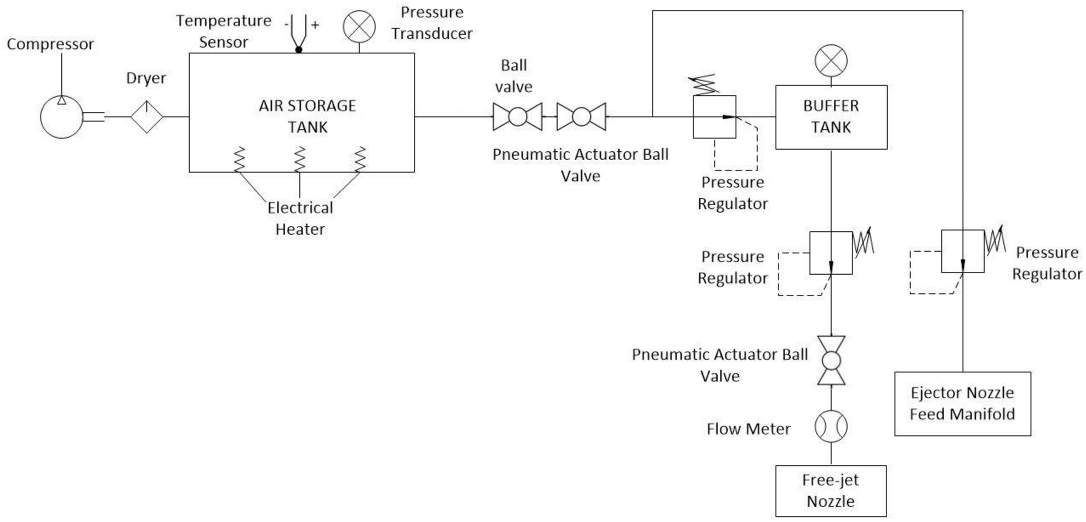

Figure 1-19. Sketch of the Test Facility in TÜBİTAK-SAGE.

1.4. Objectives and Outline of the Thesis

High Altitude Test Facility needs a vacuum system to start the free-jet nozzle. In this study, ejector system is used as a vacuum system. Although the ejector systems seem to be simple, complex interacting flow processes such as supersonic conditions, shock wave formation, the turbulent mixing and multiple shock systems take place within them. In addition to the internal flow difficulties, as mentioned in different sources, minor variations in ejector system geometry or operating conditions seriously effect operational performance of ejector system.

In this study, the purpose is to design an experimental setup for testing the article under the conditions of nozzle full-flow without any flow separation and enhance the knowledge about the high altitude test system. For this purpose; first, the design methodology for high altitude test system by numerical methods is developed. Then, by using the numerical investigation results obtained from the design methodology, an experimental setup is designed, manufactured and established at TÜBİTAK SAGE.

In the experimental study, manufactured experimental setup is tested in different configurations and operating conditions. Pressure data is measured from the different locations along the experimental setup and temperature data is measured from the test chamber, free-jet nozzle and ejector nozzle inlet during the experiments.

Lastly, numerical investigation results and experimental results are compared and discussed in detail.

CHAPTER 2

NUMERICAL METHODOLOGY

2.1. Introduction

The design of the ejector systems are performed with simple 1-D equations and experiments for a long time. However, due to the complexity of the supersonic flow, turbulent mixing and shock waves, there is a difference between numerical and experimental results. That's why correction factors are used in theoretical 1-D analysis. The experimental setups are quite expensive and can only analyze a limited number of flow conditions. Therefore, in recent years, numerical methods are commonly used in the design of the ejector systems for simulating the flow field of different geometries and flow conditions as well as for better visualization of the flow field. In this study, numerical methods are decided to be used in design.

In this chapter, brief information is given about numerical methodology and the background of the flow solver. In addition, general information about optimization techniques used in design methodology are mentioned.

2.2. The FLUENT CFD Solver

Analyses are done in ANSYS FLUENT 19.2 computational fluid dynamics tool environment. FLUENT provides comprehensive modeling capabilities for a wide range of incompressible and compressible, laminar and turbulent fluid flow problems.

2.2.1. Governing Equations

The basis of computational fluid dynamics is the fundamental governing equations – the continuity, momentum and energy equations. They are the mathematical statements of three major physical principles upon which all of fluid dynamics is based:

- Mass is conserved,
- Newton's second law,
- Energy is conserved.

In this study, single phase fluid motion is considered. Air is used as a working fluid. Velocity, V_x, V_y, V_z, pressure, p, temperature, T, density, ρ and internal energy, e, are the unknowns that can be obtained by solving the following equations.

The continuity equation in non-conservation form is given by

$$\frac{D\rho}{Dt} + \rho\nabla.\vec{V} = 0 \tag{2-1}$$

The continuity equation in conservation form is given by

$$\frac{\partial\rho}{\partial t} + \nabla.(\rho\vec{V}) = 0 \tag{2-2}$$

Body forces are neglected in momentum equations. The momentum (Navier Stokes) equations in non-conservation form can be expressed by the followings,

$$\rho\frac{Du}{Dt} = -\frac{\partial p}{\partial x} + \frac{\partial\tau_{xx}}{\partial x} + \frac{\partial\tau_{yx}}{\partial y} + \frac{\partial\tau_{zx}}{\partial z} \tag{2-3}$$

$$\rho\frac{Dv}{Dt} = -\frac{\partial p}{\partial y} + \frac{\partial\tau_{xy}}{\partial x} + \frac{\partial\tau_{yy}}{\partial y} + \frac{\partial\tau_{zy}}{\partial z} \tag{2-4}$$

$$\rho\frac{Dw}{Dt} = -\frac{\partial p}{\partial z} + \frac{\partial\tau_{xz}}{\partial x} + \frac{\partial\tau_{yz}}{\partial y} + \frac{\partial\tau_{zz}}{\partial z} \tag{2-5}$$

The momentum (Navier Stokes) equations in conservation form can be expressed by the followings,

$$\frac{\partial(\rho u)}{\partial t} + \nabla.(\rho u\vec{V}) = -\frac{\partial p}{\partial x} + \frac{\partial\tau_{xx}}{\partial x} + \frac{\partial\tau_{yx}}{\partial y} + \frac{\partial\tau_{zx}}{\partial z} \tag{2-6}$$

$$\frac{\partial(\rho v)}{\partial t} + \nabla.(\rho v\vec{V}) = -\frac{\partial p}{\partial y} + \frac{\partial\tau_{xy}}{\partial x} + \frac{\partial\tau_{yy}}{\partial y} + \frac{\partial\tau_{zy}}{\partial z} \tag{2-7}$$

$$\frac{\partial(\rho w)}{\partial t} + \nabla.(\rho w \vec{V}) = -\frac{\partial p}{\partial z} + \frac{\partial \tau_{xz}}{\partial x} + \frac{\partial \tau_{yz}}{\partial y} + \frac{\partial \tau_{zz}}{\partial z} \tag{2-8}$$

In addition, conservation of energy can be written as [32]:

$$\begin{aligned}\frac{\partial(\rho e)}{\partial t} &+ \nabla.\left(\rho e \vec{V}\right) \\ &= \rho\dot{q} + \frac{\partial}{\partial x}\left(k\frac{\partial T}{\partial x}\right) + \frac{\partial}{\partial y}\left(k\frac{\partial T}{\partial y}\right) + \frac{\partial}{\partial z}\left(k\frac{\partial T}{\partial z}\right) \\ &- p\left(\frac{\partial u}{\partial x} + \frac{\partial v}{\partial y} + \frac{\partial w}{\partial z}\right) + \lambda\left(\frac{\partial u}{\partial x} + \frac{\partial v}{\partial y} + \frac{\partial w}{\partial z}\right)^2 \\ &+ \mu\left[2\left(\frac{\partial u}{\partial x}\right)^2 + 2\left(\frac{\partial v}{\partial y}\right)^2 + 2\left(\frac{\partial w}{\partial z}\right)^2 + \left(\frac{\partial u}{\partial y} + \frac{\partial v}{\partial x}\right)^2 \right. \\ &\left. + \left(\frac{\partial u}{\partial z} + \frac{\partial w}{\partial x}\right)^2 + \left(\frac{\partial v}{\partial z} + \frac{\partial w}{\partial y}\right)^2\right]\end{aligned} \tag{2-9}$$

The pressure of an ideal gas is a function of density and temperature expressed by a special equation called equation of state and ρ is calculated by ideal gas law.

$$p = \rho RT \tag{2-10}$$

where R the specific gas constant that is calculated by using the molecular weight of the gas:

$$R = \frac{R_u}{M} \tag{2-11}$$

M is molecular weight of the gas and R_u is the universal gas constant which is equal to 8314.4621 J/mol.K. R is being equal to 287.1 J/kg.K for air. For an ideal gas, to relate the internal energy with temperature so that the energy equation can be written as temperature being the only unknown following relation can be used.

$$e = c_v T \tag{2-12}$$

In this work, viscosity, μ, and thermal conductivity, k, are assumed to be constant.

2.2.2. Turbulence Models

Turbulence is the most important challenge for fluid flow problems because of the both large and extremely small eddies and irregular motion of the fluid. Simulation of turbulent flow creates additional difficulties in the solution of governing equations. To describe the effects of turbulent fluctuations of velocities and scalar quantities in a single phase various types of models are used. The most common turbulence models are Realizable $k-\varepsilon$, $k-\omega$ and Standard SST $k-\omega$.

2.2.2.1. Realizable $\boldsymbol{k-\varepsilon}$ Turbulence Model

It is an improved method by means of calculating the turbulent viscosity and the dissipation rate. Compared to the standart $k-\varepsilon$ turbulence model, this model predicts the distribution of dissipation rate and boundary layer characteristics in large pressure gradients better [33].

2.2.2.2. $\boldsymbol{k-\omega}$ Turbulence Model

This model describes well the near-wall flows, including those with the large pressure gradients. However, it is not successful enough in calculating jet streams. Also, this model is very sensitive to the boundary conditions in the external flow and the turbulence level initial conditions [33].

2.2.2.3. Standard SST $\boldsymbol{k-\omega}$ Turbulence Model

This model is a combination of $k-\omega$ int the near-wall region and $k-\varepsilon$ in far from the wall region. It was stated that this model shows promising results in mixing layers at medium pressure gradients [33]. The SST $k-\omega$ model is similar to the standart $k-\omega$ model with including refinements [34].

- $k-\omega$ model and the $k-\varepsilon$ model are both multiplied by a blending function and both models are added together. The blending function is designed to be one in the near-wall region and activate the $k-\omega$ model, and zero away from the wall which activates the $k-\varepsilon$ model.

- The modeling constants are different.
- The SST $k-\omega$ model combines a damped cross-diffusion derivative term in the ω equation.
- Definition of the turbulent viscosity is modified.

Bartosiewicz et al. [35] compared simulation results obtained by using different turbulence model with experimental data and stated that SST $k-\omega$ model appear to be very promising for ejector analysis. Also, Kolar and Dvorak [36], verify the SST $k-\omega$ model in supersonic air ejector by comparing the numerical simulation with experimental results in terms of vacuum pressure and color schlieren pictures. As a result, in this thesis SST $k-\omega$ turbulence model is used.

2.3. FLUENT Setup

Working fluid is chosen as air. Due to the flow is compressible; air density is computed with ideal gas law. All computations are done in two-dimensional axisymmetric space with coupled pressure-based solver. Flow is solved in steady-state. As a spatial discretization,

- Gradients are computed by using least square cell-based method.
- Pressure interpolation scheme is chosen as second order which is recommended for compressible flows.
- Density, momentum, turbulent kinetic energy, specific dissipation rate and energy is computed by using second order upwind method.

2.4. Solution Domain

HATS analysis model consists of a free-jet nozzle, a test chamber that isolates the article from the outside atmosphere, a diffuser and an ejector system, which is shown schematically in Figure 2-1.

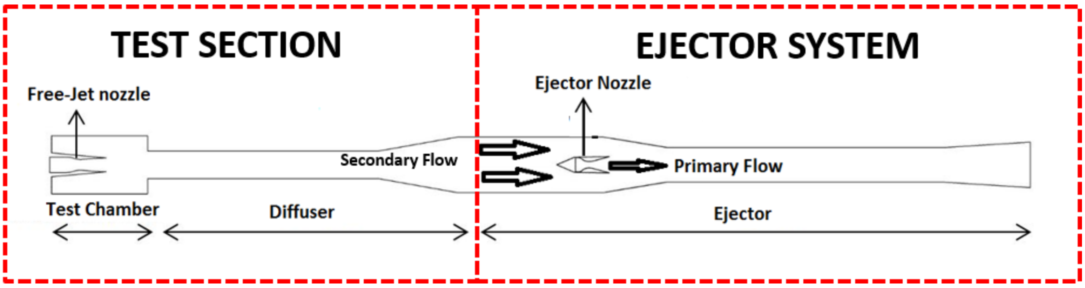

Figure 2-1. Schematics of HATS Analysis Model.

The solution domain and the boundary conditions for the Ejector System and Test Section are given respectively in Figure 2-2 and Figure 2-3.

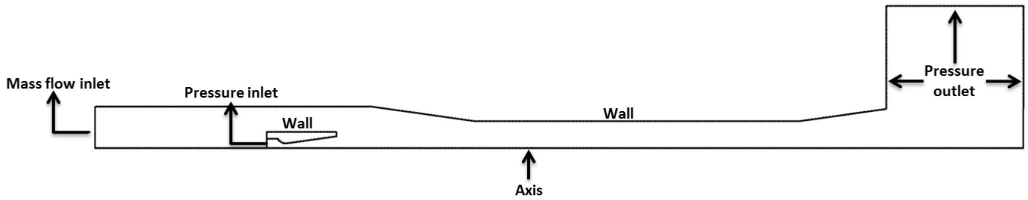

Figure 2-2. Solution Domain and the Boundary Conditions for the Ejector System.

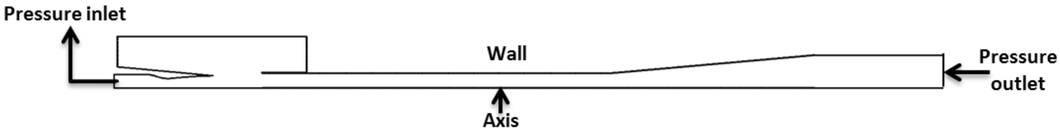

Figure 2-3. Solution Domain and the Boundary Conditions for the Test Section.

2.5. Grid Sensitivity

A grid sensitivity study is performed for the Ejector System numerical simulations which results in coarse, medium and fine grid with 50000, 110000 and 450000 elements, respectively. Ejector nozzle section ,shown in Figure 2-2, grid detail is given in Figure 2-4, Figure 2-5 and Figure 2-6 for coarse, medium and fine grid, respectively. In design methodology section, series of CFD analysis are conducted for different geometries by using optimization method in MODE FRONTIER software and mesh is generated in grid generation program by using an automated meshing script. For this reason, uniform grid is used in this study and the control on the grid spacing is performed on the cell dimensions of the geometry.

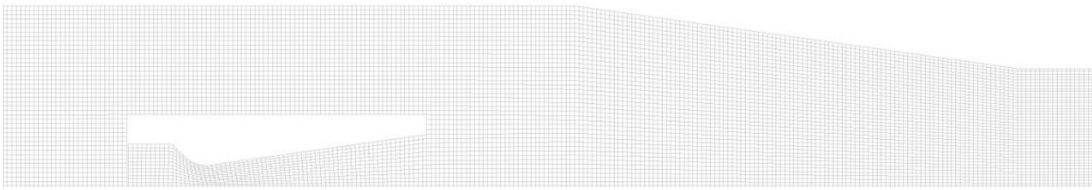

Figure 2-4. Ejector Nozzle Section Grid Detail For Coarse Grid.

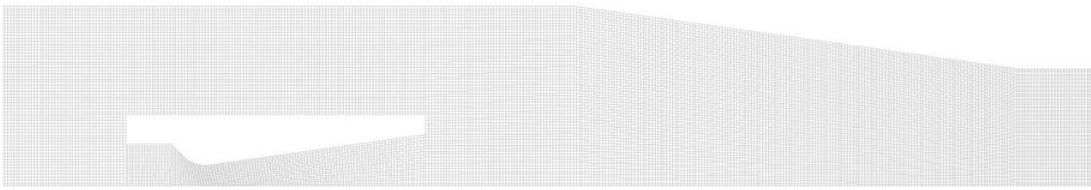

Figure 2-5. Ejector Nozzle Section Grid Detail for Medium Grid.

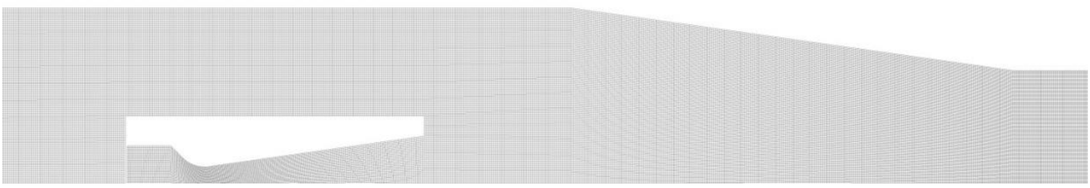

Figure 2-6. Ejector Nozzle Section Grid Detail for Fine Grid.

The grid sensitivity study for a random ejector geometry is performed by using the boundary conditions given in Table 2-1.

Table 2-1. Grid Sensitivity of Ejector System Boundary Conditions.

Parameter	**Value**
Pressure inlet total pressure, P_{t1}, bar	20
Pressure inlet total temperature, T_{t1}, K	300
Entrainment ratio, ER, $\dot{m}_s / \dot{m}_p$	0.33
Pressure outlet pressure, P_{amb}, Pa	89000
Mass flow inlet total temperature, T_{t2}, K	300

The Vacuum Pressure calculated at the mass inlet of the Ejector System is shown in Figure 2-7. The flow solver predicts a vacuum pressure, P_v, value of 32800 Pa for coarse grid, 32560 Pa for medium grid and 32400 Pa for fine grid. The value predicted using medium grid is only 0.3% higher than the value predicted using fine grid. For grid sensitivity analysis the important criteria is the Mach number, static pressure and static temperature distribution along the axis and they are plotted in Figure 2-8. In coarse grid solution, axial variation of Mach number, static pressure and static temperature cannot capture the trend of change. However, medium and fine grids show a similar trend and their predictions almost overlap, which indicate that the solution is insensitive to further grid refinement. Therefore, it is concluded that medium grid properties can be utilized in HATS simulations.

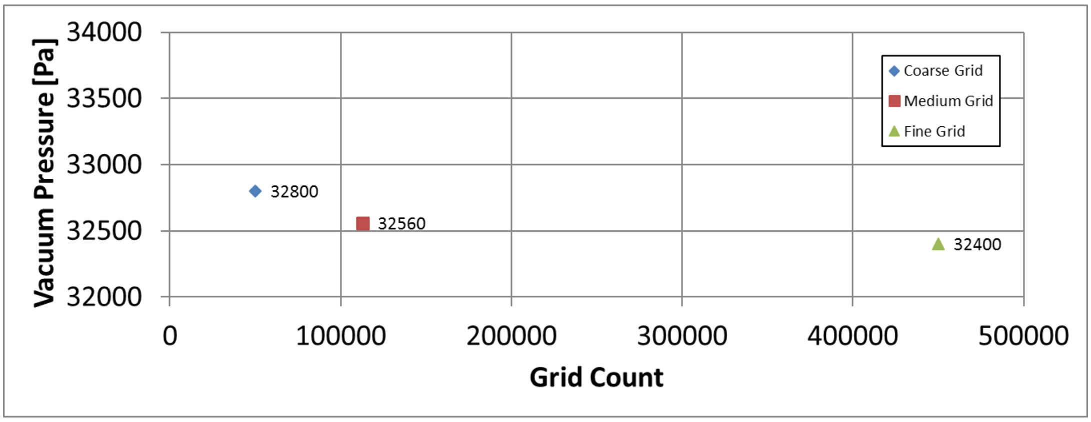

Figure 2-7. Vacuum Pressure vs. Grid Count.

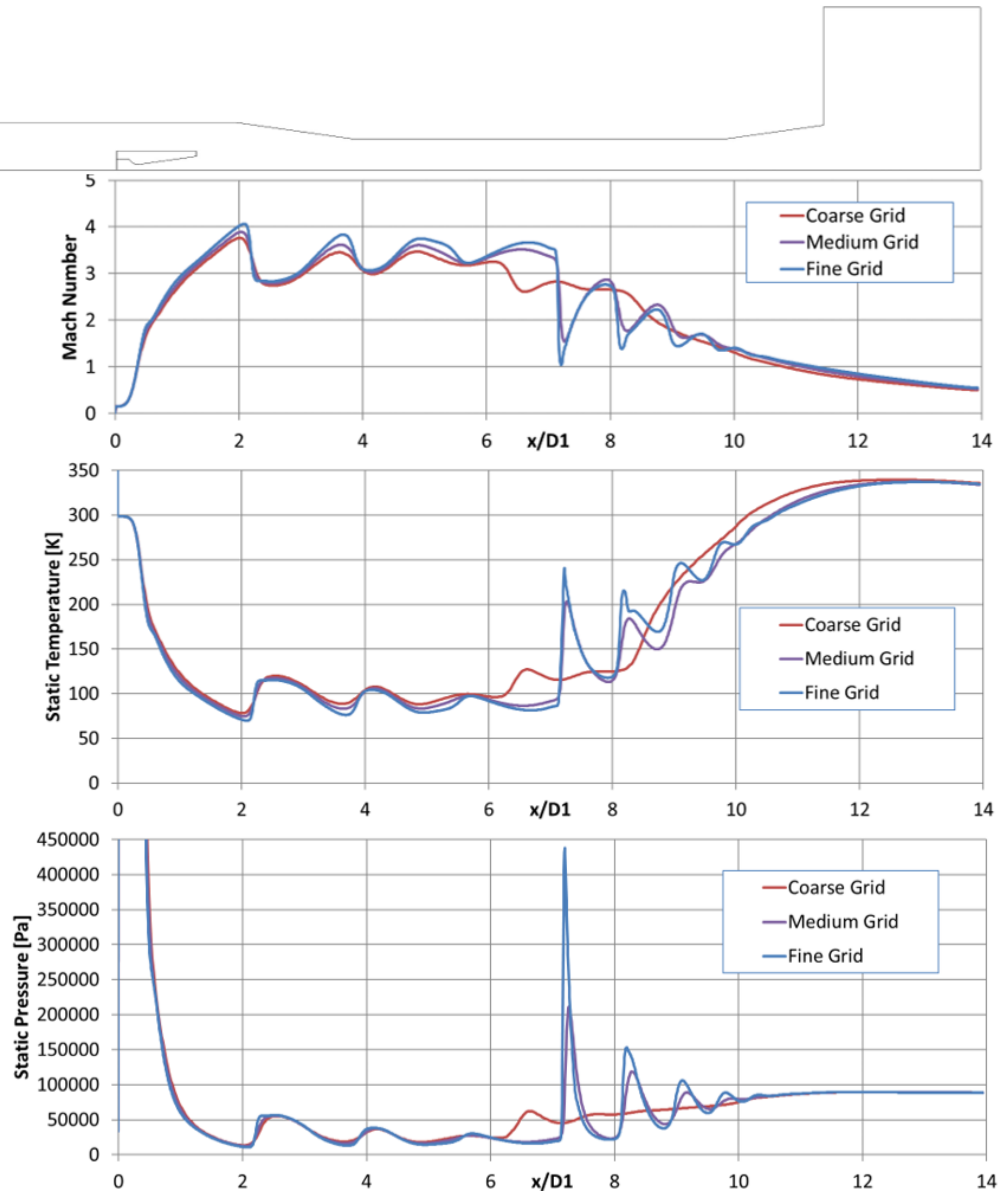

Figure 2-8. Mach Number, Static Pressure and Static Temperature Variation Along the Axis.

To observe the differences between inviscid model, realizable $k-\varepsilon$ model and SST $k-\omega$ model, numerical simulations are done by using medium grid properties and results are compared with each other. The flow solver predicts a vacuum pressure, P_v, value of 32560 Pa for SST $k-\omega$ model, 33525 Pa for realizable $k-\varepsilon$ model. Although vacuum pressure values are close to each other, normal shock location is different in two models. In inviscid model, there is a convergence problem. Vacuum pressure is oscillating between 60000 Pa and 90000 Pa, because turbulence mixing of two streams, shock wave formations and supersonic flow phenomena in diffuser may not be solved correctly due to the lack of turbulence model. As a result, the ejector diffuser cannot be started in inviscid model. Mach number, static pressure and static temperature distribution along the axis are plotted in Figure 2-9. It is seen that inviscid model is not suitable for ejector analysis.

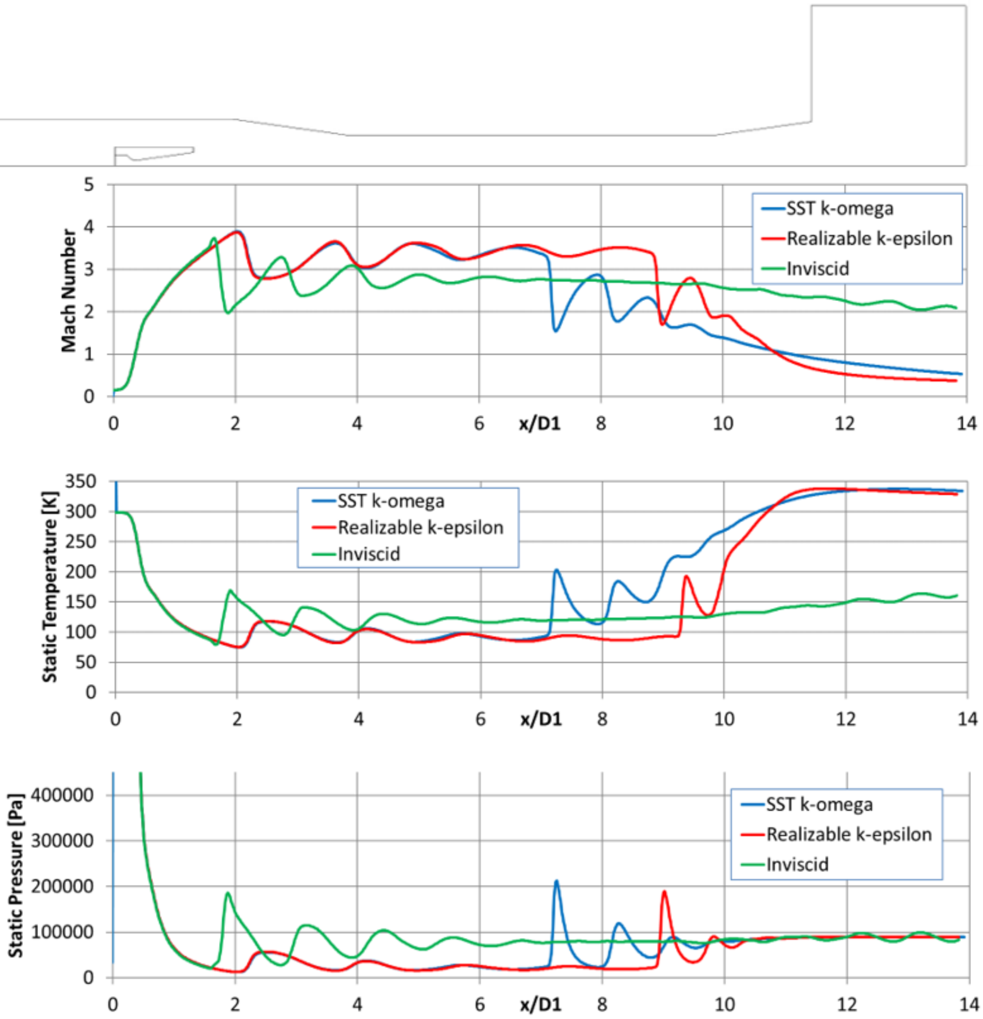

Figure 2-9. Comparison of inviscid model, realizable $k-\varepsilon$ model and SST $k-\omega$ model.

A separate grid sensitivity study is not performed for the Test section, yet the grid spacing used in the medium grid of Ejector System is used for the Test Section simulations.

2.6. Optimization Models

Optimization is the process of making something better. It involves trying variations on an initial concept and using the information gained to improve the idea. Coupling the optimization algorithms and CFD codes conveys numerous advantage to the design procedure. In this study, the aim of using an optimization algorithm is observing the effect of each parameters on the vacuum pressure, P_v. A multiobjective genetic algorithm-2 (MOGA-2) is used as an optimization procedure to explore the design space [37]. MOGA-2 is able to hold some best solutions without bringing the premature convergence into local optimal points. That means, by using this optimization algorithm whole design space can be explored without saturating or being stuck in some local optimums [38]. In this study, default parameters in MODE FRONTIER software are used for MOGA-2.

CHAPTER 3

DESIGN METHODOLOGY

One of the main objective of the present study is to develop a design methodology for HATS. The flowchart of the proposed design methodology is given in Figure 3-1.

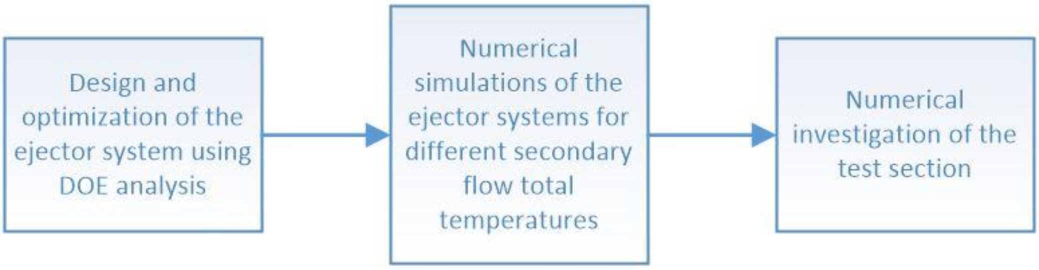

Figure 3-1. The Flowchart of the Proposed Design Methodology.

The design methodology separates the design problem into two parts. In the first step, the design and optimization of the Ejector System is accomplished by carrying out a Design of Experiment (DOE) Analysis while the Ejector nozzle total pressure, Ejector Nozzle Total Temperature, Entrainment Ratio (ER), Ambient Pressure and Free-Jet Nozzle Total Temperature kept constant. The objective in the DOE analysis is to find the optimum ejector geometry which minimizes the test section diffuser exit pressure. Once the ejector geometry ensuring the minimum diffuser exit pressure is found, the diffuser exit pressure value for that specific geometry is known by the numerical results. This pressure value is applied as a pressure outlet boundary condition to the Test Section numerical simulations.

In the second step, the numerical simulations for the Ejector System are repeated for the different secondary flow total temperatures using the geometry obtained from the DOE analysis, since the effect of total temperature of the secondary flow on the DOE analysis can be neglected. At this stage of the design procedure the pressure values at the mass inlet of the Ejector system, which is assumed as the outlet pressure of the constant area diffuser has been found.

As a third step, the numerical investigation of the Test Section is accomplished by applying the diffuser exit pressure, which is found in the first and second step, as a boundary condition to the numerical simulations. At this stage of the design procedure, first the L/D ratio of the constant area diffuser is set to 10, which is high enough to isolate the mixing effect in diffuser [25], and the numerical simulations are performed. The vacuum pressures calculated in Step 2 for different secondary flow total temperatures are used as a 'outlet pressure' boundary condition at the exit of the constant area diffuser. Optimum diameter for test section diffuser starting condition is found for different free-jet nozzle geometries operating at different secondary flow total temperatures. For the same ejector system geometry, by choosing the optimum diameter for the constant area diffuser, it is guaranteed that the HATS can start regardless of the free-jet nozzle used in the test. The main aim of these analyses is to find a minimum constant area diffuser length which does not promote unstart of the test facility. The design problem in this stage lacks the effect of the test article blockage.

In order to validate the design procedure, a combined numerical analysis of the HATS is performed in three different operating conditions, then ejector system and test section numerical analysis' results are compared with HATS combined numerical analysis' results.

3.1. Design and Optimization of the Ejector System

The design and optimization of the Ejector System is accomplished using Design of Experiment (DOE) Analysis while the Ejector Nozzle Total Pressure, Ejector Nozzle Total Temperature, Entrainment Ratio, Ambient Pressure and Free-Jet Nozzle Total Temperature kept constant. The objective in the DOE analysis is to find the ejector system geometry, which minimizes the diffuser exit pressure. The main geometrical parameters of interest in the DOE analysis are shown in Figure 3-2.

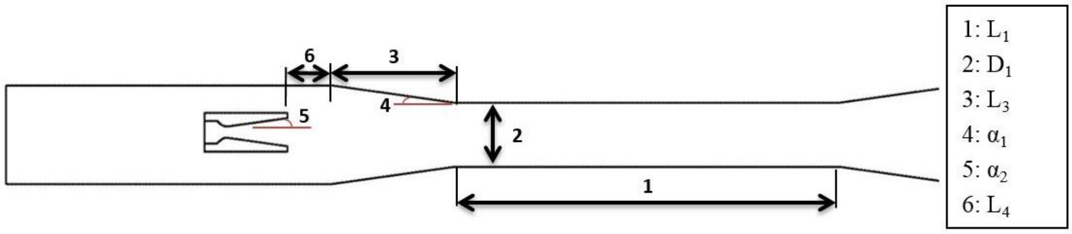

Figure 3-2. Geometrical Parameters for the DOE Analysis.

The solution domain for the numerical simulations along with the boundary conditions are given in Figure 2-2 and boundary conditions given in Table 3-1.

Table 3-1. Ejector System Boundary Conditions.

Parameter	Value
Pressure inlet total pressure, P_{t1}, bar	20
Pressure inlet total temperature, T_{t1}, K	300
Entrainment ratio, ER, $\dot{m}_s / \dot{m}_p$	0.33
Pressure outlet pressure, P_{amb}, Pa	89000
Mass flow inlet total temperature, T_{t2}, K	400

For each 6 geometric parameter shown in Figure 3-2 upper and lower limits for DOE analysis are given in Table 3-2.

Table 3-2. Lower and Upper Limit of Geometric Parameters.

Parameter	Lower limit	Upper limit
L_1	$4*D_1$	$14*D_1$
D_1	-	-
L_3	D_1	$3*D_1$
α_1	6	20
α_2	6	20
L_4	$0.3*D_1$	$1.5*D_1$

Then, parametric sensitivity analysis has been done by using 'Design by Analysis' technique. Series of CFD analysis has been conducted by using MODE FRONTIER software. Main objective of the analysis is to minimize the mass flow inlet static pressure, P_v by exploring the effect of each parameters. Because of MOGA-2 (multi objective genetic algorithm) is commonly used for minimizing or maximizing a variable problem by investigating the design space [38], it is chosen as an optimization method in MODE FRONTIER. For each analysis in MODE FRONTIER,

- Parameters are updated by optimization algorithm,
- Geometry is created in CAD software,
- Geometry is exported from CAD software,
- Mesh is generated in grid generation program by using an automated meshing script,
- Boundary conditions given in Table 3-1 are defined and CFD analysis is done in FLUENT 19.2 by using journal script.
- Mass flow inlet static pressure, P_v is saved. Analysis loop is given in Figure 3-3.

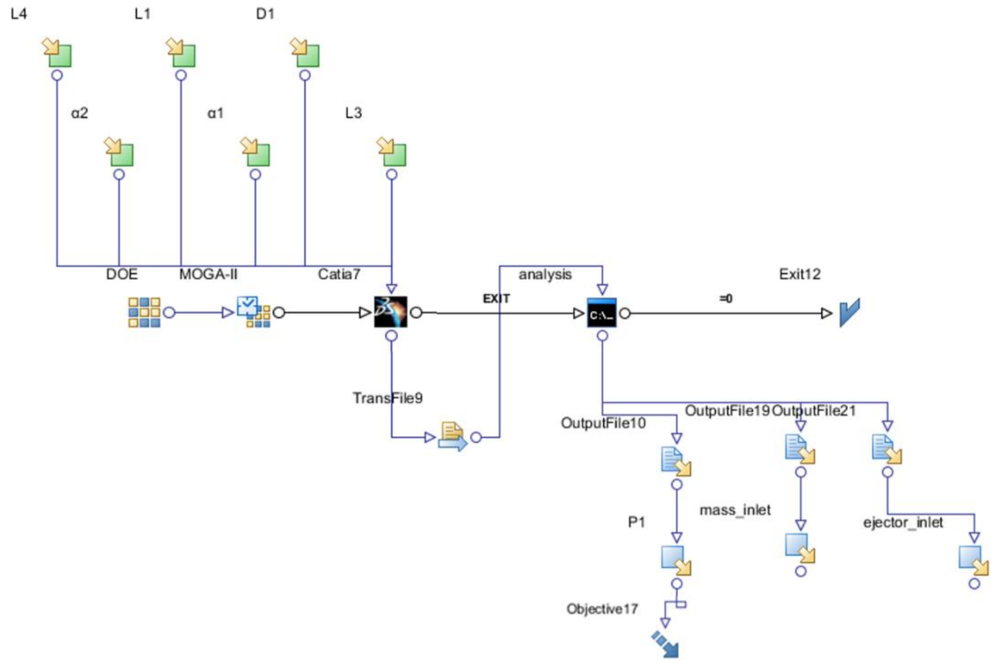

Figure 3-3. Analysis Loop Used in MODE FRONTIER.

Nearly 1000 analysis are done by using MODE FRONTIER and results are shown in Figure 3-4.

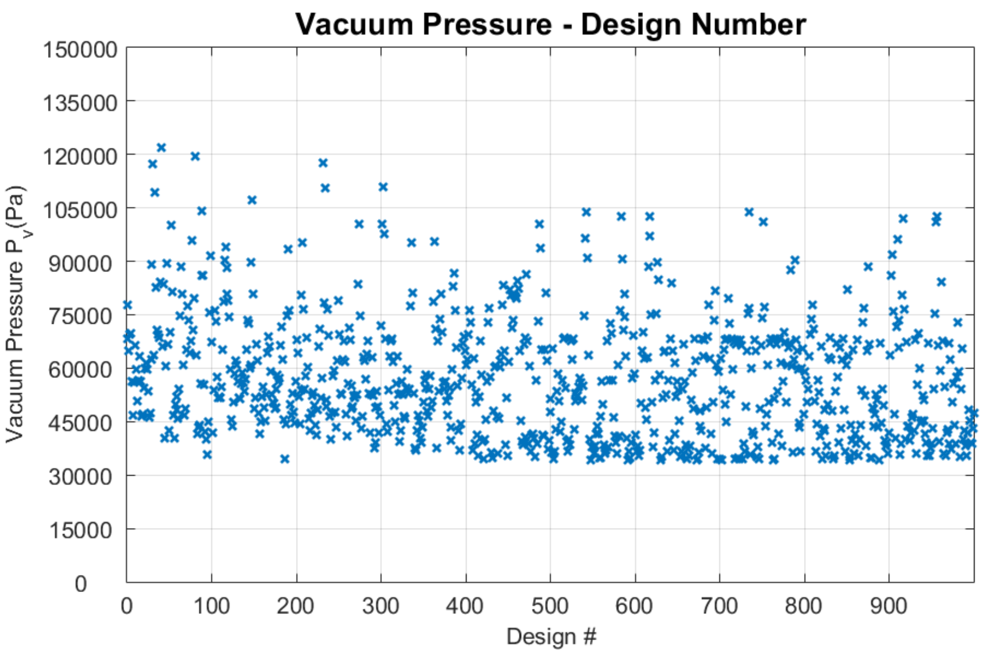

Figure 3-4. Results of 'Design by Analysis' done in MODE FRONTIER.

Results are investigated by using JMP 7 software and outputs are shown in Figure 3-5.

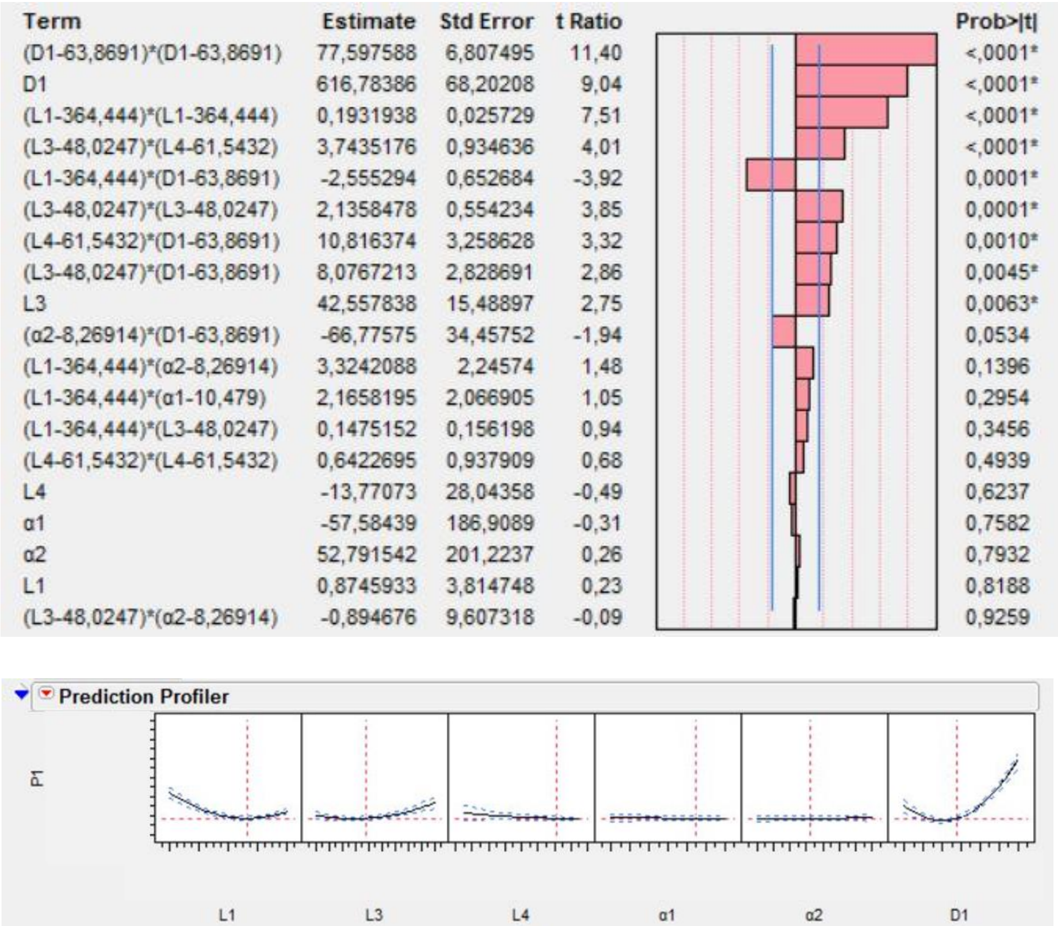

Term	Estimate	Std Error	t Ratio	Prob>|t|
(D1-63,8691)*(D1-63,8691)	77,597588	6,807495	11,40	<,0001*
D1	616,78386	68,20208	9,04	<,0001*
(L1-364,444)*(L1-364,444)	0,1931938	0,025729	7,51	<,0001*
(L3-48,0247)*(L4-61,5432)	3,7435176	0,934636	4,01	<,0001*
(L1-364,444)*(D1-63,8691)	-2,555294	0,652684	-3,92	0,0001*
(L3-48,0247)*(L3-48,0247)	2,1358478	0,554234	3,85	0,0001*
(L4-61,5432)*(D1-63,8691)	10,816374	3,258628	3,32	0,0010*
(L3-48,0247)*(D1-63,8691)	8,0767213	2,828691	2,86	0,0045*
L3	42,557838	15,48897	2,75	0,0063*
(α2-8,26914)*(D1-63,8691)	-66,77575	34,45752	-1,94	0,0534
(L1-364,444)*(α2-8,26914)	3,3242088	2,24574	1,48	0,1396
(L1-364,444)*(α1-10,479)	2,1658195	2,066905	1,05	0,2954
(L1-364,444)*(L3-48,0247)	0,1475152	0,156198	0,94	0,3456
(L4-61,5432)*(L4-61,5432)	0,6422695	0,937909	0,68	0,4939
L4	-13,77073	28,04358	-0,49	0,6237
α1	-57,58439	186,9089	-0,31	0,7582
α2	52,791542	201,2237	0,26	0,7932
L1	0,8745933	3,814748	0,23	0,8188
(L3-48,0247)*(α2-8,26914)	-0,894676	9,607318	-0,09	0,9259

Figure 3-5. Outputs of JMP 7 custom DOE.

By analyzing the numerical results, most dominant parameters are determined as D_1 and L_1. It can be seen that in Figure 3-4, there are many designs with close P_v values. Among them, the final ejector system geometry is determined by using optimum D_1 value and minimum L_1/D_1 to get shorter and efficient system. The final geometry is given in Figure 3-6. This geometry is the baseline design.

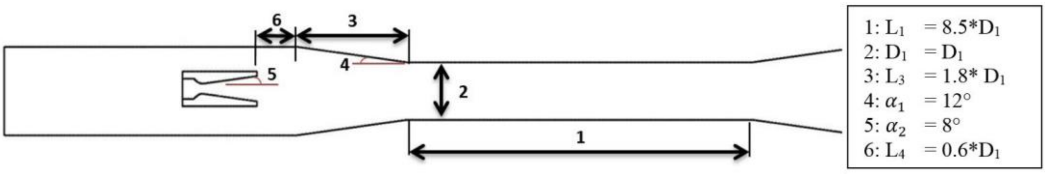

Figure 3-6. Designed Dimensionless Ejector Geometry by DOE.

The Static Pressure, Mach Number and Static Temperature contour plot for chosen ejector system geometry is given in Figure 3-7. The minimum mass flow inlet static pressure P_v, is predicted by flow solver as a 32200Pa.

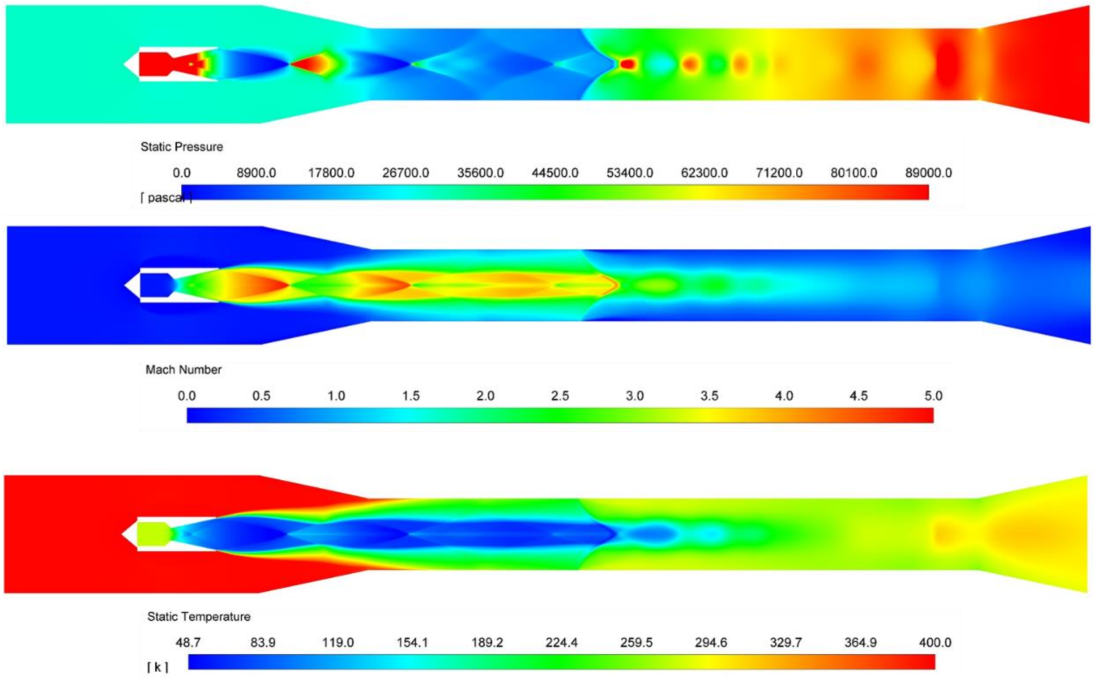

Figure 3-7. Static Pressure, Mach Number and Static Temperature Contour Plot for Designed Ejector System.

3.2. Numerical Investigation of the Ejector System for Different Secondary Flow Total Temperatures

Due to the flight Mach number and altitude temperature, free-jet nozzle total temperature changes. The numerical simulations for the Ejector System are repeated for the different secondary flow total temperatures (T_{t2}) using the geometry obtained from the DOE analysis. Results are given in Figure 3-8 and Figure 3-9. It is clearly seen that when the free-jet nozzle total temperature increases, vacuum pressure P_v, also increases and this rise show a trend similar to linear. For different free-jet nozzles, different vacuum pressure values should be used in test section investigations.

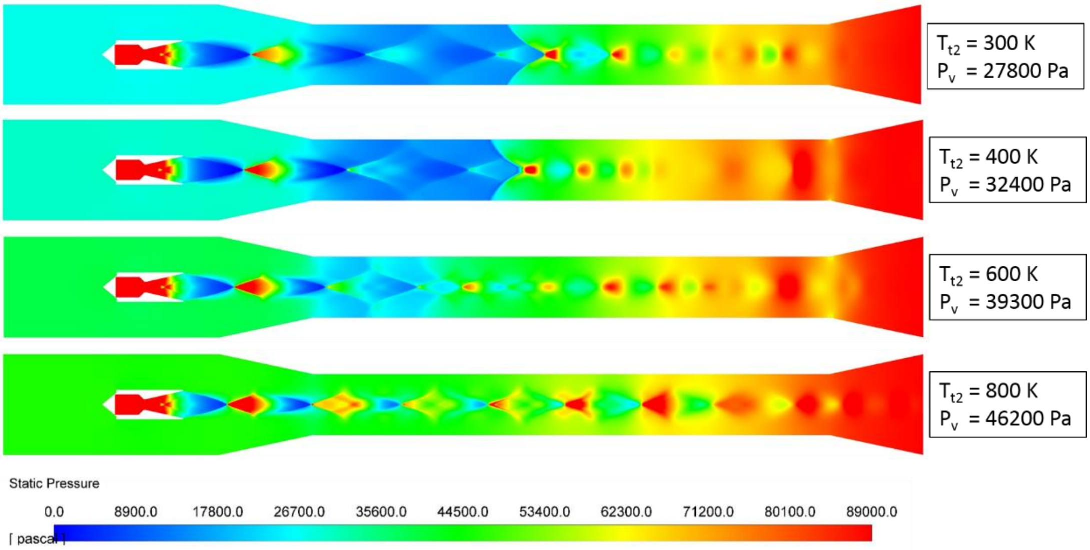

Figure 3-8. Pressure Contour Plot of Ejector System for Different T_{t2}.

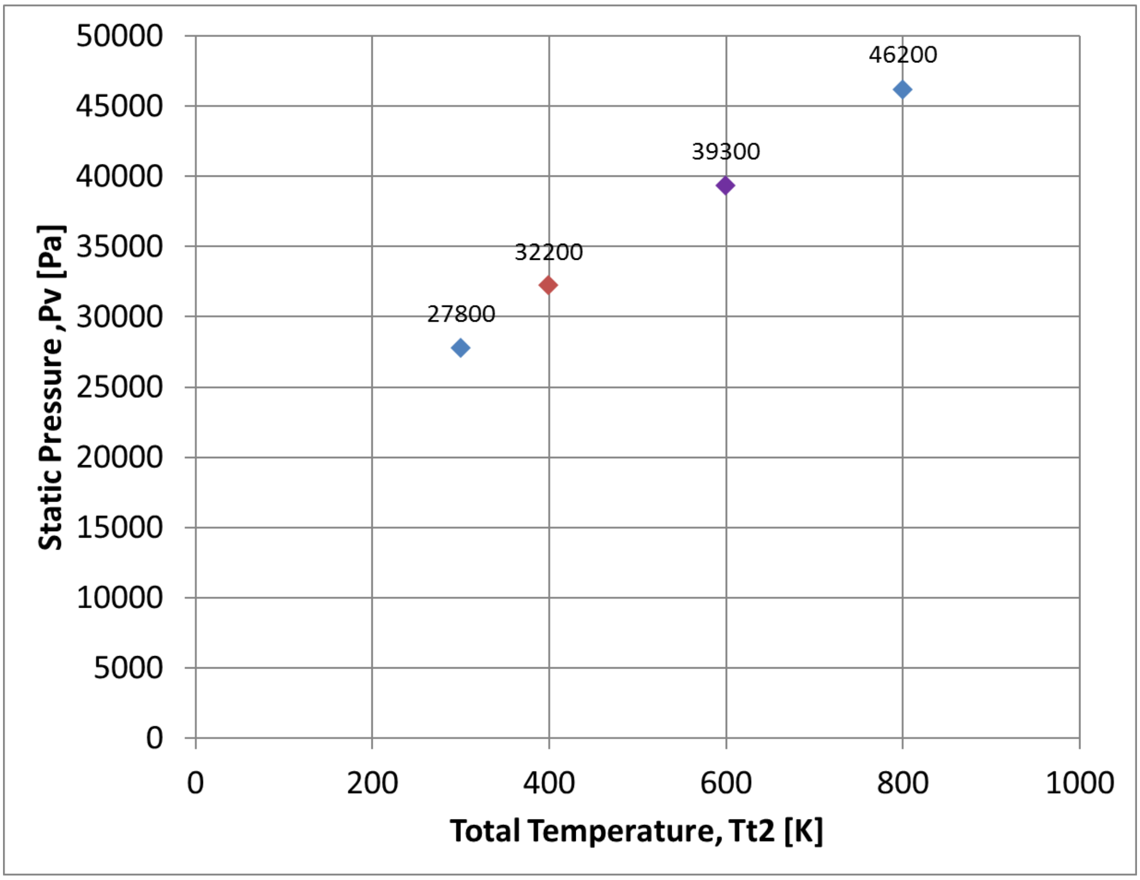

Figure 3-9. Vacuum Pressure ,P_v, for different T_{t2}.

3.3. Numerical Investigations of the Test Section

The numerical investigations of the test section are accomplished by applying the P_v calculated in Section 3.1 as a pressure outlet boundary condition of the test section diffuser exit. At this stage of the design procedure, numerical simulations are performed for constant L/D ratio of the constant area diffuser taken from literature as 10 [25]. Since the L/D ratio is set to a high enough value to isolate the effect of the constant area diffuser length, optimum diameter D_2, for facility start has been found for 2, 2.5 and 3 Mach free-jet nozzle geometries operating at different secondary flow total temperatures as shown in Figure 3-9. Boundary conditions for test section analyses are given in Table 3-3. Nozzle exit pressures (P_{ex}) are calculated by using following equation.

$$P_{ex} = P_{t2} \, (1 + \frac{\gamma - 1}{2} \, M^2)^{\frac{\gamma}{1-\gamma}} \tag{3-1}$$

Table 3-3. Test Section Boundary Conditions and Nozzle Properties.

	Free-jet Nozzle		
Parameter	**2 Mach**	**2.5 Mach**	**3 Mach**
Pressure inlet total pressure, P_{t2}, bar	0.92	1.59	2.58
Pressure inlet total temperature, T_{t2}, K	400	600	700
Pressure outlet pressure, P_v, Pa	32200	39300	42750
Pressure outlet total temperature, T_{t2}, K	400	600	700
Nozzle exit diameter, D_{ex2}	0.79*D_2	0.85*D_2	0.92*D_2
Nozzle exit pressure, P_{ex2}, Pa	11758	9305	7023

Diffuser diameter D_2 has a great importance for free-jet nozzle starting process. It should be higher than the nozzle exit diameter and it should be as small as possible for free-jet nozzle start. After numerous CFD simulations, D_2 is determined as 0.8*D_1. Pressure contour plot and temperature contour plot of test sections with 2, 2.5 and 3 Mach nozzle are given in Figure 3-10 and Figure 3-11. Although the diffuser exit pressure condition is changed for each free-jet nozzle, both three nozzles are started at given test section geometry.

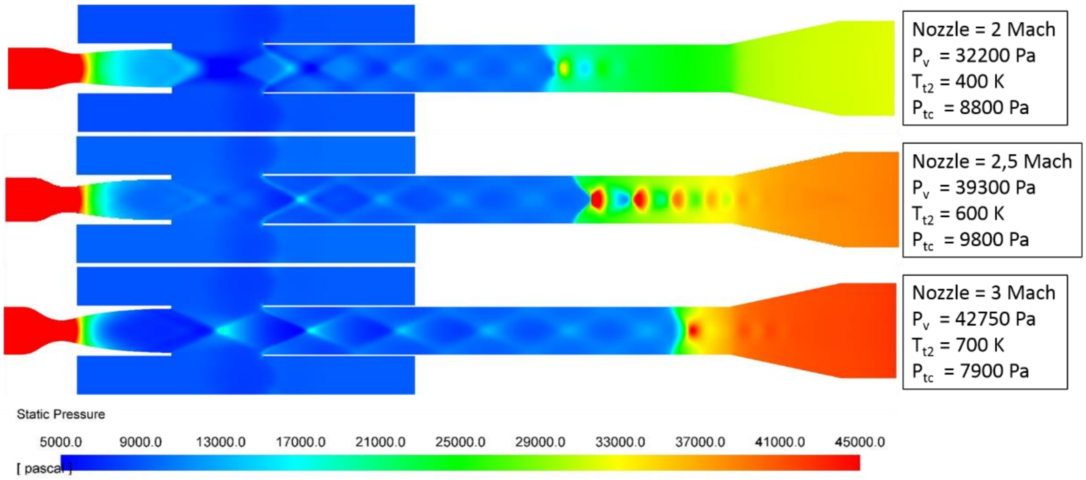

Figure 3-10. Pressure Contour Plot of Three Different Test Section.

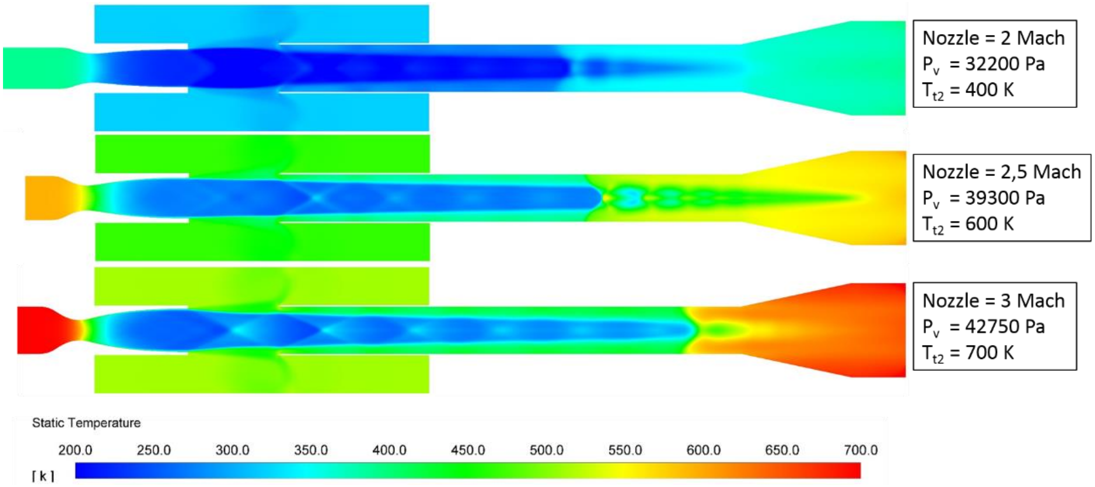

Figure 3-11. Temperature Contour Plot of Three Different Test Section.

Mach number contour plot and Mach number distribution along the axis of test section with 2 Mach, 2.5 Mach and 3 Mach free-jet nozzle are respectively given in Figure 3-12, Figure 3-13 and Figure 3-14. In Figure 3-12, due to the nozzle exit pressure is much higher than the test chamber pressure (11758 Pa > 8800 Pa), free-jet nozzle becomes under-expanded and 3 Mach region is formed in test chamber. If the test chamber pressure is increased by using bleed air, 2 Mach free-jet nozzle can be worked as an ideally-expanded and the mach distributions change.

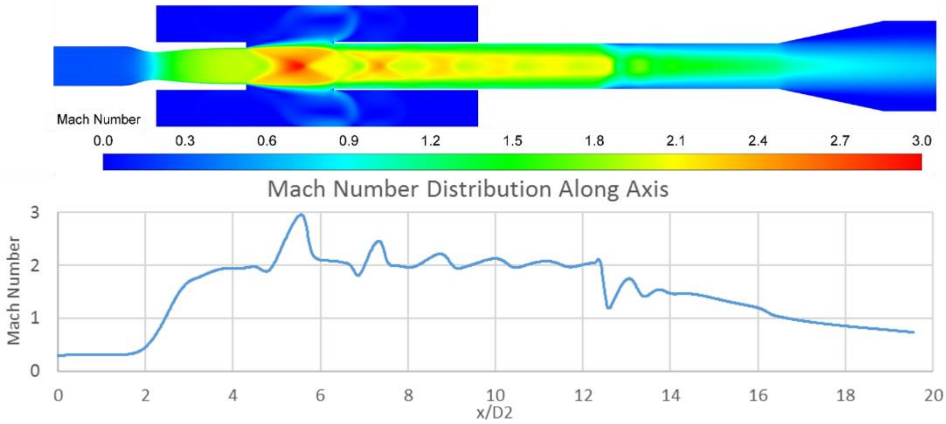

Figure 3-12. Mach Number Contour Plot of Test Section for M = 2 Free-jet Nozzle.

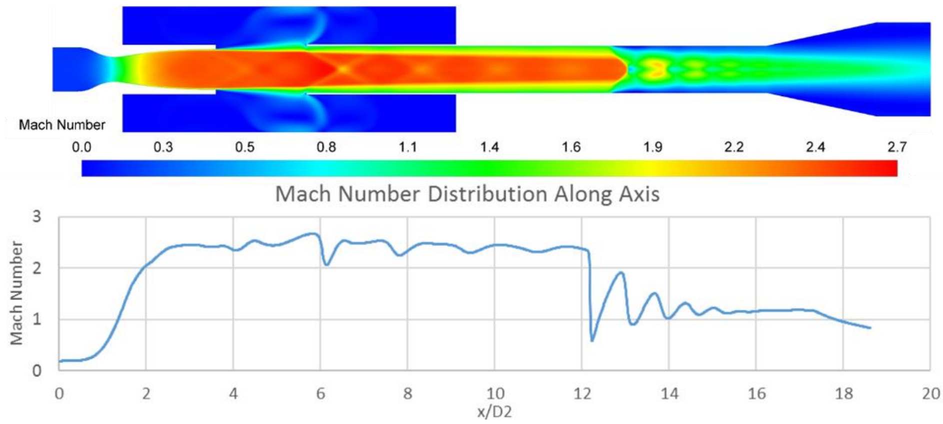

Figure 3-13. Mach Number Contour Plot of Test Section for M = 2.5 Free-jet Nozzle.

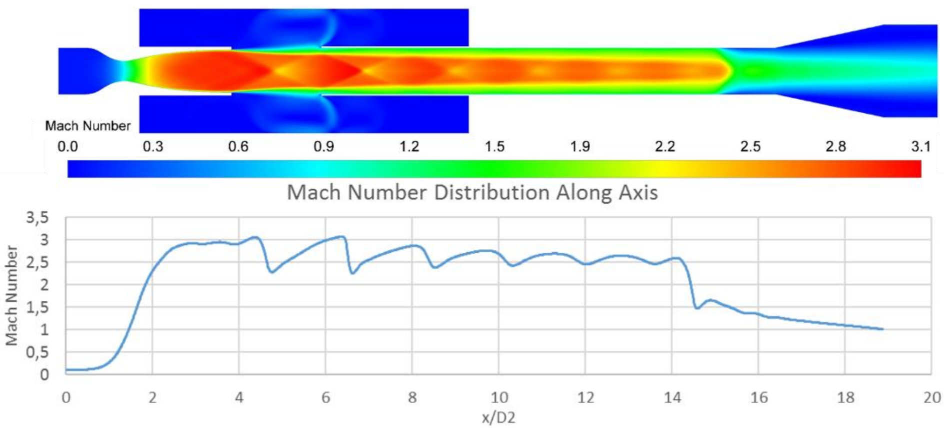

Figure 3-14. Mach Number Contour Plot of Test Section for M = 3 Free-jet Nozzle.

3.4. Combined Numerical Analyses of the High Altitude Test System

A combined numerical analysis of the HATS are performed in three different operating conditions respectively 2 Mach, 2.5 Mach and 3 Mach Free-jet Nozzles given in 3.3. Then, ejector system and test section numerical analysis' results are compared with HATS combined numerical analysis' results. Boundary conditions for combined numerical analysis are given in Figure 3-15 and Table 3-4.

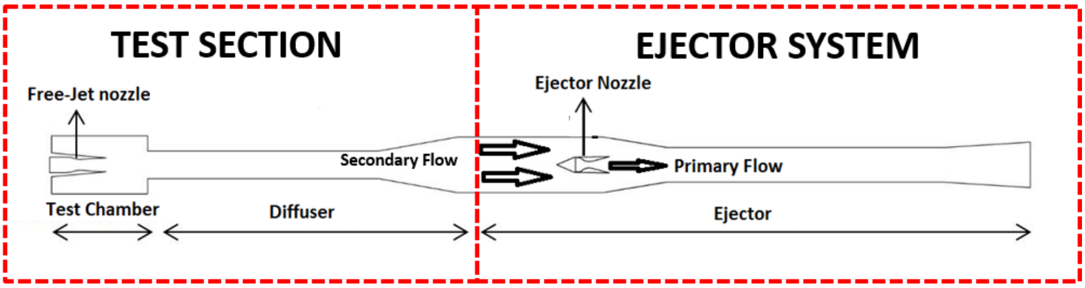

Figure 3-15. Combined Analysis Model Schematic.

Table 3-4. Combined System Boundary Conditions.

Parameter	**Value**
Pressure inlet total pressure, P_{t1}, bar	20
Pressure inlet total temperature, T_{t1}, K	300
Entrainment ratio, ER, $\dot{m}_s / \dot{m}_p$	0.33
Pressure outlet pressure, P_{amb}, Pa	88400
Pressure outlet temperature, T_{amb}, K	300
Free-jet nozzle total pressure, P_{t2}, bar	2Mach → 0.92 2.5Mach → 1.59 3 Mach → 2.58
Free-jet nozzle total temperature, T_{t2}, K	2Mach → 400 2.5Mach → 600 3 Mach → 700

3.4.1. Combined Numerical Analysis of HATS with 2 Mach Free-Jet Nozzle

Test Section Diffuser Exit Pressure P_v, was calculated in 3.1 and given in Figure 3-9 as 32200 Pa. It shows a great fit (1.09% difference) with the combined analysis results, which is 32050 Pa. The pressure, mach number and temperature contour plots of Combined HATS Analysis are given in Figure 3-16, Figure 3-17 and Figure 3-18 respectively.

Test Chamber Pressure P_{tc}, was calculated in 3.3 and given in Figure 3-10 as 8800 Pa. It shows a good fit (4.7% difference) with the combined analysis results, which is 8400 Pa.

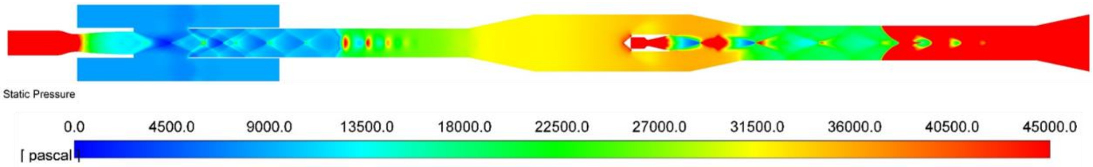

Figure 3-16. Pressure Contour Plot of Combined HATS Analysis with 2 Mach Free-Jet Nozzle.

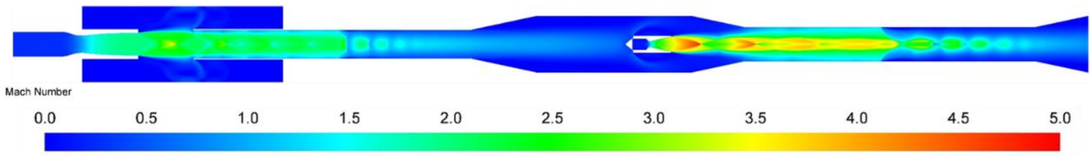

Figure 3-17. Mach Number Contour Plot of Combined HATS Analysis with 2 Mach Free-Jet Nozzle.

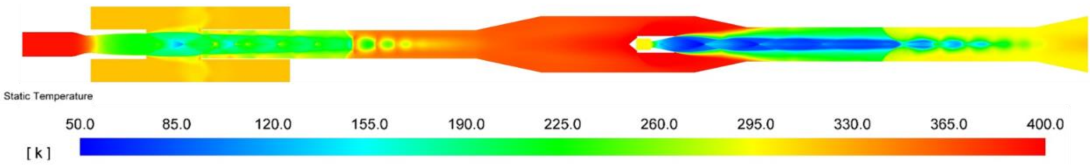

Figure 3-18. Temperature Contour Plot of Combined HATS Analysis with 2 Mach Free-Jet Nozzle.

Table 3-5. Numerical Analysis' Results Comparison for 2 Mach Free-jet Nozzle.

Parameter	Ejector Analysis	Combined Analysis	Difference %
P_v, Pa	32400	32050	-1.09
P_{tc}, Pa	8800	8400	-4.7

3.4.2. Combined Numerical Analysis of HATS with 2.5 Mach Free-Jet Nozzle

Test Section Diffuser Exit Pressure P_v, was calculated in 3.1 and given in Figure 3-9 as 39300 Pa. It shows a great fit (1.4% difference) with the combined analysis results, which is 38750 Pa. The pressure, mach number and temperature contour plots of Combined HATS Analysis are given in Figure 3-19, Figure 3-20 and Figure 3-21 respectively.

Test Chamber Pressure P_{tc}, was calculated in 3.3 and given in Figure 3-10 as 9800 Pa. It shows a good fit (3.4% difference) with the combined analysis results, which is 9480 Pa.

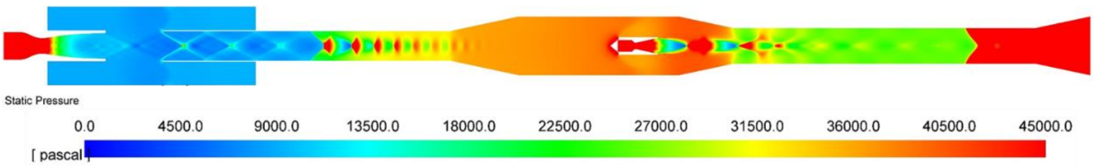

Figure 3-19. Pressure Contour Plot of Combined HATS Analysis with 2.5 Mach Free-Jet Nozzle.

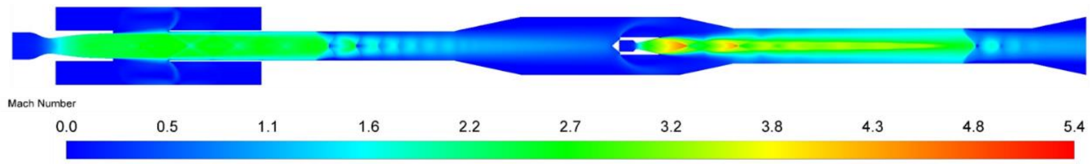

Figure 3-20. Mach Number Contour Plot of Combined HATS Analysis with 2.5 Mach Free-Jet Nozzle.

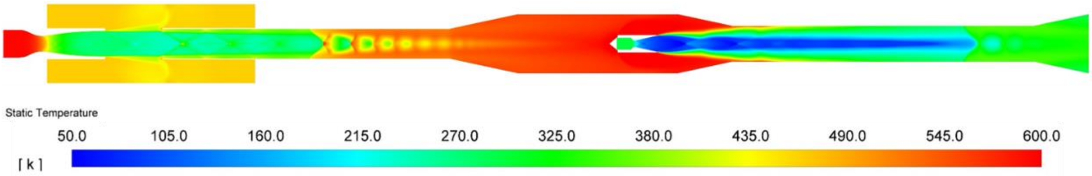

Figure 3-21. Temperature Contour Plot of Combined HATS Analysis with 2.5 Mach Free-Jet Nozzle.

Table 3-6. Numerical Analysis' Results Comparison for 2.5 Mach Free-jet Nozzle.

Parameter	Ejector Analysis	Combined Analysis	Difference %
P_v, Pa	39300	38750	-1.4
P_{tc}, Pa	9800	9480	-3.4

3.4.3. Combined Numerical Analysis of HATS with 3 Mach Free-Jet Nozzle

Test Section Diffuser Exit Pressure P_v, was interpolated by using the data given in Figure 3-9 as 42750 Pa. It shows a great fit (1.2% difference) with the combined analysis results, which is 43300 Pa. The pressure, mach number and temperature contour plots of Combined HATS Analysis are given in Figure 3-22, Figure 3-23 and Figure 3-24 respectively.

Test Chamber Pressure P_{tc}, was calculated in 3.3 and given in Figure 3-10 as 7900 Pa. It shows a good fit (4% difference) with the combined analysis results, which is 7600 Pa.

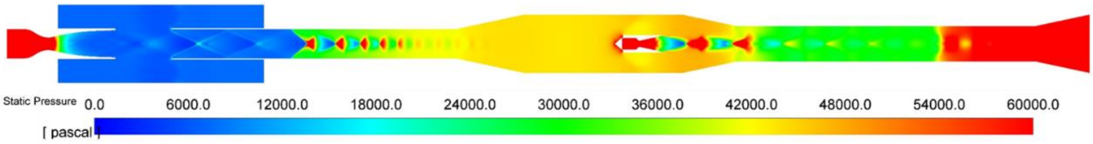

Figure 3-22. Pressure Contour Plot of Combined HATS Analysis with 3 Mach Free-Jet Nozzle.

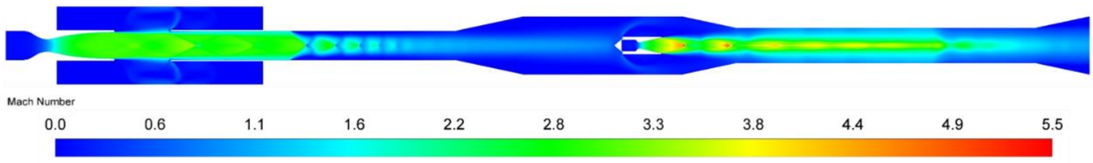

Figure 3-23. Mach Number Contour Plot of Combined HATS Analysis with 3 Mach Free-Jet Nozzle.

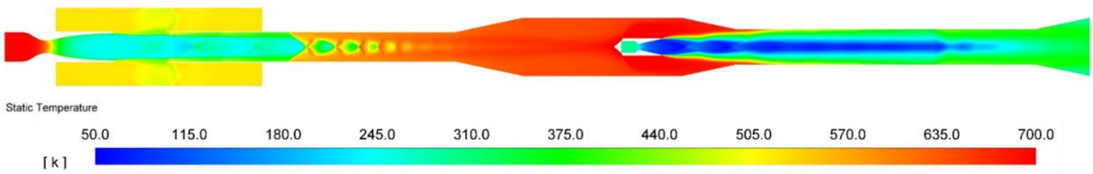

Figure 3-24. Temperature Contour Plot of Combined HATS Analysis with 3 Mach Free-Jet Nozzle.

Table 3-7. Numerical Analysis' Results Comparison for 3 Mach Free-jet Nozzle.

Parameter	Ejector Analysis	Combined Analysis	Difference %
P_v, Pa	42750	43300	+1.2
P_{tc}, Pa	7900	7600	-4

CHAPTER 4

EXPERIMENTAL STUDY

4.1. Introduction

Computational methods are commonly used in aerodynamic design, however, there remain many instances where ground testing is necessary to validate the methodology, to refine the design or to provide further insight into the flow physics [39]. Experiments of high altitude test system has a huge importance in altitude simulation testing, because; 1-D, 2-D analysis and numerical investigations done by flow solvers are not fully capable to solve complex flow processes taking place within the system such as supersonic conditions, shock wave formation, turbulent mixing and multiple shock systems.

By using the numerical solutions given in Chapter 3, an experimental setup is designed and manufactured. The baseline design is the optimum design given in Figure 3-6.

After the manufacturing process, experimental setup is established in TÜBİTAK-SAGE High Altitude Test Facility. This All mechanical components used in the experimental setup are selected from catalogues to make the experimental setup cost-effective. In addition, all mechanical components are chosen as AISI 304 Stainless Steel.

In this chapter, experimental setup design and manufacturing process are presented.

4.2. Experimental Setup Design and Manufacturing

Maximum experimental setup length is determined as a 6 meter by the infrastructure limits of TUBİTAK-SAGE High Altitude Test Facility. To satisfy this length limit, the maximum mass flow rate of ejector nozzle $\dot{m}_p$, is set to 3kg/s and then the whole system is sized. Designed experimental setup is given in Figure 4-1. Maximum length of the system is 5015 mm and the height is 350 mm which is shown in Figure 4-2. The manufactured experimental setup pictures are given in Figure 4-3 and Figure 4-4. Main parts of the experimental setup is shown in Figure 4-5 and the list of the main parts is given in Table 4-1. Parts are connected with each other by using flanges.

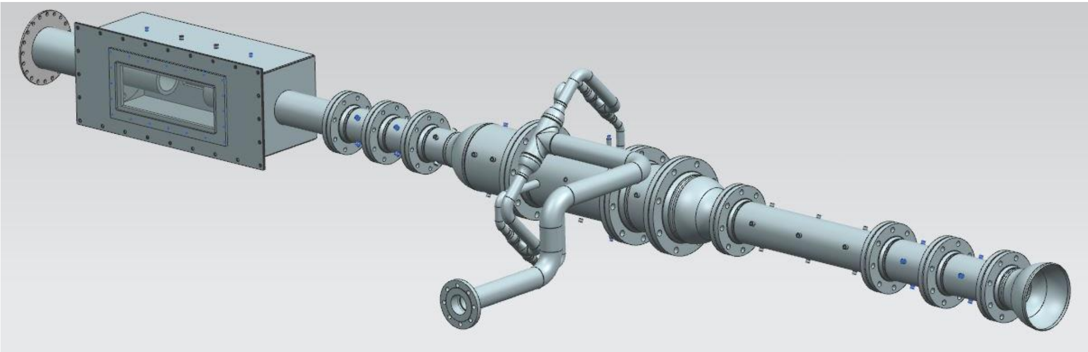

Figure 4-1. Experimental Setup CAD Model.

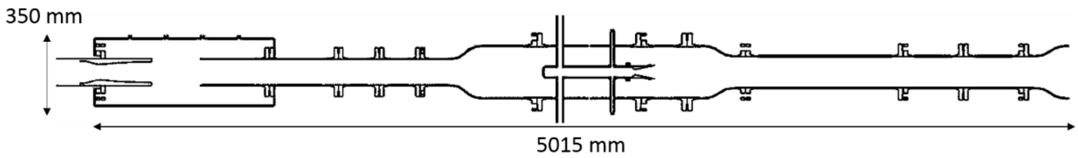

Figure 4-2. Basic Dimensions of the Experimental Setup.

Figure 4-3. Manufactured Experimental Setup-1.

Figure 4-4. Manufactured Experimental Setup-2.

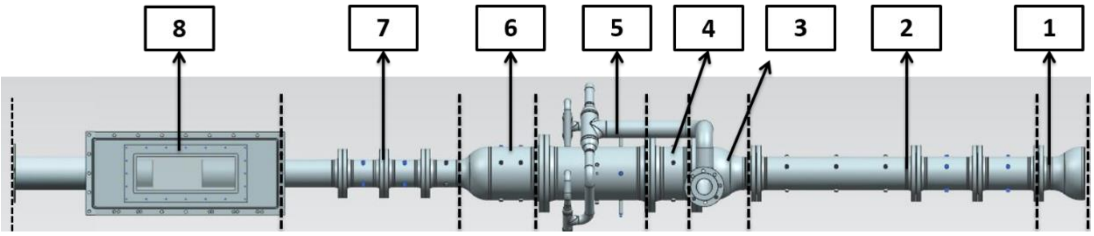

Figure 4-5. Main Parts of the Experimental Setup.

Table 4-1. List of Main Parts of Experimental Setup.

Number	Part Name
1	Subsonic Diffuser
2	Ejector Diffuser
3	Transition Cone
4	Nozzle Exit Plane (NXP) Extension
5	Ejector Nozzle Feed Manifold
6	Diffuser-Ejector Nozzle Feed Manifold Connection
7	Test Section Diffuser
8	Test Chamber

4.2.1. Subsonic Diffuser

Subsonic diffuser shown in Figure 4-6 is used for slowing down the flow and reduce the exit velocity. There is no design criteria for this part of the system. Exit cone is formed by welding Concentric Reduction to DN150 welding neck flange.

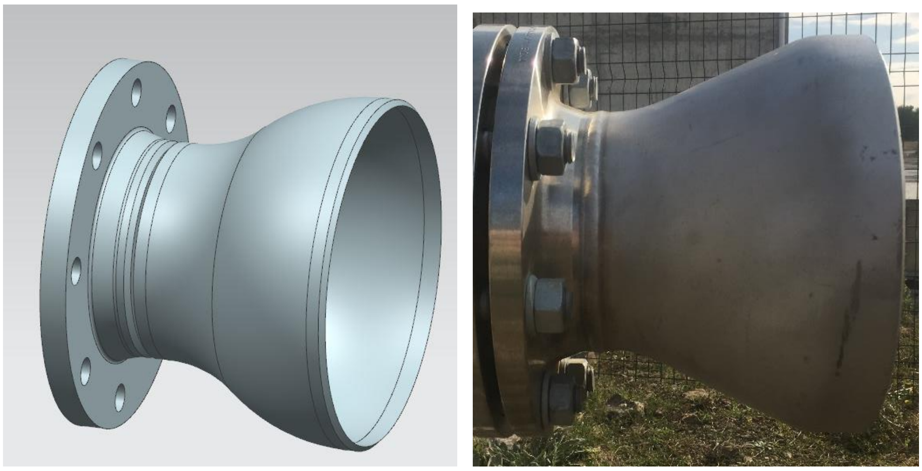

Figure 4-6. Exit Cone Part CAD Model and Exit Cone.

4.2.2. Ejector Diffuser

Ejector Diffuser is one of the most important part of the experimental setup, due to the length and the diameter of the diffuser has a great influence on the performance of ejector system. Diameter of the ejector diffuser is determined by proportioning the dimensions given in Section 3.1. Then, ejector diffuser pipe is chosen from the pipe catalogue as a DN150 with 5mm thickness. Inner diameter of the pipe, D_1=158.3 mm.

To observe the ejector diffuser L/D ratio effect on the performance of the system, ejector diffuser is manufactured as modular. It can be shortened or extended by integrating or removing the parts. Long and short ejector diffusers are given in Figure 4-7. One long and two short ejector diffusers are manufactured. Ejector diffusers are formed by welding the DN150 pipe to DN150 welding neck flanges.

As seen from the Figure 4-7 and Figure 4-8, there are couplings located on the pipes. Pipes are drilled at certain points and couplings are welded to outer surface of the pipes to mount pressure transmitter. Couplings are ¼ NPT.

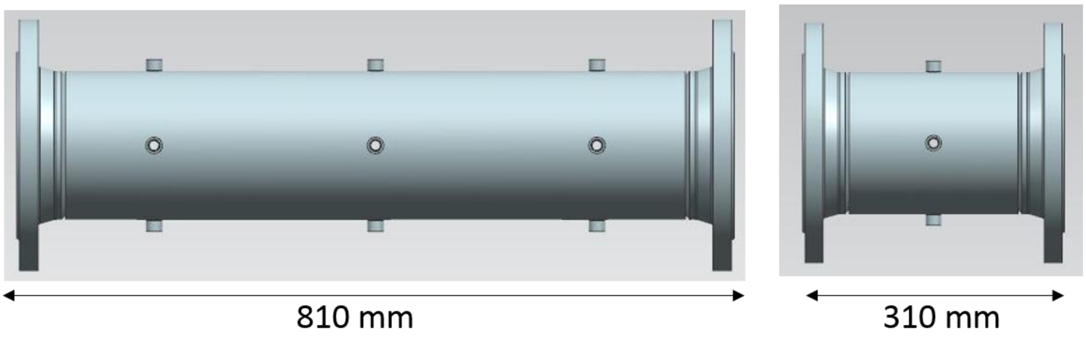

Figure 4-7. Ejector Diffuser Parts CAD model.

Figure 4-8. Ejector Diffusers.

4.2.3. Transition Cone

In Section 3.1, transition cone angle effect on the performance of the system has been investigated in detail, however; due to the high cost of the manufacturing process of the cone geometry, transition cone is replaced with concentric reduction. These cones are shown in Figure 4-9. Transition cone is formed by welding Concentric Reduction (DN150 to DN250) to DN150 and DN250 welding neck flanges.

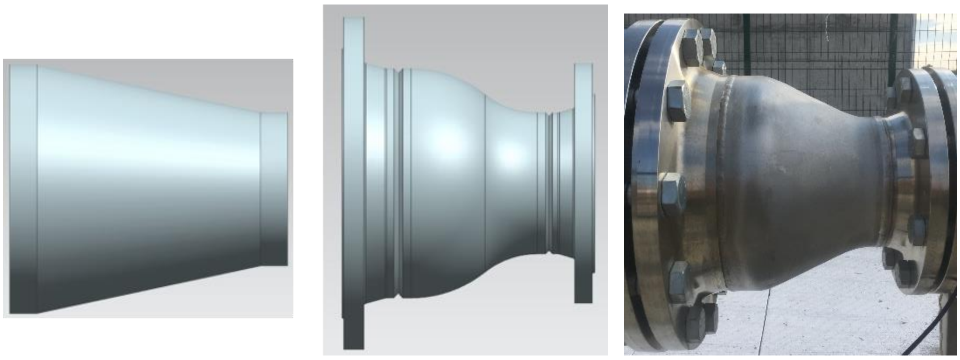

Figure 4-9. Left: Designed Cone CAD Model – Middle: Cone CAD Model – Right: Cone.

4.2.4. Nozzle Exit Plane (NXP) Extension

In Section 3.1, the effect of Nozzle Exit Plane (NXP) Location, L_4 is analyzed. For testing the effect of L_4, this part is manufactured. Experiments are carried out with and without this part given in Figure 4-10. Part is formed by welding the DN 250 pipe to DN250 welding neck flanges.

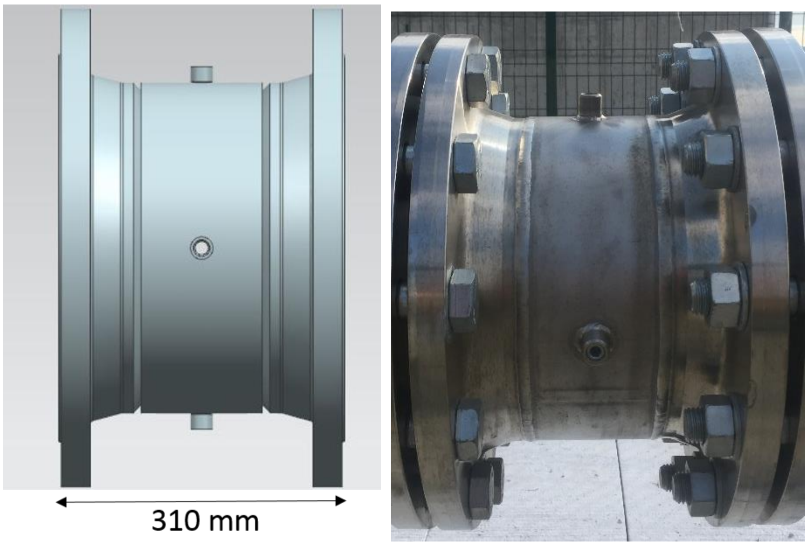

Figure 4-10. NXP Location Changer Part CAD model and Manufactured Part.

4.2.5. Diffuser Ejector Nozzle Feed Manifold Connection

In Section 3.3, diffuser exit cone angle effect on the performance of the diffuser has been investigated, however; due to the high cost of the manufacturing process of the cone geometry, cone is replaced with concentric reduction. The part is shown in Figure 4-11 and Figure 4-12. In Section 3.3, D_2 was calculated by numerical investigations as $0.8*D_1$.

So, D_2 is found as $0.8 \times 158.3 = 126.64\, mm$. From the standard pipe catalogue, DN125 pipe with 4mm thickness, ID = 131.7 mm OD = 139.7 mm is chosen.

This part consists of Concentric Reduction (DN125 to DN250), DN125 - DN250 pipes and DN125 - DN250 welding neck flanges.

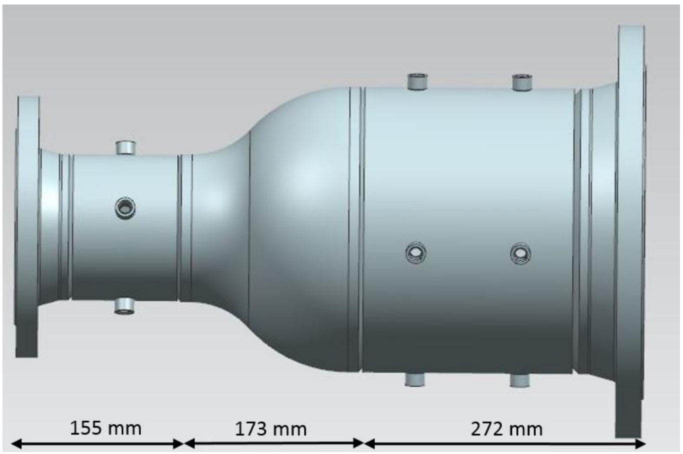

Figure 4-11. Diffuser- Ejector Nozzle Feed Manifold Connection Part CAD Model.

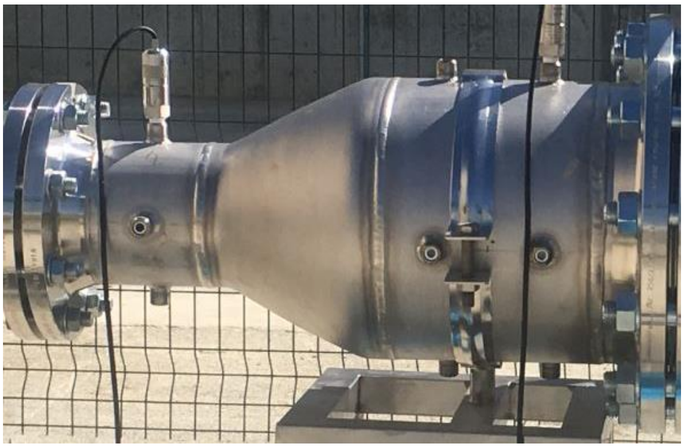

Figure 4-12. Diffuser- Ejector Nozzle Feed Manifold Connection Part.

4.2.6. Test Section Diffuser

Test section diffuser is one of the most important part of the test section part of the experimental setup, due to the great influence of the length and the diameter of the diffuser on the performance of free-jet nozzle. Diameter of the test section D_2 is determined D_2 is found as $126.64\,mm$ in Section 4.2.5. From the standard pipe catalogue, DN125 pipe with 4mm thickness, ID = 131.7 mm OD = 139.7 mm is chosen.

To observe the test section diffuser L/D ratio effect on the performance of the system, test section diffuser is manufactured as modular. It can be shortened or extended by integrating or removing the parts. Test section diffusers are given in Figure 4-13 and Figure 4-14. Test section diffusers are formed by welding the DN125 pipe to DN125 welding neck flanges.

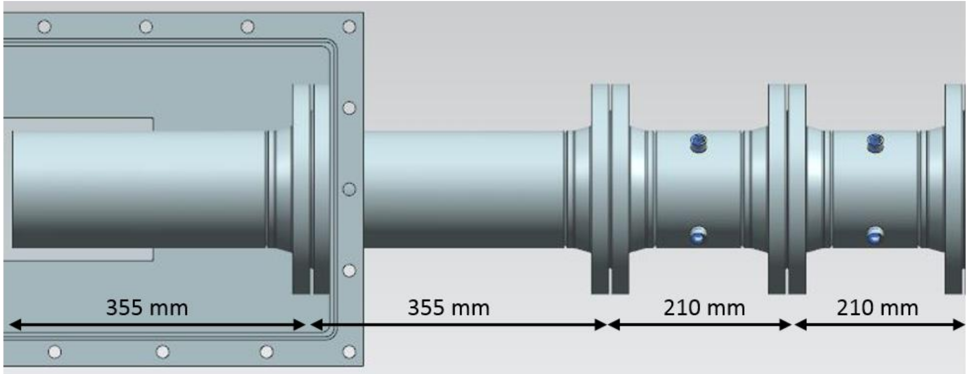

Figure 4-13. Test Section Diffusers CAD Model.

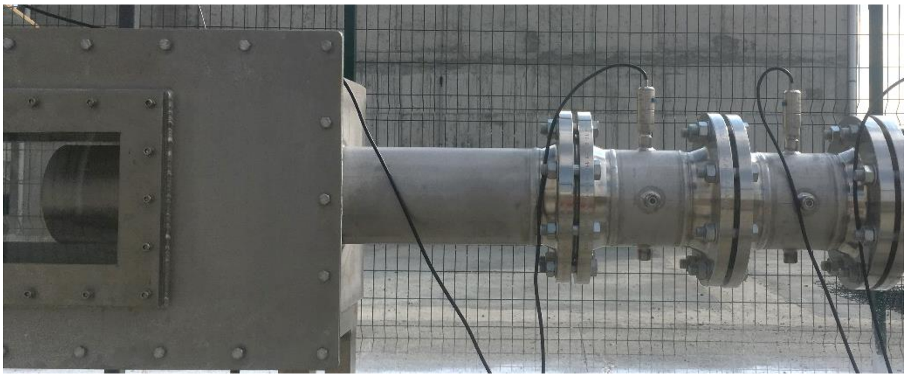

Figure 4-14. Test Section Diffusers.

4.2.7. Ejector Nozzle Feed Manifold

This part is the most difficult part in the whole design and manufacturing process of the experimental setup. The difficulties are due to the following reasons.

- Design of inner pipe containing the high pressure gas during the experiment to which the ejector nozzle is connected.
- Connection of the outer pipes with the inner pipe by blocking the secondary flow as minimum as possible.
- Alignment problem of the inner pipe.

- Support design for the inner pipe to resist the ejector nozzle thrust.
- Measuring the total pressure and total temperature of the ejector nozzle.

By considering these issues, ejector nozzle feed manifold is designed.

Ejector nozzle dimensions are calculated by using the values given in Table 4-2 and using following equation.

Table 4-2. Inputs for Ejector Nozzle Dimensioning.

γ	1,4
$\dot{m}_p$ (kg/s)	3
P_{t1} (Pa)	20×10^5
T_{t1} (K)	280
R (J/kg)	287
P_{ex} (Pa)	30000

$$A_{th} = \frac{\dot{m}_p}{P_{t1}} \sqrt{T_{t1}} \frac{1}{\sqrt{\frac{\gamma}{R} \left(\frac{2}{\gamma + 1}\right)^{\frac{\gamma+1}{\gamma-1}}}} \tag{4-1}$$

D_{th} is calculated as 28.36 mm. By using the following equation nozzle exit mach number is calculated as M=3.4.

$$P_{ex} = P_{t2} \left(1 + \frac{\gamma - 1}{2} M^2\right)^{\frac{\gamma}{1-\gamma}} \tag{4-2}$$

By using the calculated Mach number, Nozzle Exit Diameter is calculated using following,

$$\left(\frac{A\_e}{A\_th}\right)^2 = \frac{1}{M^2} \left(\frac{2}{\gamma + 1} \left(1 + \frac{\gamma - 1}{2} M^2\right)\right)^{\frac{\gamma+1}{\gamma-1}} \tag{4-3}$$

D_{ex} is calculated as 35.36 mm. Ejector nozzle is given in Figure 4-15.

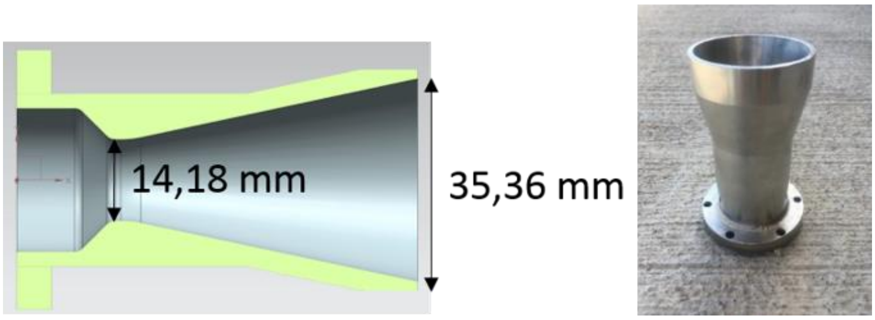

Figure 4-15. Ejector Nozzle.

Inner pipe dimensions are determined as mentioned below,

- Support number is chosen as 4 to establish the alignment of the inner pipe easier.
- Support pipes are used both for support mission and measurement interface.
- Supports are welded to both inner pipe and outer DN250 pipe.

Air should be incompressible in the pipes for system safety. To satisfy this requirement, maximum air velocity in the pipes are determined as 0.3 Mach ≈ 100 m/s. By using the following continuity equation,

$$\dot{m}_p = \frac{P_{t1}}{R\,T_{t1}}\,U\,A \tag{4-4}$$

For $\dot{m}_p$= 3kg/s, $P_{t1} = 20 \times 10^5\ Pa$, $T_{t1} = 290\ K$ and U=100m/s,

Total area is found as A=1.248×10^{-3}m^2.

For inner pipe, $D_{pipe} > 40$ mm.

There are 4 feeding pipe. So, Area for 1 pipe is calculated as, $\frac{A}{4} = 3.12 \times 10^{-4}$m^2.

For feeding pipes, $D_{pipe} > 20$ mm.

From standard pipe catalogue,

- Inner pipe is chosen as inner diameter, ID = 50 mm. Thickness is determined as t = 5 mm, due to the high-pressure gas and the welding connections with feeding pipes and supports.
- Feeding pipes are chosen as DN25 pipe with inner diameter, ID = 27.7 mm and thickness, t = 3 mm.

4 feeding pipes are connected to each other by using piping elements tees, reductions and elbows. It is ended with DN80 flange to connect air supply line.

Designed and manufactured ejector nozzle feed manifold is given in Figure 4-16, Figure 4-17, Figure 4-18 and Figure 4-19.

There are couplings located on the pipes. Pipes are drilled at certain points and couplings are welded to outer surface of the pipes to mount pressure transmitter and thermocouple. Pressure transmitter couplings are ¼ NPT and thermocouple couplings are 1/8 BSP.

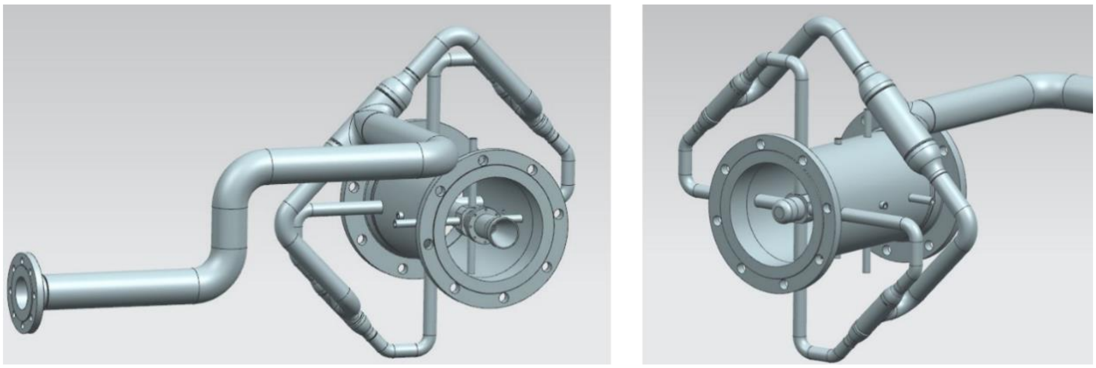

Figure 4-16. Ejector Nozzle Feed Manifold CAD Model.

Figure 4-17. Ejector Nozzle Feed Manifold.

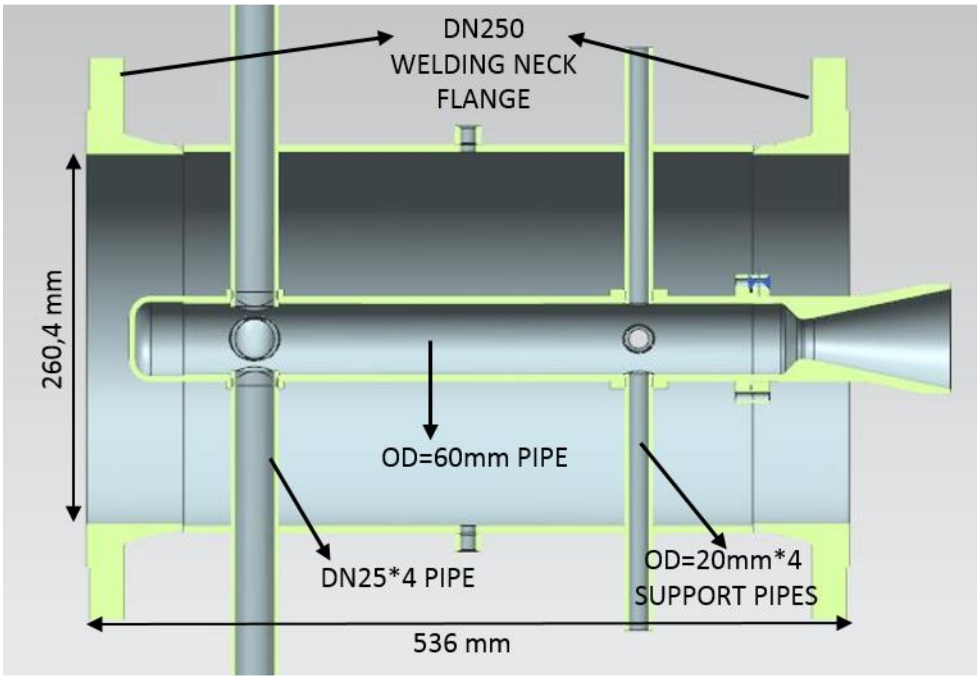

Figure 4-18. Ejector Nozzle Feed Manifold CAD Model Section View.

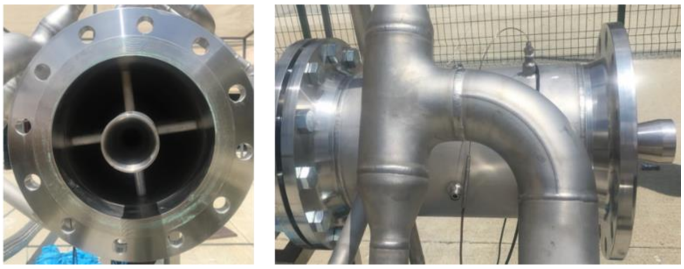

Figure 4-19. Ejector Nozzle Feed Manifold Detail.

4.2.8. Test Chamber

There is no specific design criteria for test chamber dimensions. So, it is manufactured big enough to mount free-jet nozzle and internal part of the diffuser as 350mm*350mm*930mm. DN150 flange is welded to one side of the test chamber to mount free-jet nozzle easily. In addition, DN125 flange is welded to the other side of the test chamber to change internal diffuser part easily. To connect the free-jet nozzle with air supply, there is a connection pipe and flange which are welded to test chamber outer wall. 2 Mach free-jet nozzle with 105,5 mm nozzle exit diameter is manufactured to mount in test chamber.

In the future, test article can be mounted in the test chamber and visualization methods can be applied. Due to this, there are glass interfaces on both sides of the test chamber. In addition, there are couplings located on the test chamber wall. Couplings are welded to mount pressure transmitter and thermocouple. Pressure transmitter couplings are ¼ NPT and thermocouple couplings are 1/8 BSP. Test chamber is given in Figure 4-20, Figure 4-21, Figure 4-22, Figure 4-23 and Figure 4-24.

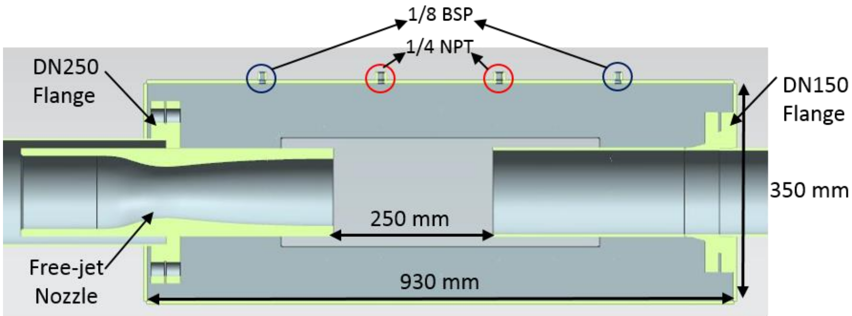

Figure 4-20. Test Chamber CAD Model Section View.

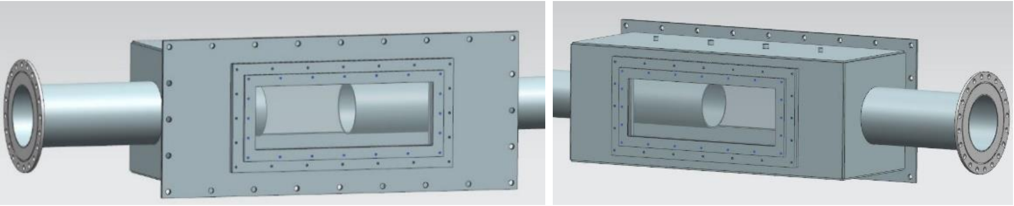

Figure 4-21. Test Chamber CAD Model.

Figure 4-22. Test Chamber.

Figure 4-23. Inside of the Test Chamber.

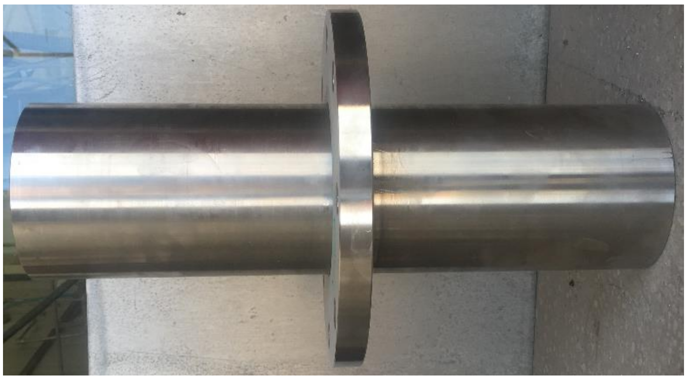

Figure 4-24. Free-jet Nozzle.

4.3. Measurements

In the experimental setup; pressure, temperature and mass flow rate measurement devices are utilized. The specifications of measurement devices used in the experimental setup are given in Table 4-3.

Table 4-3. Experimental Setup Sensor Specifications.

Descriptions	Specifications
Pressure Transducer	KISTLER 4260 A
Temperature Sensor	OMEGA T-TYPE Thermocouple
Mass Flow Rate Sensor	SAGE 200 thermal mass flow meter

4.3.1. Pressure Measurements

In the experiments, pressure value along the experimental setup is recorded by KISTLER 4260A (Figure 4-25) piezo-resistive 0-1 bara pressure sensor and the ejector nozzle total pressure is recorded by KISTLER 4260A piezo-resistive 0-35 bara pressure sensor. The data is recorded at a rate of 25kHz. However, due to the test duration is about 10 minutes, test data is downsampled before processing. Sensors are mounted to the experimental setup by using ¼ NPT couplings.

Figure 4-25. Kistler 4260A piezoresistive pressure transmitter.

4.3.2. Temperature Measurements

Temperature data at the test chamber and ejector nozzle inlet are collected by using T-type thermocouples. Recording of data was done at a rate of 10Hz. Allocation of the thermocouples in the test chamber and ejector nozzle can be seen in Figure 4-26 and Figure 4-27.

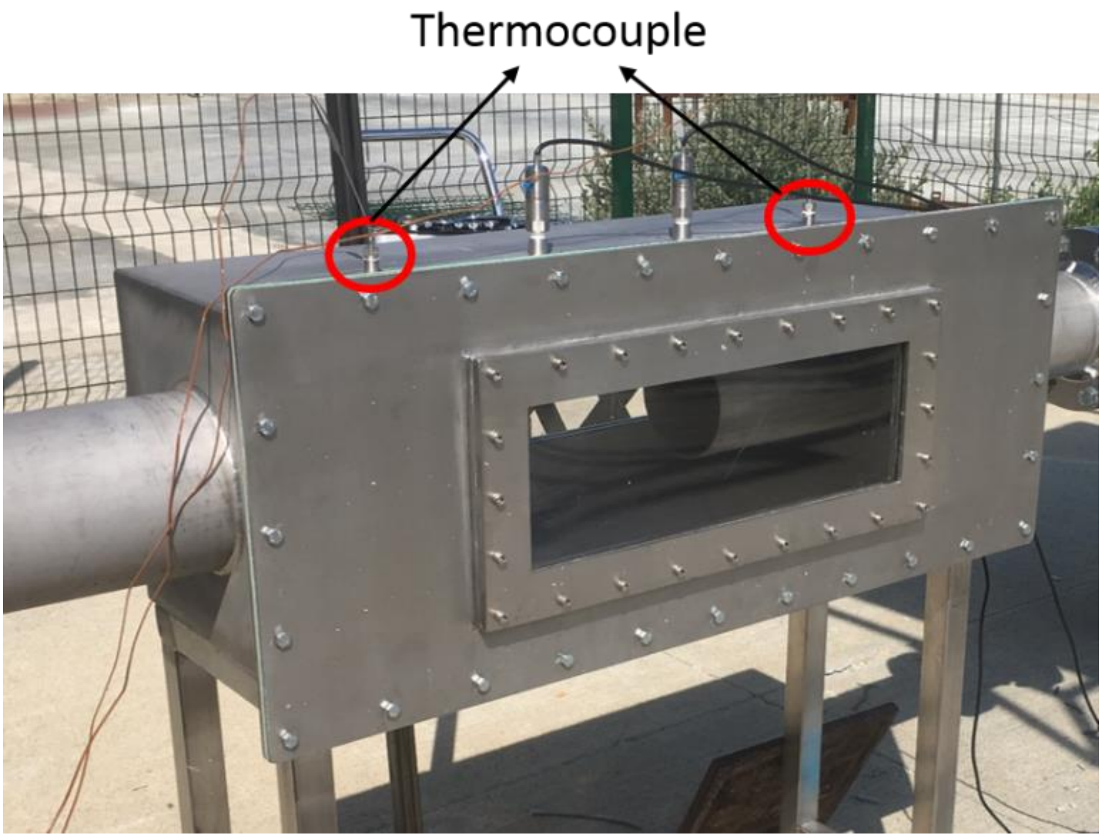

Figure 4-26. Allocation of Thermocouples on the Test Chamber.

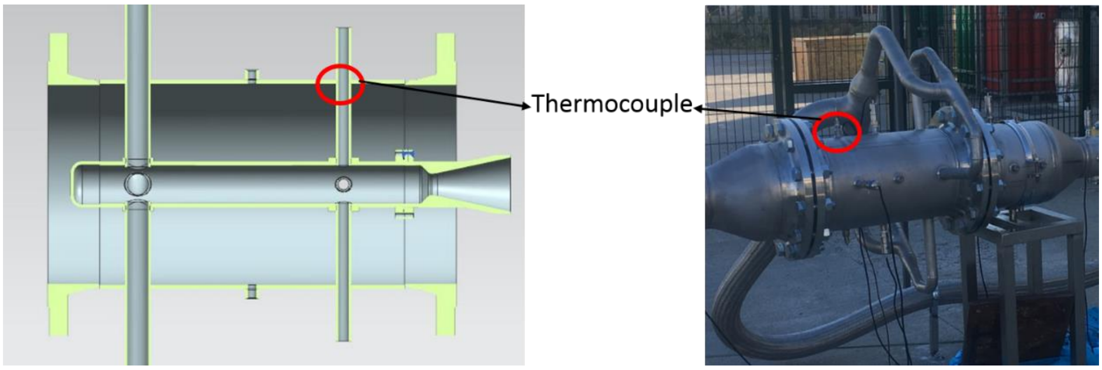

Figure 4-27. Allocation of thermocouple on Ejector Nozzle Feed Manifold.

4.3.3. Mass Flow Rate Measurements

Mass flow rate of the ejector nozzle can be calculated by using the geometry of the nozzle, recorded total pressure and total temperature data. Nonetheless, due to the pressure drop in long pipes downstream of the free-jet nozzle, mass flow rate has to be recorded. Free-jet nozzle mass flow rate is recorded by SAGE 200 thermal mass flow meter shown in Figure 4-28. The data is recorded at a rate of 1Hz.

Figure 4-28. SAGE Thermal Mass Flow Meter.

CHAPTER 5

RESULTS AND DISCUSSIONS

Experiments are done to investigate the effect of length to diameter ratio of ejector diffuser (L_1/D_1), NXP length (L_4), and ER on the performance of high altitude test system. The results obtained from the experiments and the numerical simulations of the High Altitude Test Model are given in this chapter. Numerical simulations are performed for the configurations which are employed in the experiments. Then, experimental results are presented in detail. Lastly, the numerical and experimental results are compared with each other.

5.1. Experimental Matrix

For an ejector system, there are four basic geometric parameters: transition cone angle (α_1), Length to Diameter Ratio of Ejector Diffuser (L_1/D_1), NXP length (L_4), Ejector Nozzle diverging half-angle (α_2). Among them, α_1 is not applicable due to the usage of standard reduction instead of transition cone, which is mentioned in Section 4.2.3, and α_2 is fixed as 12º in Section 3.1. Parameters used in analyses are shown in Figure 5-1. By using these parameters and the Entrainment Ratio (ER), test matrix is generated which is given in Table 5-1.

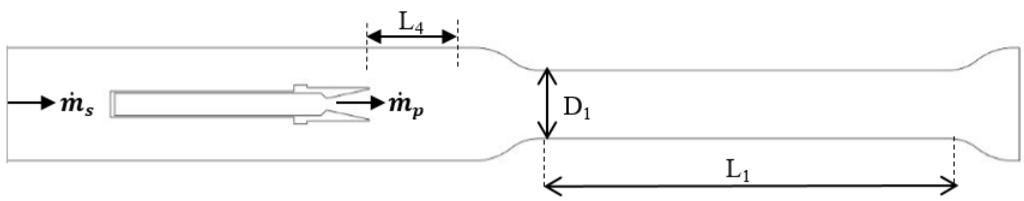

Figure 5-1. Experimental Setup Parameters.

Table 5-1. Experimental Matrix.

CASE ID	L_1/D_1	ER ($\dot{m}_s / \dot{m}_p$)	NXP Extension	L_4 (mm)
1	9.7	0.34	YES	250
2	7.75	0.34	YES	250
3	5.8	0.34	YES	250
4	9.7	0.34	NO	14
5	7.75	0.34	NO	14
6	5.8	0.34	NO	14
7	9.7	0.16	YES	250
8	9.7	0.25	YES	250
9	9.7	0.33	YES	250
10	9.7	0.36	YES	250
11	9.7	0.44	YES	250
12	9.7	0.47	YES	250
13	9.7	0.57	YES	250

5.2. Numerical Simulations

There are some differences between simulations done in this chapter and simulations done in Sections 3.1 and 3.3. These are,

- In experimental study, air storage tank is not heated. Due to the heat loss in the experimental setup, ejector nozzle total temperature T_{t1} is measured as 280K and Free-jet nozzle total temperature T_{t2} is measured as 300K at steady-state.
- Instead of subsonic diffusers and transition cone, standard reductions are used in experimental setup. So, these components are changed in the HATS analysis model.

HATS analysis model is rebuilt considering the changes made in manufacturing of experimental setup. Updated HATS analysis model is given in Figure 5-2.

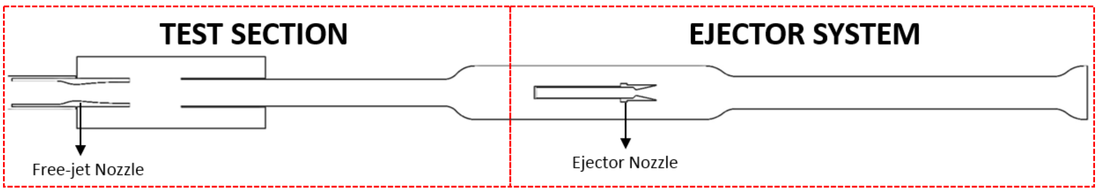

Figure 5-2. Updated HATS Analysis Model Schematic.

Combined numerical simulations for HATS analysis model (with L_1/D_1=9.7 and NXP Extension exist) are performed with boundary conditions given in Table 5-2.

Table 5-2. HATS Analysis Model Boundary Conditions.

Parameter	**Value**
Pressure inlet total pressure, P_{t1}, bar	20
Pressure inlet total temperature, T_{t1}, K	280
Free-jet nozzle mass flow rate, $\dot{m}_s$, kg/s	ER= 0.16 → 0.5 ER= 0.25 → 0.75 ER= 0.33 → 1 ER= 0.36 → 1.1 ER= 0.44 → 1.32 ER= 0.47 → 1.41 ER= 0.57 → 1.71
Free-jet nozzle total temperature, T_{t2}, K	300
Pressure outlet pressure, P_{amb}, Pa	88400
Pressure outlet temperature, T_{amb}, K	300

5.2.1. Numerical Simulation Results for Case 7 (ER = 0.16)

Due to the difference between the free-jet nozzle exit pressure and the test chamber pressure normal shock occurs inside the free-jet nozzle and both nozzle and test section diffuser are not started. It can be seen in Figure 5-3.

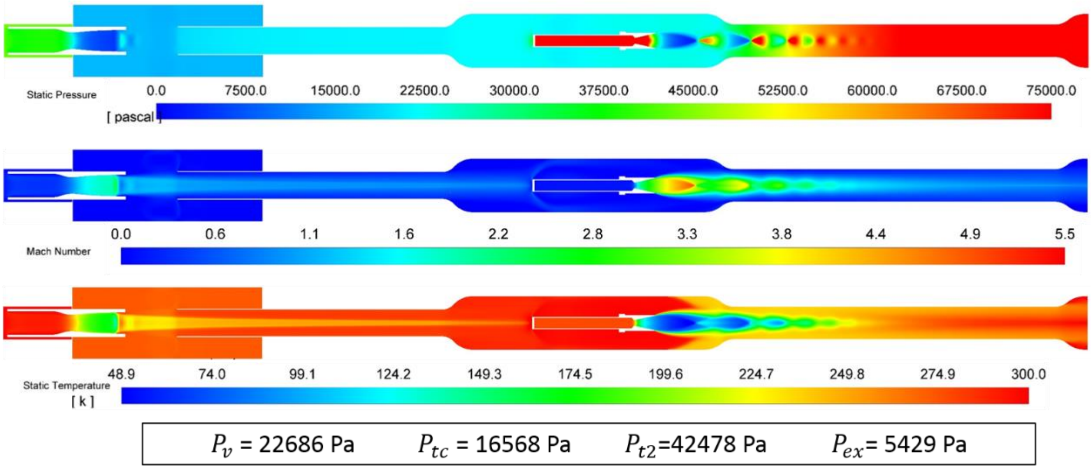

Figure 5-3. CFD Results for ER = 0.16.

5.2.2. Numerical Simulation Results for Case 8 (ER = 0.25)

In this case, free-jet nozzle is started but test section diffuser is partially started, because; the mass flow rate of the free-jet nozzle is not enough to start the diffuser.

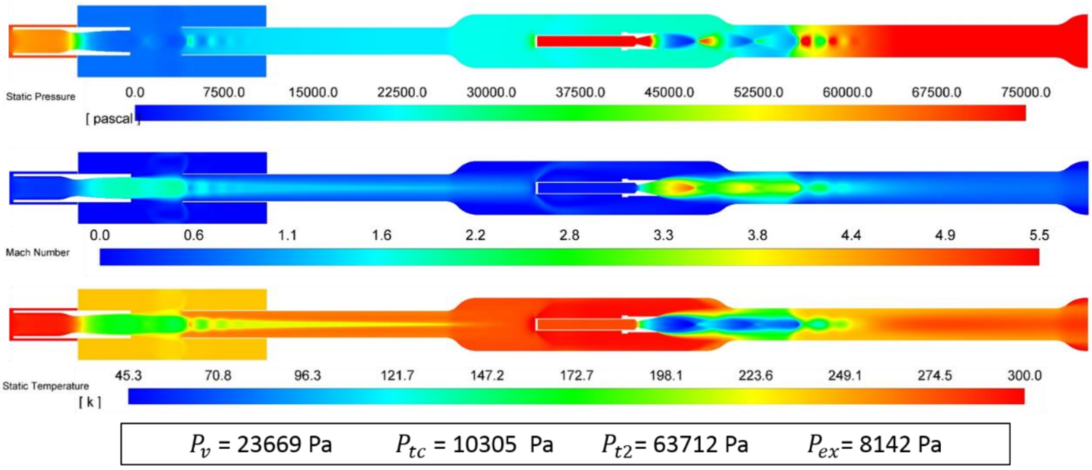

Figure 5-4. CFD Results for ER = 0.25.

5.2.3. Numerical Simulation Results for Case 9 (ER = 0.33)

This is the design condition of the system. Both free-jet nozzle and the test section diffuser is started. Test section diffuser diameter is determined for this ER value. So, test chamber pressure P_{tc} gets the lowest value for this geometry and boundary conditions.

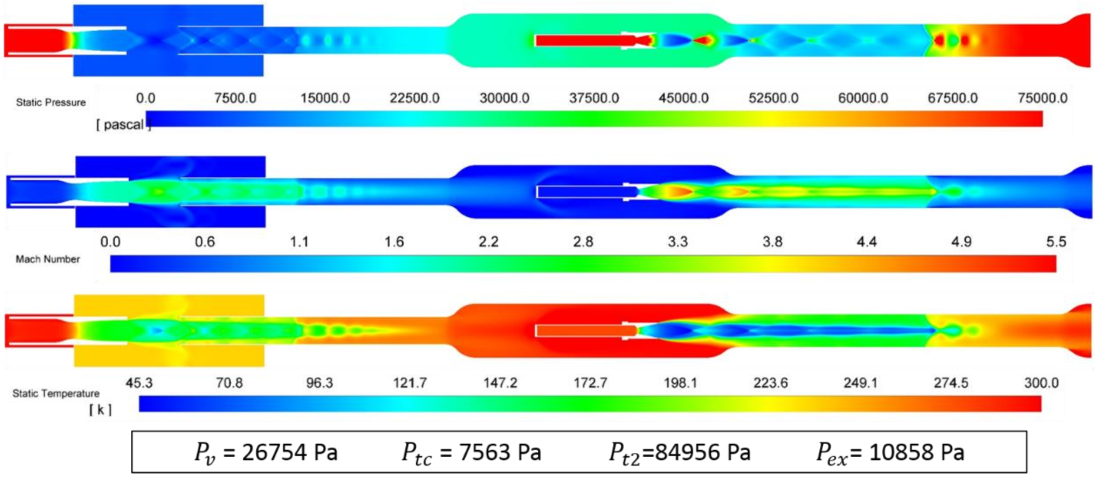

Figure 5-5. CFD Results for ER = 0.33.

5.2.4. Numerical Simulation Results for Case 10 (ER = 0.36)

When the free-jet nozzle mass flow rate is higher than the design point (ER=0.33), test chamber pressure starts to increase.

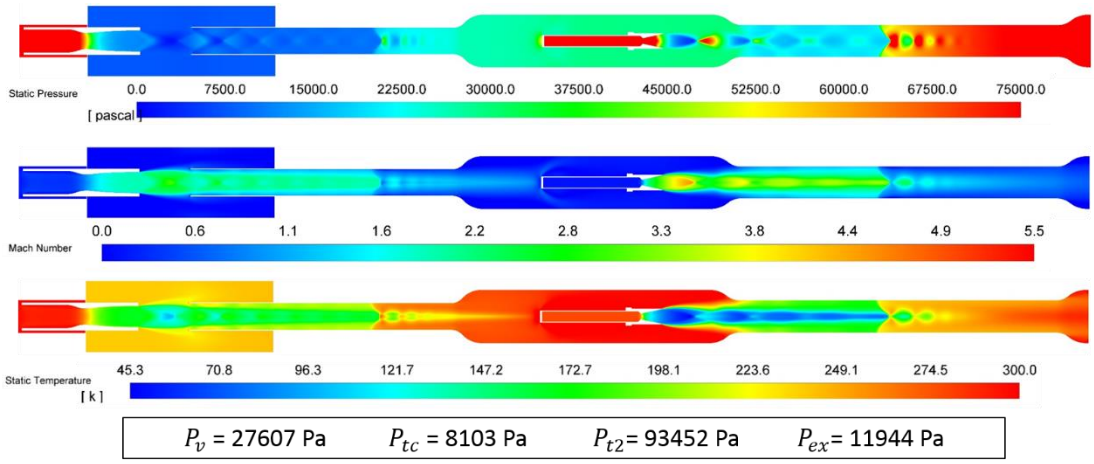

Figure 5-6. CFD Results for ER = 0.36.

5.2.5. Numerical Simulation Results for Case 11 (ER = 0.44)

Vacuum pressure P_v continuously increases with increase in ER, however, due to the increase in free-jet nozzle mass flow rate ($\dot{m}_s$), test chamber pressure increases after design point (ER= 0.33) of the system.

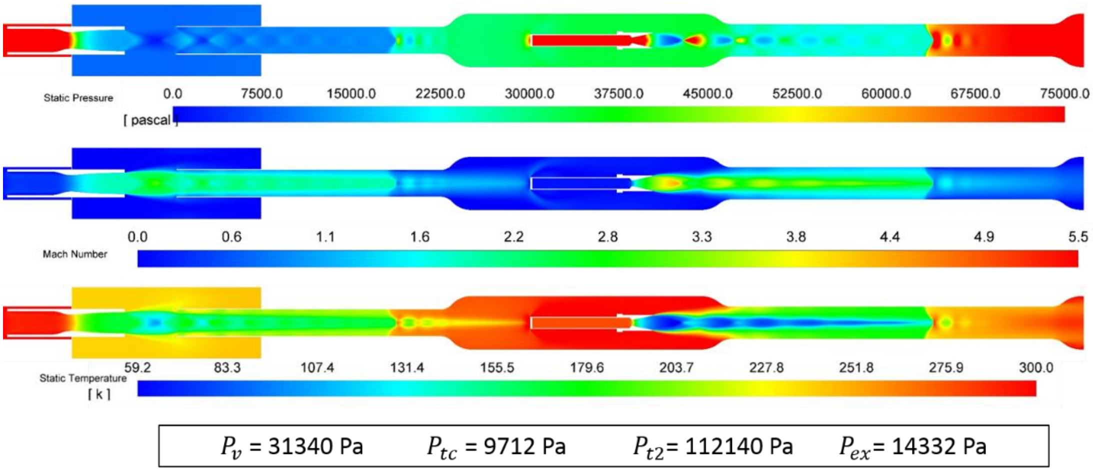

Figure 5-7. CFD Results for ER = 0.44.

5.2.6. Numerical Simulation Results for Case 12 (ER = 0.47)

When the total mass flow rate increases, ejector performance drops because the diameter of the ejector system is determined for a given mass flow rates. With higher ejector diameter, Vacuum pressure P_v value becomes lower than 32435 Pa.

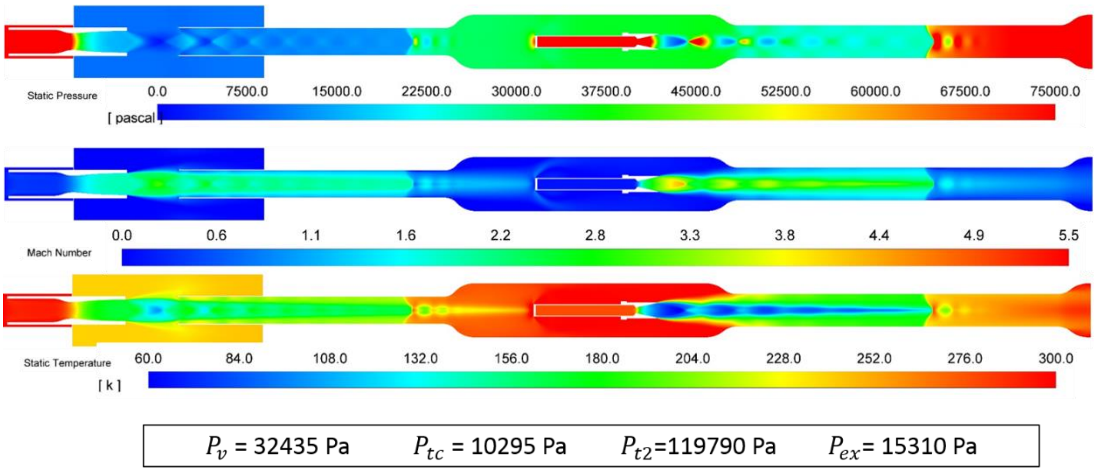

Figure 5-8. CFD Results for ER = 0.47.

5.2.7. Numerical Simulation Results for Case 13 (ER = 0.57)

In this case, Vacuum pressure P_v becomes 39800 Pa, which is much higher than the P_v value in Section 5.2.1. However, due to the test section diffuser diameter is constant, when the free-jet nozzle mass flow rate increases, test section diffuser performance increases. In addition, when the free-jet nozzle mass flow rate increases, the nozzle exit pressure also increases. This comparison should be made by using different free-jet nozzles.

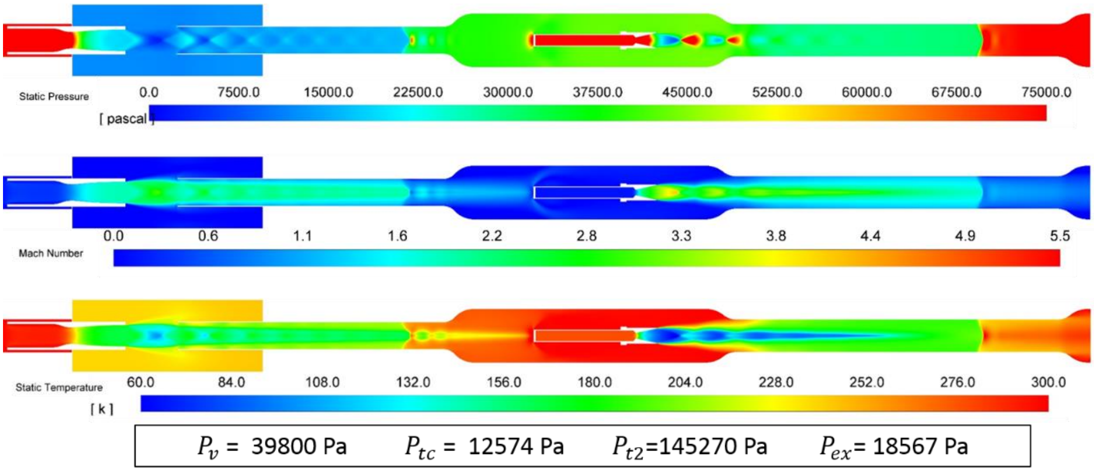

Figure 5-9. CFD Results for ER = 0.57.

5.3. Experimental Results

Experiments are performed in the experimental setup established in TÜBİTAK SAGE High Altitude Test Facility. Pressure, temperature and mass flow rate data are measured by sensors during the test. The pressure transmitter output is sampled at the rate of 25kHz, the thermocouple output is sampled at the rate of 10Hz and the mass flow meter output is sampled at the rate of 1Hz with NI cDAQ-9189 data acquisition system. The test duration is nearly 5-10 minutes. That means nearly 7.5 million pressure output are recorded for each test. It is not possible to process that amount of data. So, the pressure output is downsampled at the rate of 10Hz same with thermocouple output.

There is no filter needed for thermocouple and mass flow meter data. However, the oscillations of the pressure data that is caused most probably by the supersonic transient flow conditions in the experimental setup and vibration of the system can be eliminated by filtering. 2nd order Lowpass Butterworth Filter is used as a filtering method. Raw data and the filtered data for Case 1 in Table 5-1 are given in Figure 5-10 and Figure 5-11 as an example. Due to the controlling parameters of the pressure regulator, ejector nozzle total pressure is oscillating in each increment but the amplitude of the oscillations diminishes in time. Also, the temperature data for both ejector nozzle and test chamber is given in Figure 5-12. Temperature of the ejector nozzle continuously decreases, however, test section temperature becomes constant when the free-jet nozzle is started.

The data used in the experimental results evaluation is cropped at design point (P_{t1} = 20bar) as shown with yellow boxes in Figure 5-11. Then, the mean and standard deviation is calculated for each set of data. In the all experimental results figure, the deviation of each pressure data is given with a band.

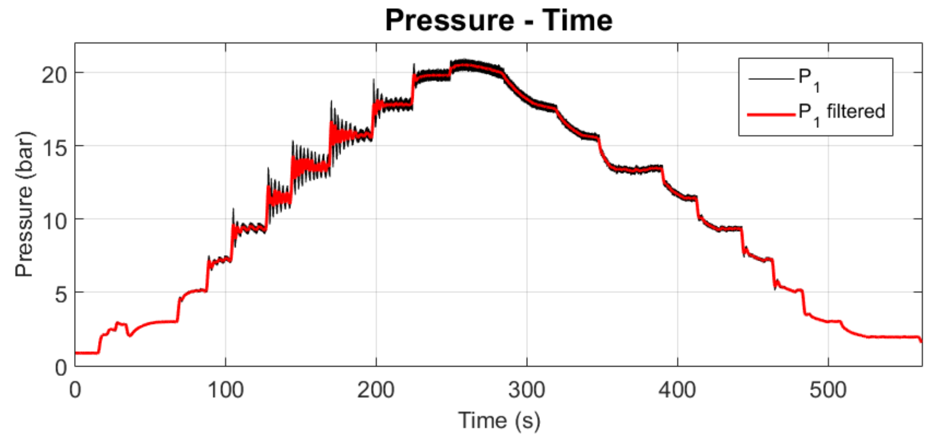

Figure 5-10. Raw and Filtered Ejector Nozzle Pressure Data of Case 1.

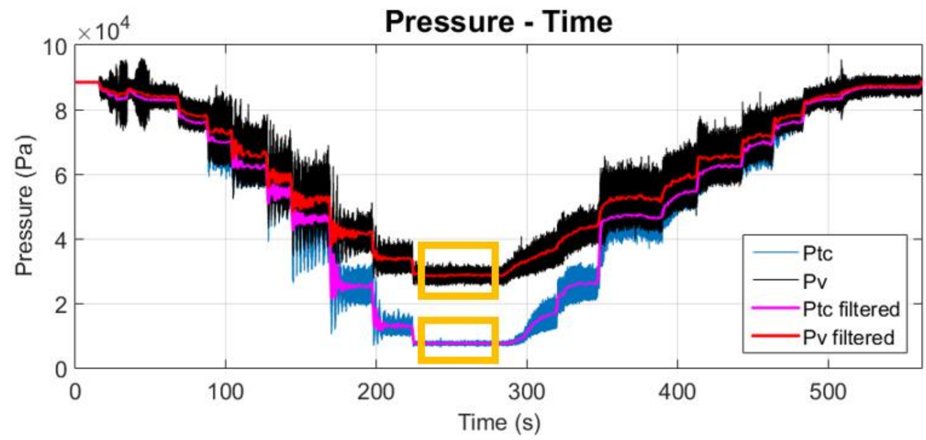

Figure 5-11. Raw and Filtered Vacuum Pressure and Test Chamber Pressure Data of Case 1.

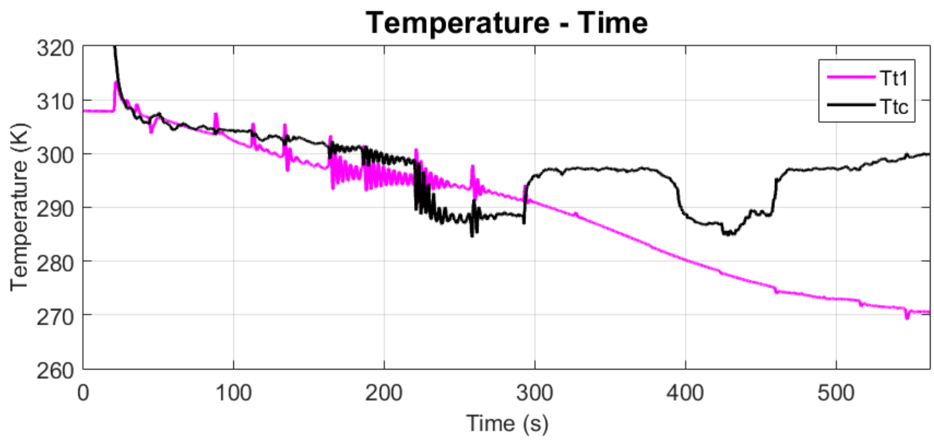

Figure 5-12. Raw Temperature Data of Case 1.

In Case 1 to Case 6, secondary flow feeding line is not connected to the test facility. That means, $\dot{m}_s$ is not controlled and free-jet nozzle sucks air from atmosphere. The mass flow rate of the sucked air for these tests at design point (P_{t1} = 20 bar) conditions are calculated by numerical analysis. However, the mass flow rate is not measured by the mass flow meter as shown in Figure 5-13.

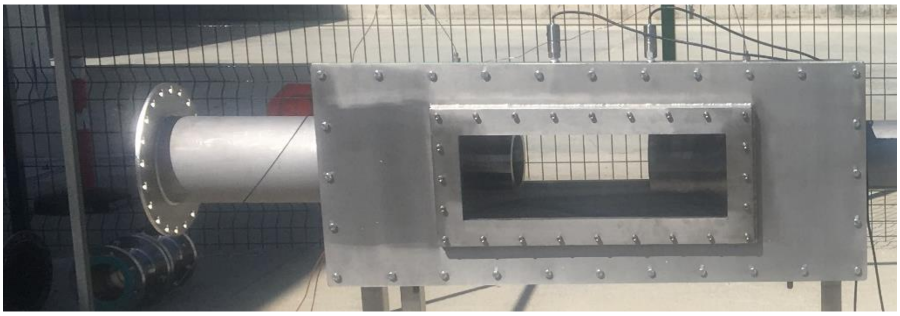

Figure 5-13. Secondary Flow Configuration for Case 1 to Case 6.

In Case 7 to Case 13, secondary flow line is connected to the test facility. That means, $\dot{m}_s$ is controlled by the pressure actuator and measured by the mass flow meter given in Figure 5-14.

Figure 5-14. Secondary Flow configuration for Case 7 to Case 13.

Experimental results for Case 1 – Case 13 are given in Figure 5-15 to Figure 5-27.

5.3.1. Experimental Results for Case 1: $L_1/D_1 = 9.7$ NXP = Exist ER = 0.34

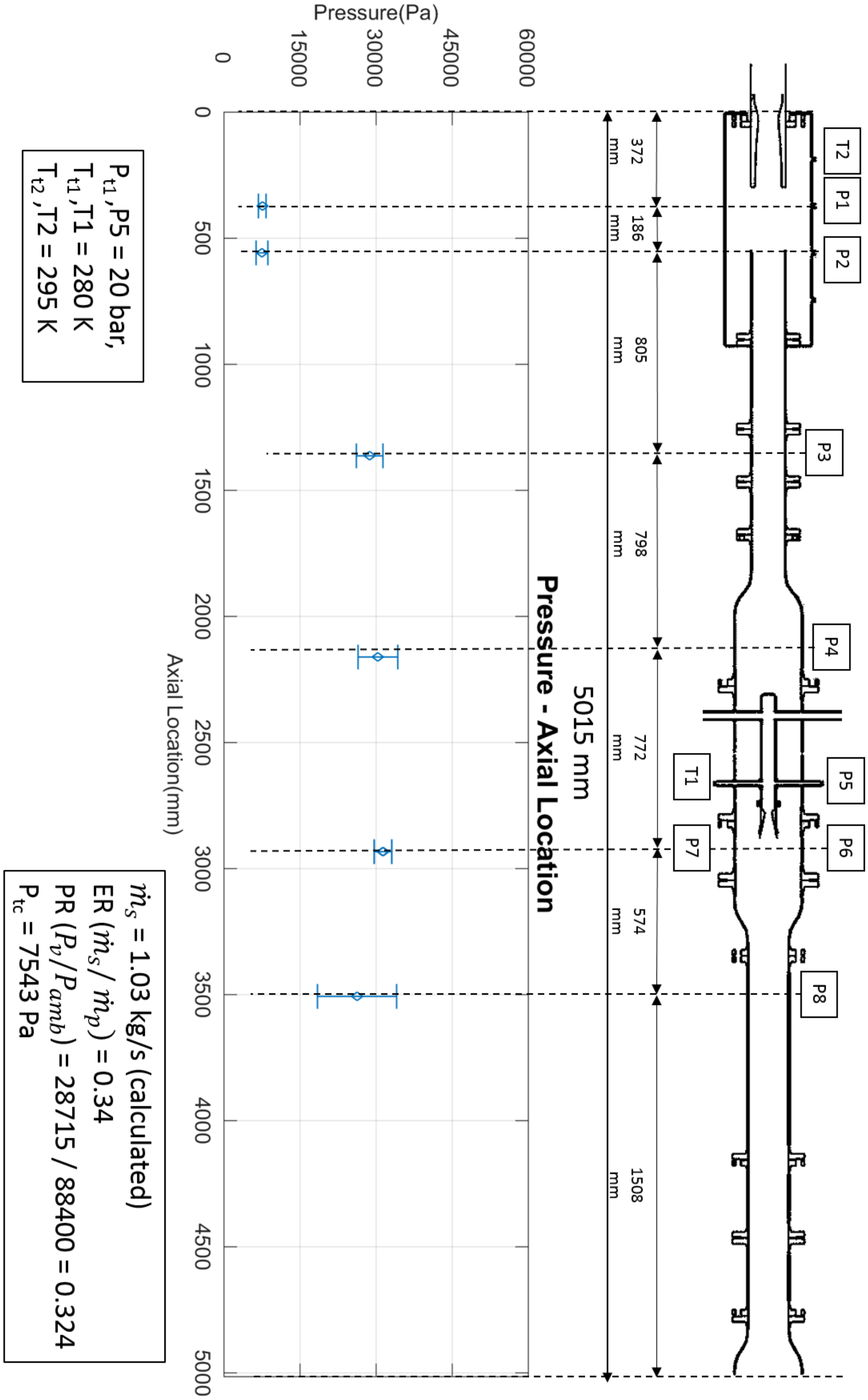

Figure 5-15. Case 1 Experimental Results.

5.3.2. Experimental Results for Case 2: L_1/D_1 = 7.75 NXP = Exist ER = 0.34

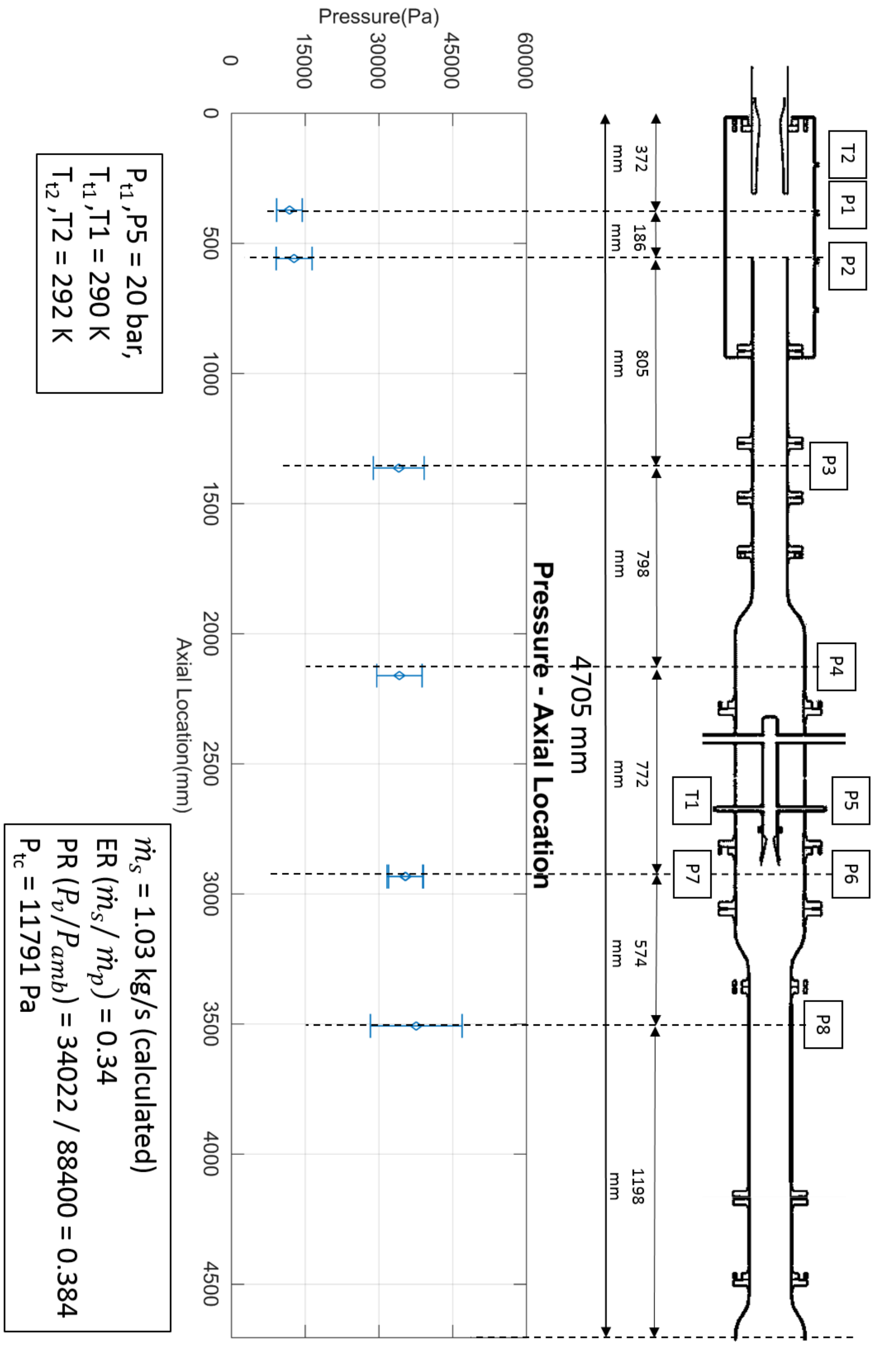

Figure 5-16. Case 2 Experimental Results.

5.3.3. Experimental Results for Case 3: L_1/D_1 = 5.8 NXP = Exist ER = 0.34

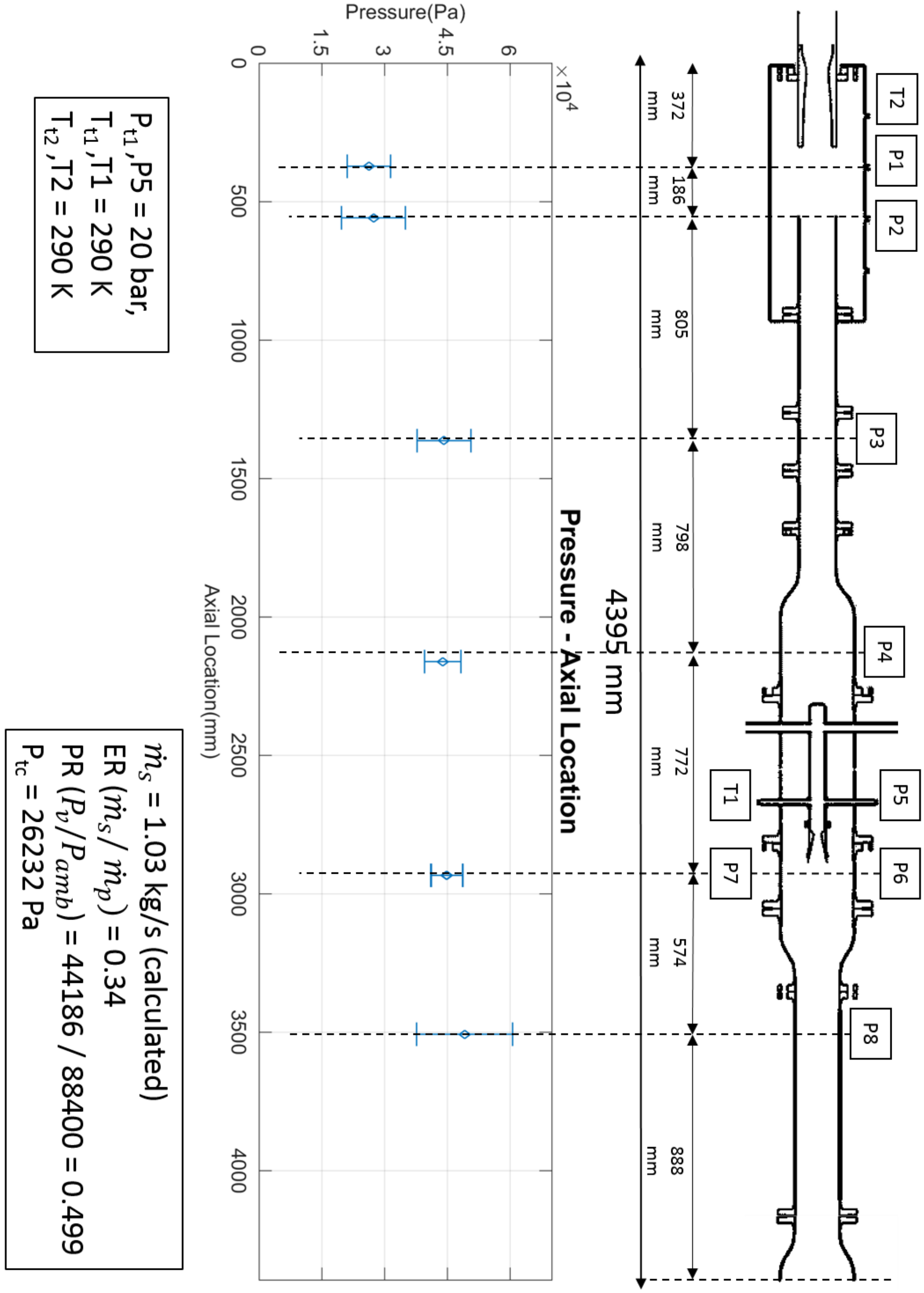

Figure 5-17. Case 3 Experimental Results.

5.3.4. Experimental Results for Case 4: L_1/D_1 = 9.7 NXP = No ER = 0.34

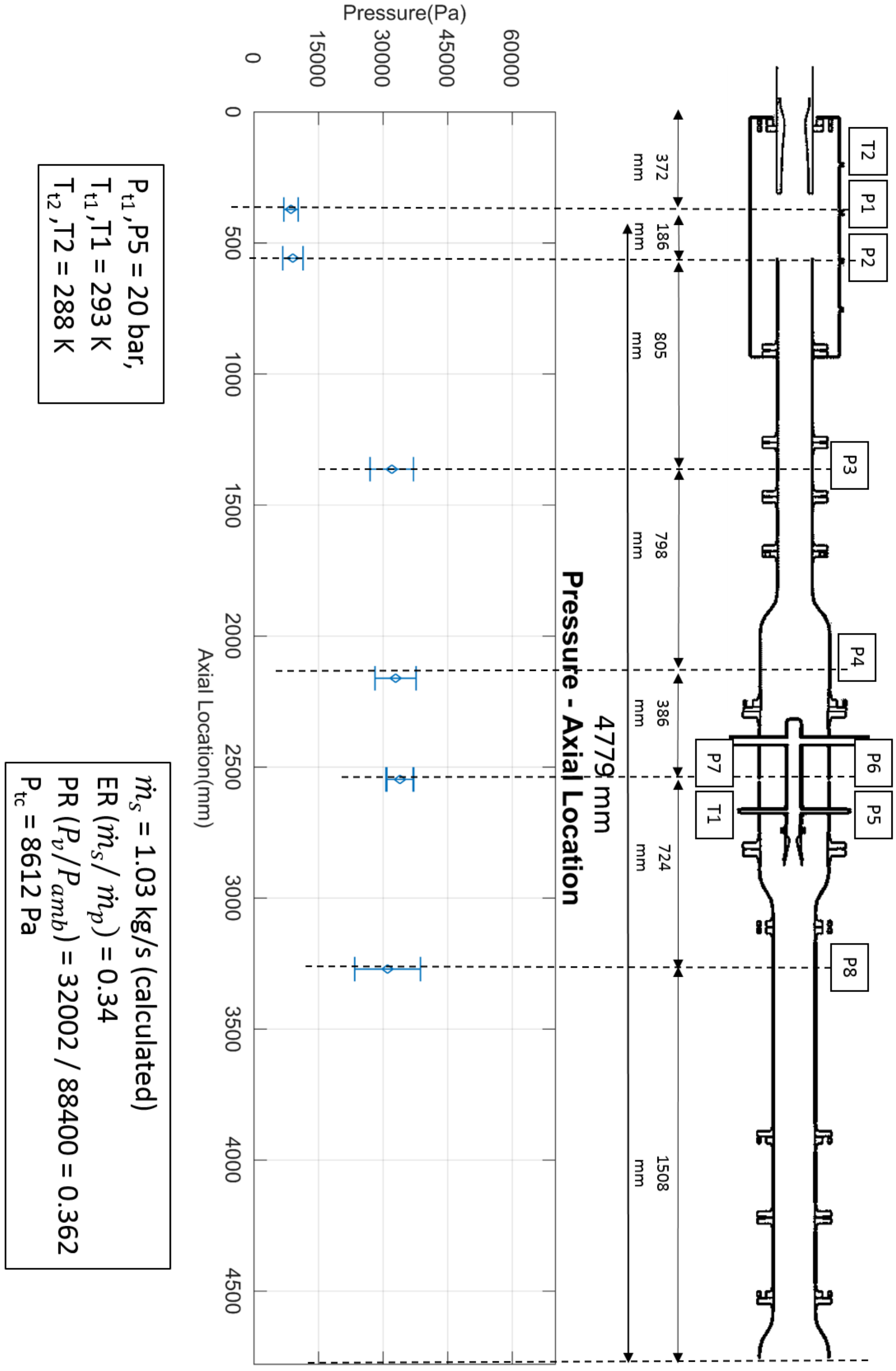

Figure 5-18. Case 4 Experimental Results.

5.3.5. Experimental Results for Case 5: $L_1/D_1 = 7.75$ NXP = No ER = 0.34

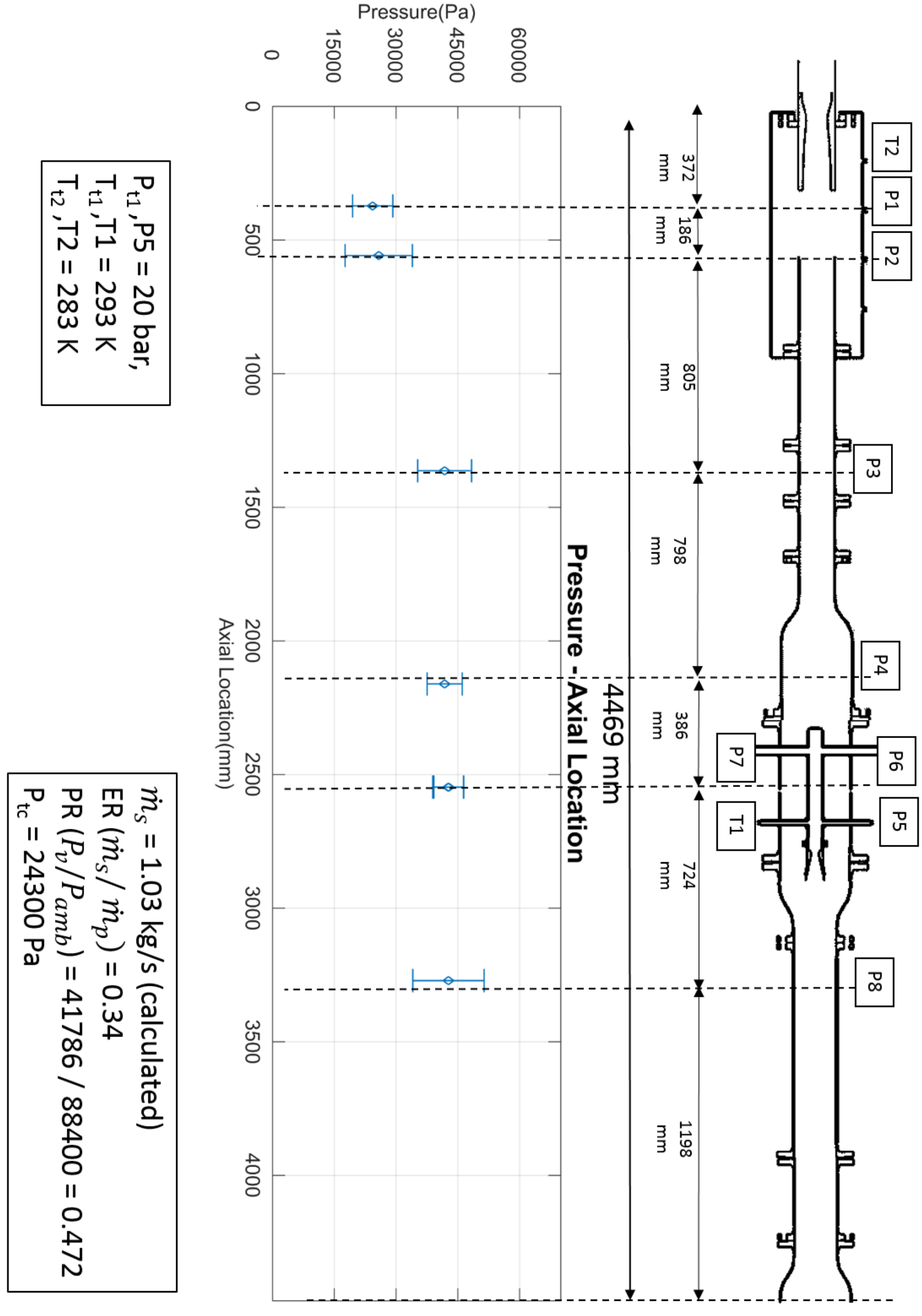

Figure 5-19. Case 5 Experimental Results.

5.3.6. Experimental Results for Case 6: $L_1/D_1 = 5.8$ NXP = No ER = 0.34

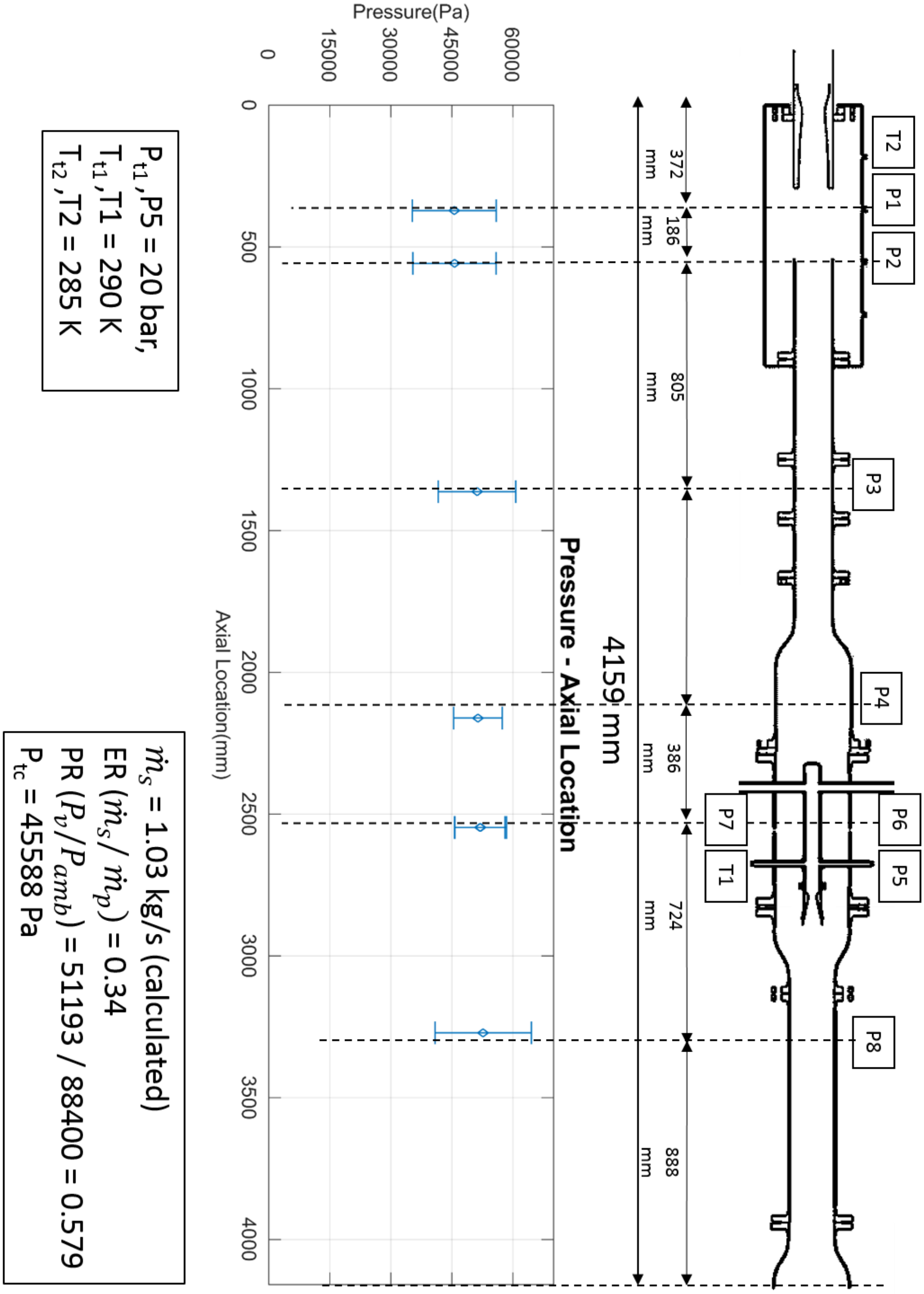

Figure 5-20. Case 6 Experimental Results.

5.3.7. Experimental Results for Case 7: L_1/D_1 = 9.7 NXP = Exist ER = 0.16

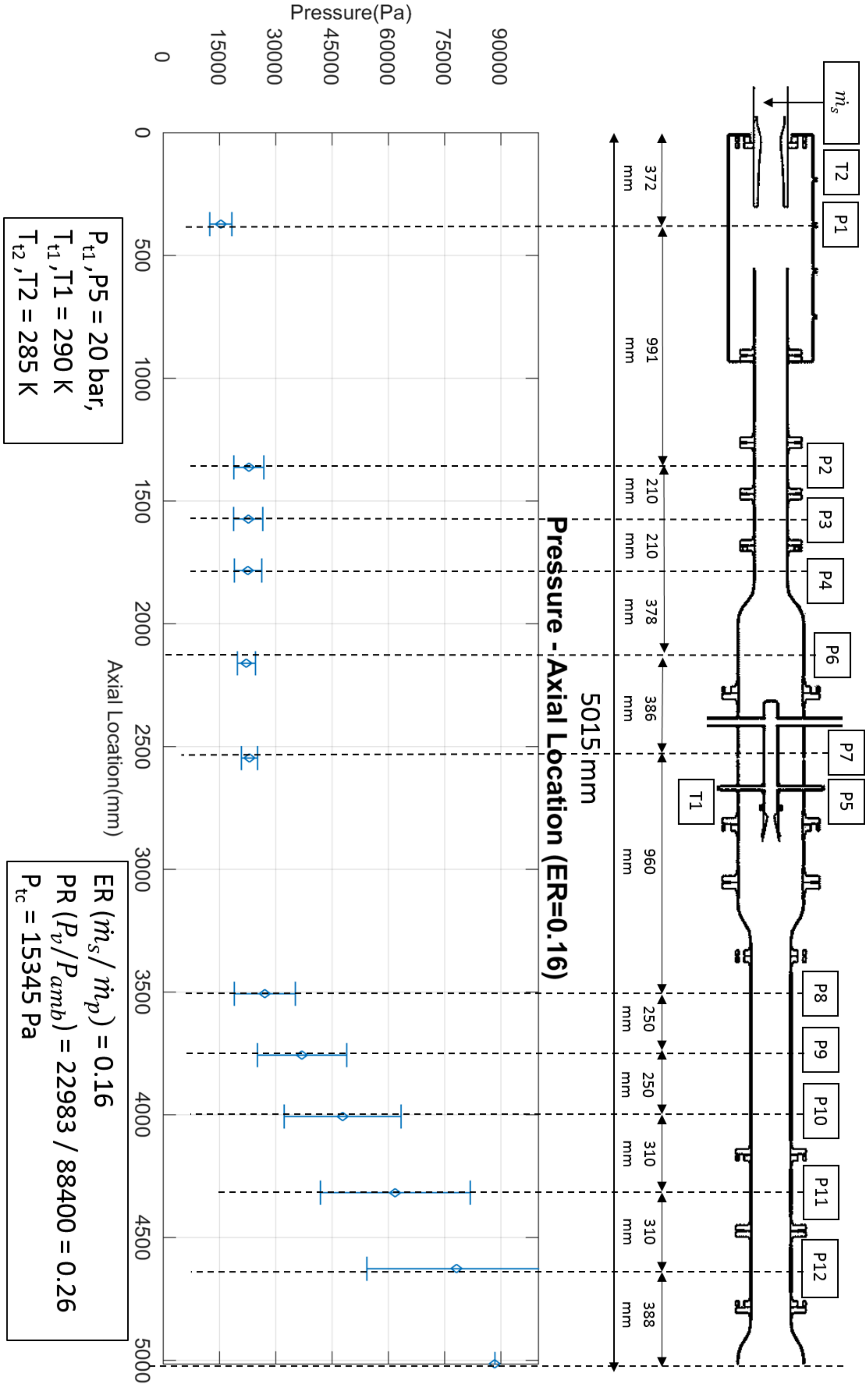

Figure 5-21. Case 7 Experimental Results.

5.3.8. Experimental Results for Case 8: $L_1/D_1 = 9.7$ NXP = Exist ER = 0.25

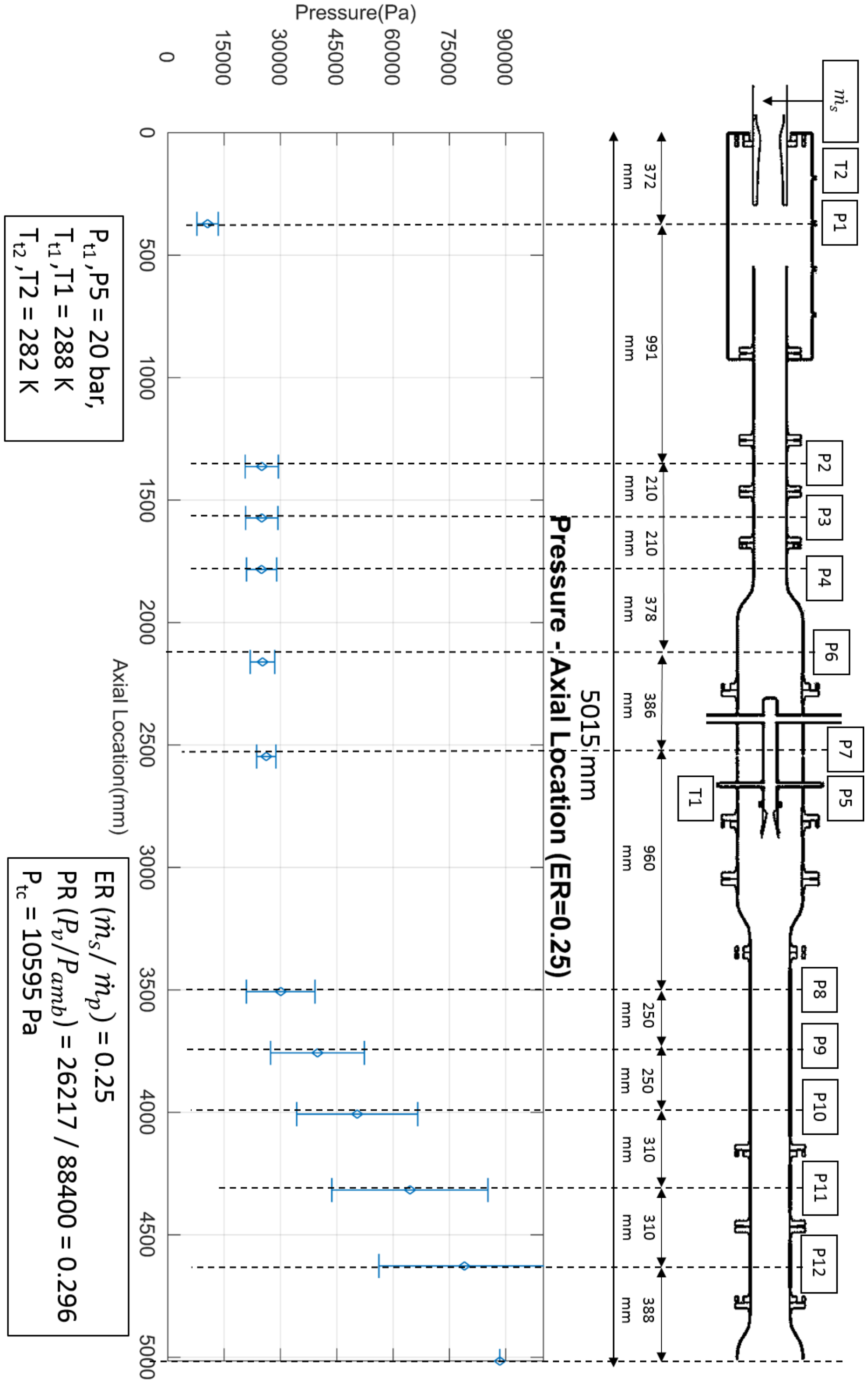

Figure 5-22. Case 8 Experimental Results.

5.3.9. Experimental Results for Case 9: L_1/D_1 = 9.7 NXP = Exist ER = 0.33

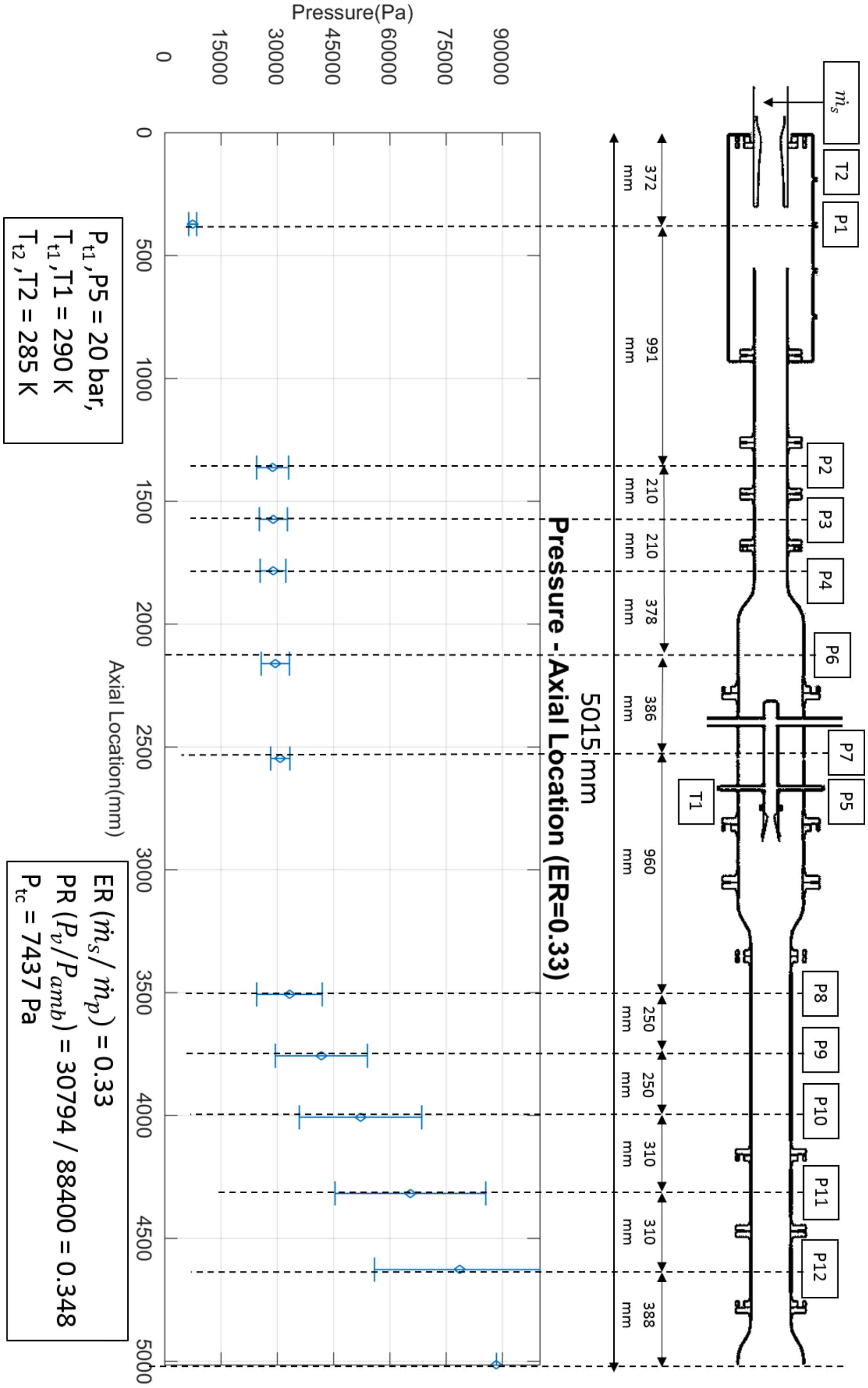

Figure 5-23. Case 9 Experimental Results.

5.3.10. Experimental Results for Case 10: L_1/D_1 = 9.7 NXP = Exist ER = 0.36

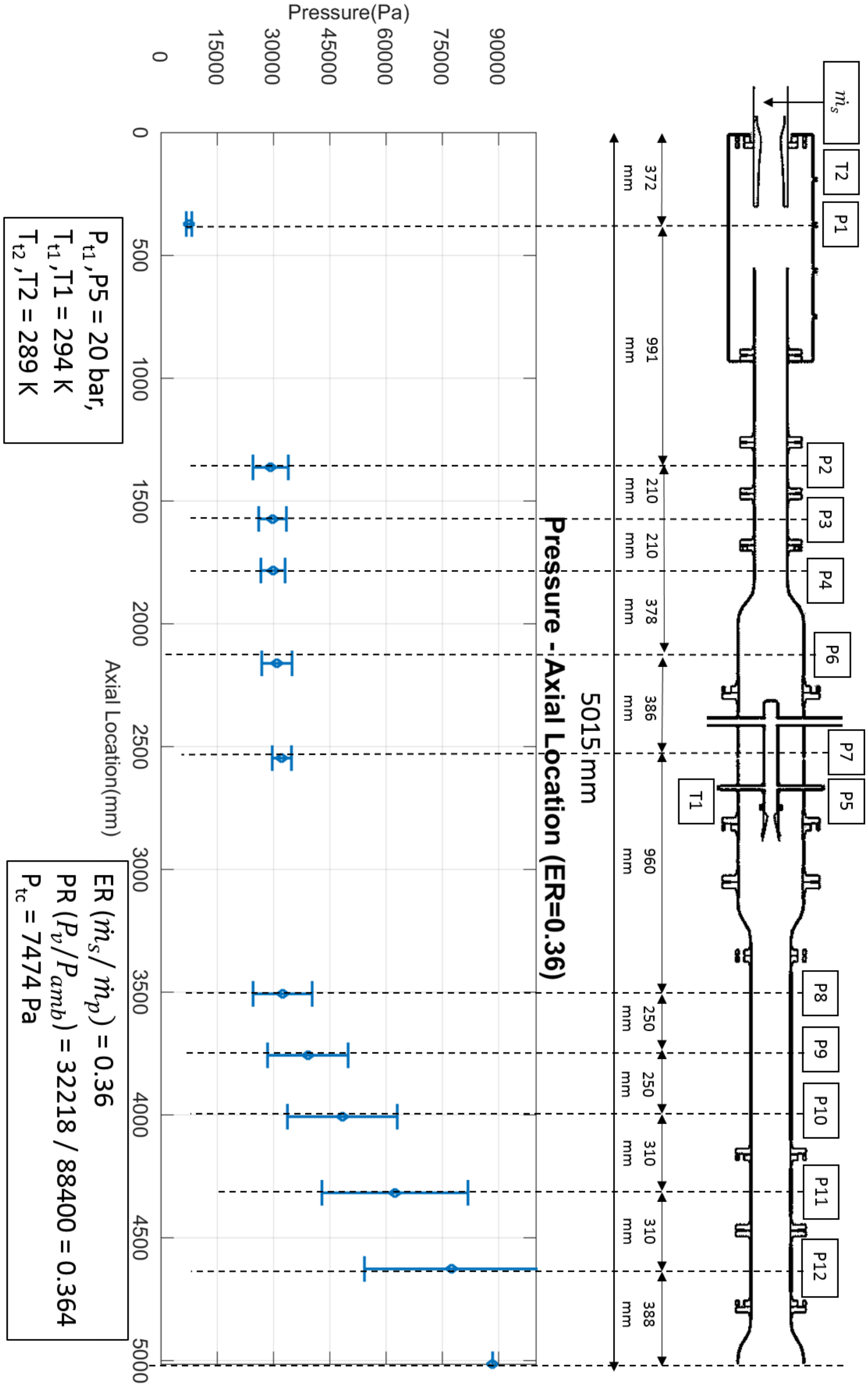

Figure 5-24. Case 10 Experimental Results.

5.3.11. Experimental Results for Case 11: L_1/D_1 = 9.7 NXP = Exist ER = 0.44

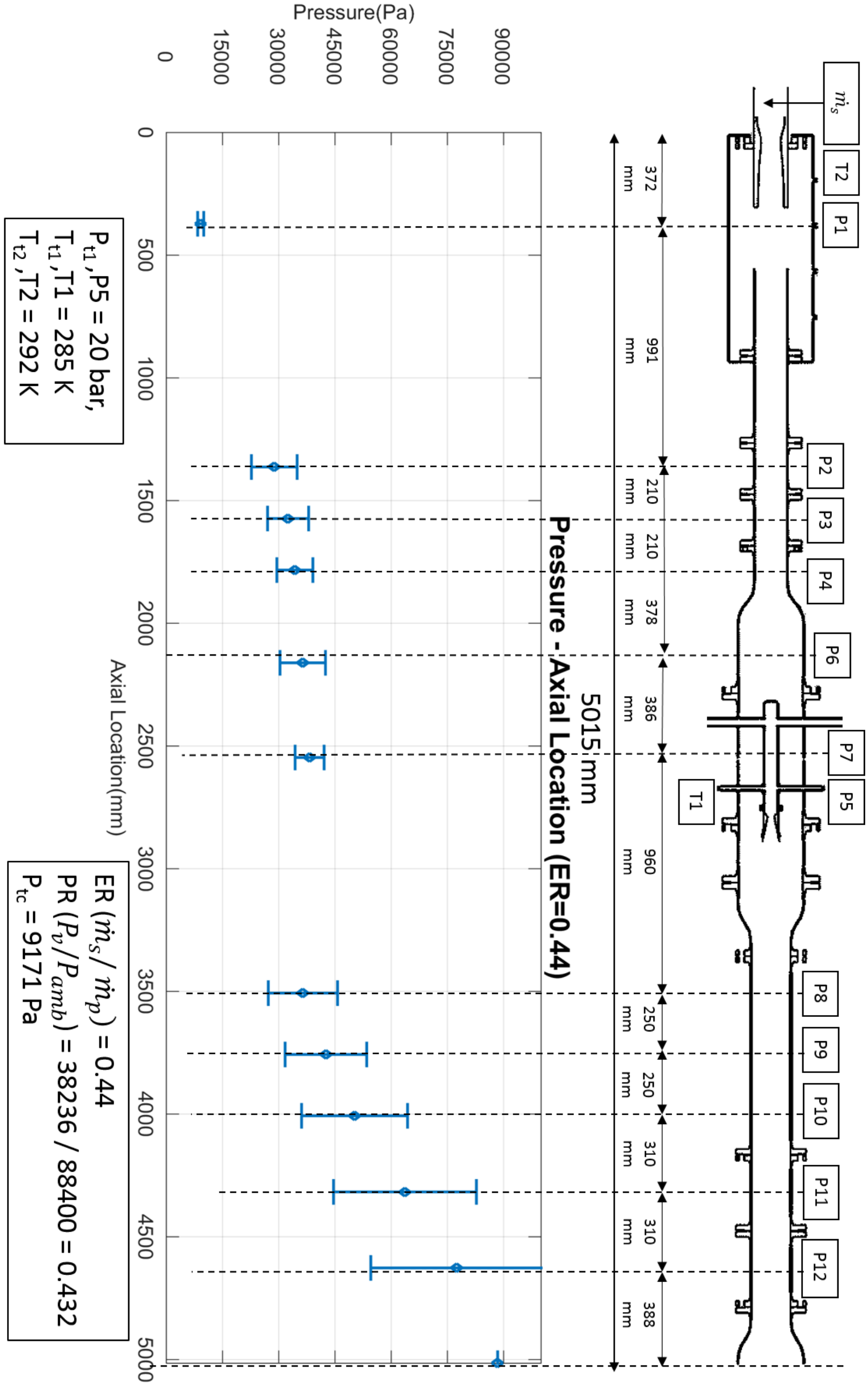

Figure 5-25. Case 11 Experimental Results.

5.3.12. Experimental Results for Case 12: L_1/D_1 = 9.7   NXP = Exist ER = 0.47

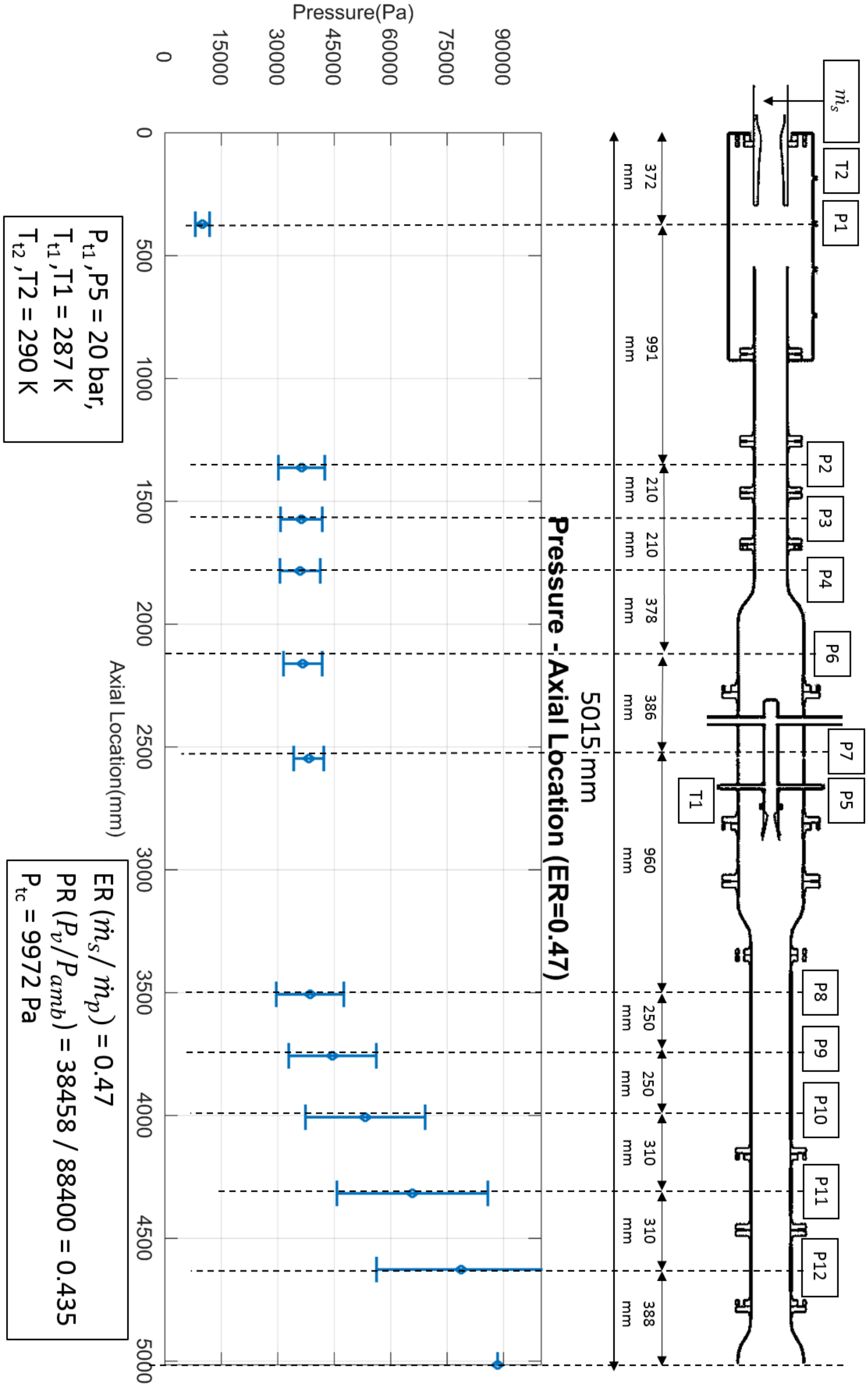

Figure 5-26. Case 12 Experimental Results.

5.3.13. Experimental Results for Case 13: L_1/D_1 = 9.7 NXP = Exist ER = 0.57

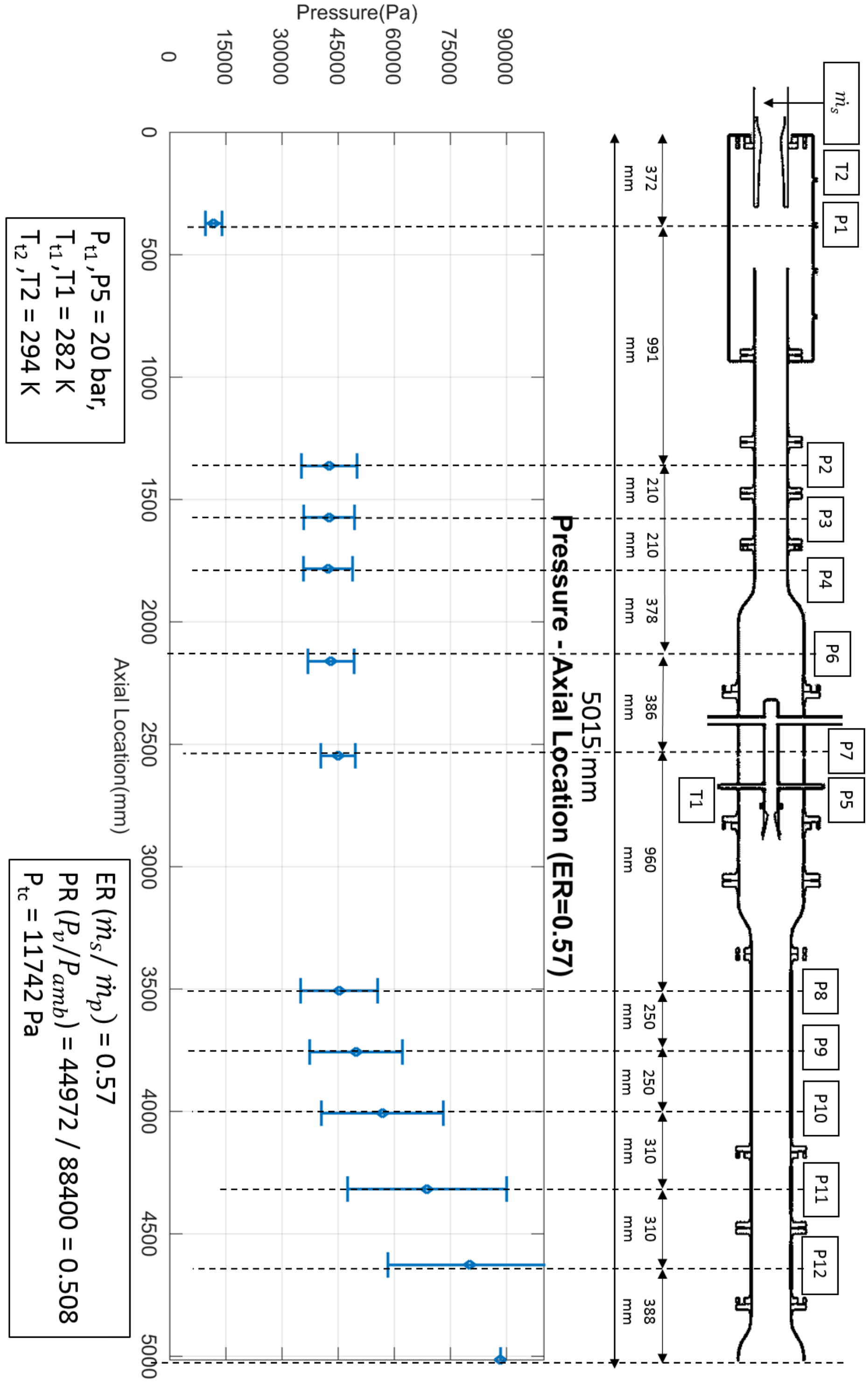

Figure 5-27. Case 13 Experimental Results.

5.4. Summary of Experimental Results

In this section, experimental results will be evaluated with respect to the length to diameter ratio of ejector diffuser (L_1/D_1), Nozzle Exit Plane –NXP- length (L_4), and Entrainment Ratio. Nozzle exit pressure is an important parameter in evaluation of the test chamber pressure value. It is calculated by using following equations for manufactured Mach 2 free-jet nozzle with inputs given in Table 5-3. Results are given in Table 5-4. These values will be used in evaluation of the experimental results.

Table 5-3. Inputs for Free-jet Nozzle Inlet and Exit Pressure Calculations.

γ	1,4
T_{t2} (K)	300
R (J/kg)	287
r_{th2} (mm)	40.07

$$P_{t2} = \frac{\dot{m}_s}{A_{th2}} \sqrt{T_{t2}} \frac{1}{\sqrt{\frac{\gamma}{R}\left(\frac{2}{\gamma+1}\right)^{\frac{\gamma+1}{\gamma-1}}}} \qquad (5\text{-}1)$$

$$P_{ex2} = P_{t2}\,(1 + \frac{\gamma-1}{2}\,M^2)^{\frac{\gamma}{1-\gamma}} \qquad (5\text{-}2)$$

Table 5-4. Mach 2 Free-jet Nozzle Exit Pressure Values for Each $\dot{m}_s$ and Entrainment Ratio.

ER	**$\dot{m}_s$ (kg/s)**	**P_{t2} (Pa)**	**P_{ex2} (Pa)**
0.16	0.5	42478	5429
0.25	0.75	63712	8142
0.33	1	84956	10858
0.36	1.1	93452	11944
0.44	1.32	112140	14332
0.47	1.41	119790	15310
0.57	1.71	145270	18567

5.4.1. Effect of the Length to Diameter Ratio of Ejector Diffuser

Case 1, Case 2 and Case 3 results are compared to see the effect of L_1/D_1 with respect to Vacuum Pressure (P_v) and Test Chamber Pressure (P_{tc}). Results are given in Table 5-5 and Figure 5-28, Figure 5-29. σ values show the standard deviation of the data. It is seen that when the L_1/D_1 ratio decreases, ejector performance drops. Then,

- The vacuum pressure and test chamber pressure increase,
- Amplitude of oscillations in the pressure data increases which is due to the fact that test section nozzle and diffuser are not started or partially started and pressure starts oscillating due to the moving waves in the system.

When the test chamber pressure value is greater than the free-jet nozzle exit pressure value given in Table 5-4 the amplitude of oscillations becomes higher.

Table 5-5. Comparison for Case 1, Case 2 and Case 3 Results.

	Case 1		**Case 2**		**Case 3**	
	Value	σ%	Value	σ%	Value	σ%
P_v (Pa)	28715	9.1	34022	13.5	44186	14.5
P_{tc} (Pa)	7543	9.9	11791	22	26232	19.7

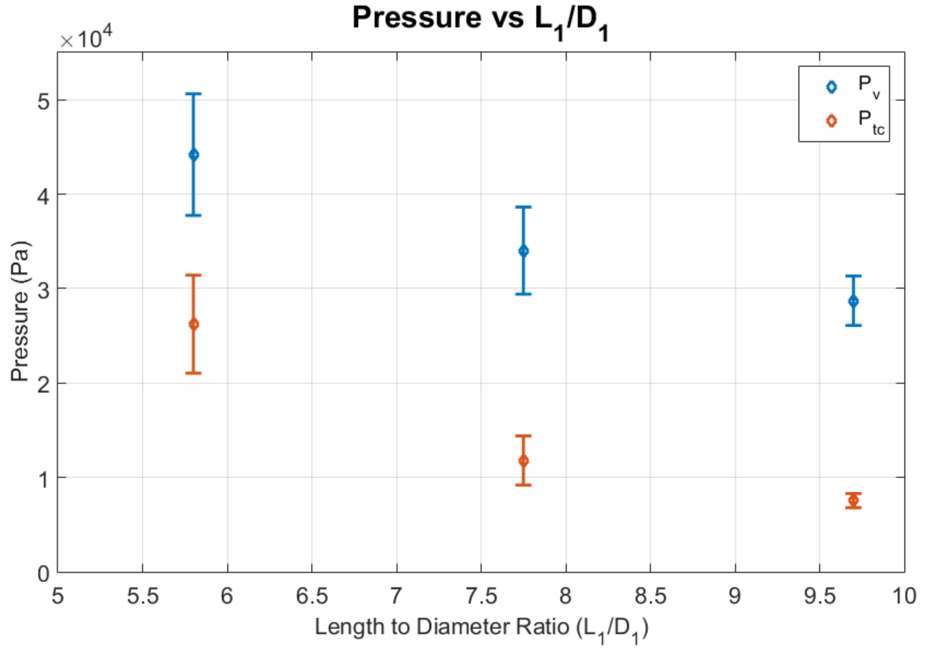

Figure 5-28. Pressure vs Length to Diameter Ratio for Case 1, Case 2 and Case 3.

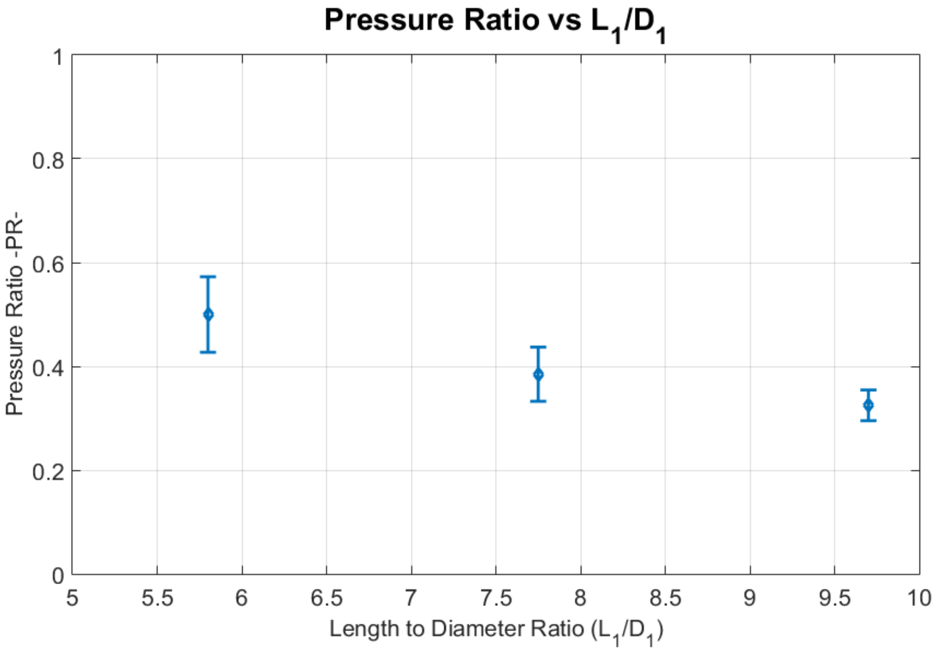

Figure 5-29. Pressure Ratio vs Length to Diameter Ratio for Case 1, Case 2 and Case 3.

5.4.1.1. Effect of Nozzle Exit Plane –NXP- Length

Case 1 & Case 4, Case 2 & Case 5 and Case 3 & Case 6 results are compared to see the effect of NXP length with respect to Vacuum Pressure (P_v) and Test Chamber Pressure (P_{tc}). Results are given in Table 5-6, Table 5-7, Table 5-8 and Figure 5-30, Figure 5-31. It is seen that when the NXP extension is removed, ejector performance drops. Then,

- The vacuum pressure and test chamber pressure increases,
- Amplitude of oscillations in the pressure data increases which is due to the fact that test section nozzle and diffuser are not started or partially started and pressure starts oscillating due to the moving waves in the system.

When the test chamber pressure value and free-jet nozzle exit pressure value become closer to each other, the amplitude of oscillations become smaller.

Table 5-6. Comparison for Case 1, Case 4 Results.

	Case 1		**Case 4**	
	Value	σ%	Value	σ%
P_v (Pa)	28715	9.1	32002	15.7
P_{tc} (Pa)	7543	9.9	8612	19.3

Table 5-7. Comparison for Case 2, Case 5 Results.

	Case 2		**Case 5**	
	Value	σ%	Value	σ%
P_v (Pa)	34022	13.5	41786	15.7
P_{tc} (Pa)	11791	22	24300	20.1

Table 5-8. Comparison for Case 3, Case 6 Results.

	Case 3		**Case 6**	
	Value	σ%	Value	σ%
P_v (Pa)	44186	14.5	51193	18.6
P_{tc} (Pa)	26232	19.7	45588	22.6

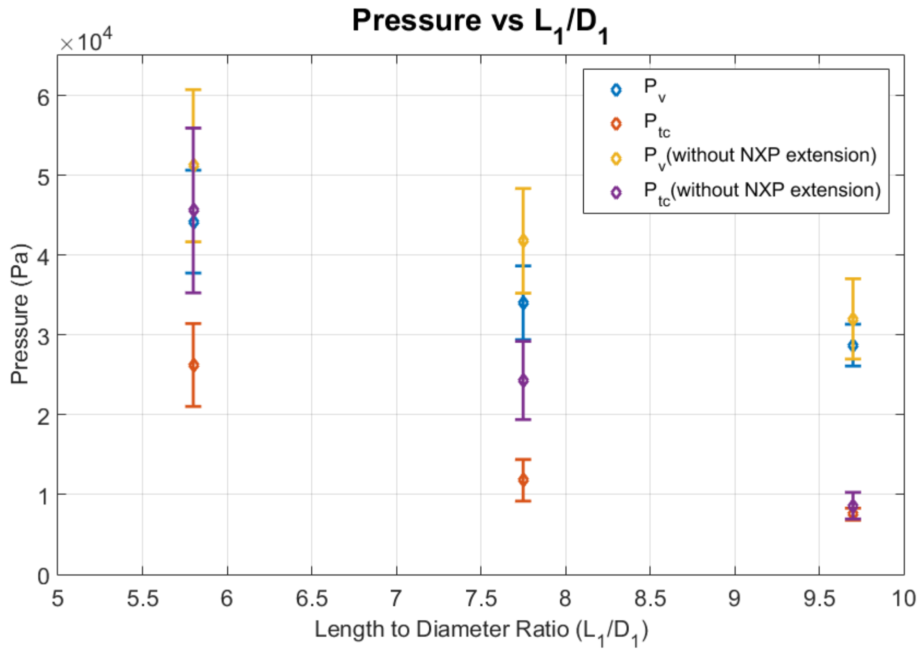

Figure 5-30. Pressure vs Length to Diameter Ratio with and without NXP Extension.

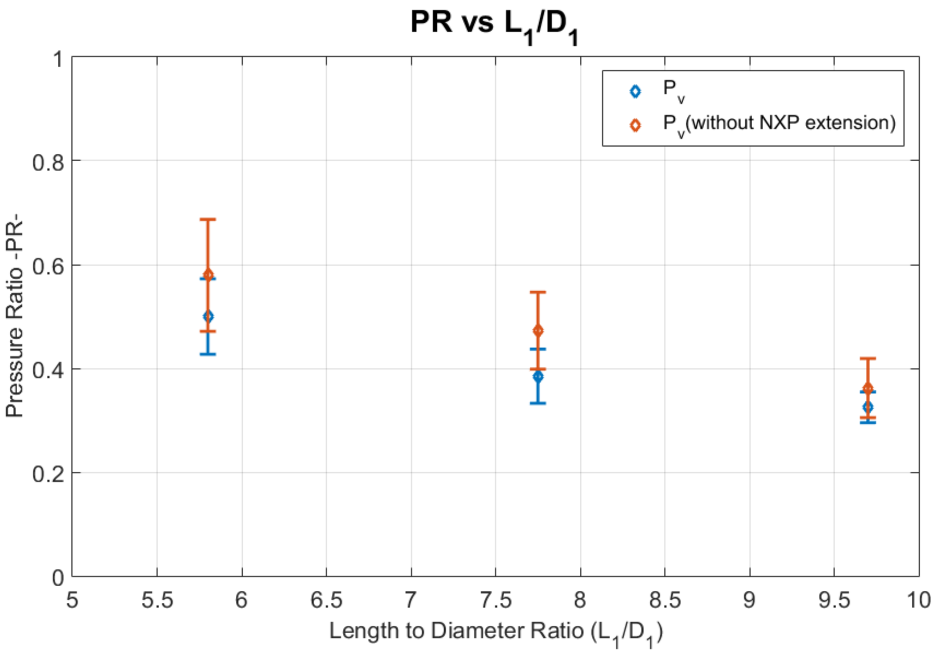

Figure 5-31. Pressure Ratio vs Length to Diameter Ratio with and without NXP Extension.

5.4.1.2. Effect of Entrainment Ratio

The performance of an ejector system is typically categorized by pressure ratio (PR) at a specific entrainment ratio (ER). Efficient ejector means getting a lower pressure ratio at a specific entrainment ratio. These tests are done by using the maximum L_1/D_1 ratio and NXP Extension. The performance of the manufactured experimental setup is given in Table 5-9, Figure 5-32 and Figure 5-33.

In Figure 5-32 it is seen that, when the entrainment ratio increases, vacuum pressure also increases, however test chamber pressure shows a different trend. The reason is the free-jet nozzle parameters used in these tests. In case 7, nozzle exit pressure is calculated as 5430 Pa, but P_{tc}=15345 Pa. So, the nozzle is unstarted and the amplitude of oscillations in pressure data is high. However, in case 10, nozzle exit pressure is calculated as 11944 Pa which is smaller than the P_{tc}=7474 Pa. That’s why the nozzle and the diffuser are started and amplitude of oscillations become smaller.

Another important result is that, the ejector and test section diffuser diameter are determined for the ER = 0.33 in Design Methodology chapter. It can be said that, the experimental setup shows the best performance in the range where the ER is close to 0.33.

Table 5-9. Comparison of Pressure Ratio for Different Entrainment Ratio.

		P_v (Pa)		**P_{tc} (Pa)**		
Experiment ID	**ER**	**Value**	**σ%**	**Value**	**σ%**	**PR**
Case 7	0.16	22983	9.3	15345	19.2	0.26
Case 8	0.25	26217	9.8	10595	16.1	0.296
Case 9	0.33	30794	8.3	7437	14.2	0.348
Case 10	0.36	32218	7.9	7474	9.9	0.364
Case 11	0.44	38236	10.1	9171	8.8	0.432
Case 12	0.47	38458	10.3	9972	19.1	0.435
Case 13	0.57	44972	10.2	11742	18.8	0.508

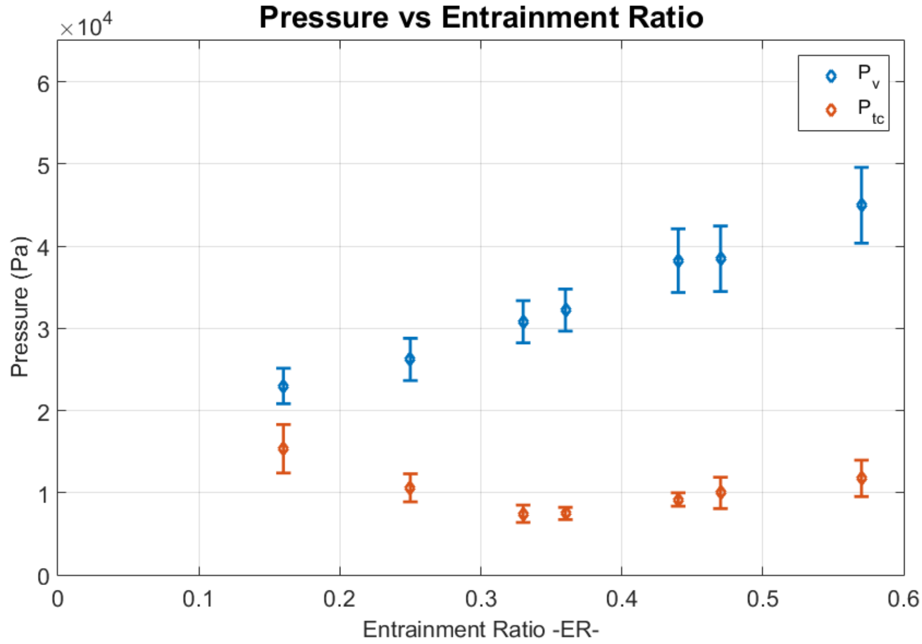

Figure 5-32. Pressure vs. Entrainment Ratio.

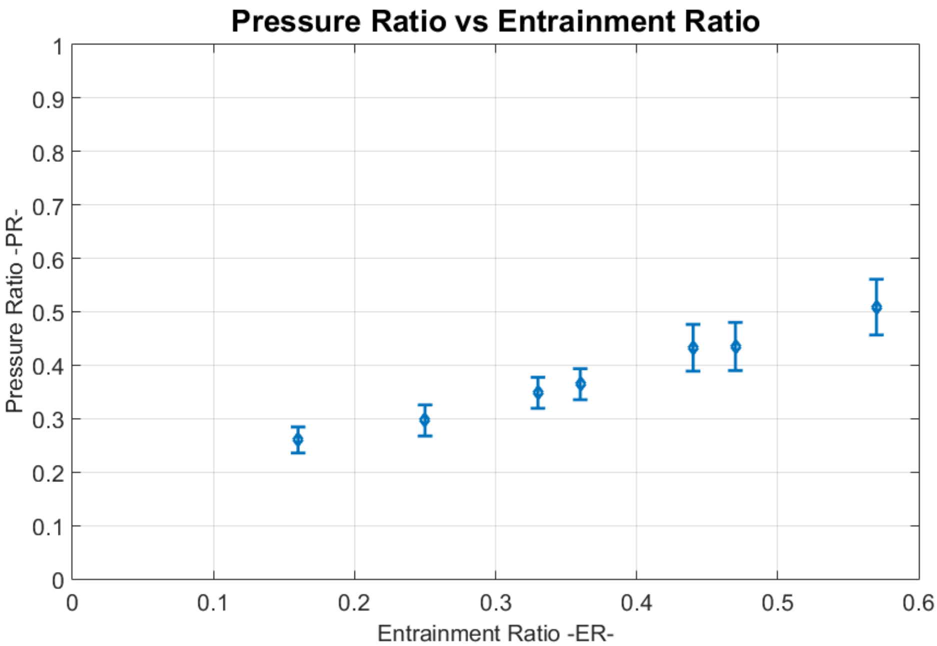

Figure 5-33. Pressure Ratio vs. Entrainment Ratio.

5.5. Comparison of the Results

For manufactured system, both numerical investigations and experimental results are given in previous sections. In this section, results are combined and evaluated together. For each entrainment ratio,

- Experimental setup and pressure transmitter locations are given,
- Pressure contour plot of CFD analysis is given,
- Pressure value of each location found in CFD analysis and measured in experiments are given on the same graph,
- Vacuum pressure (P_v) and test chamber pressure (P_{tc}) values found in CFD analysis and measured in experiments are given in a box.

For the design condition (Case 9) Turbulent intensity (TI) and y^+ of ejector diffuser and test section diffuser walls are given.

At the end of this part, all vacuum pressure (P_v) and test chamber pressure (P_{tc}) values at different entrainment ratio conditions are evaluated together.

5.5.1. Results Comparison for Case 7 ER = 0.16

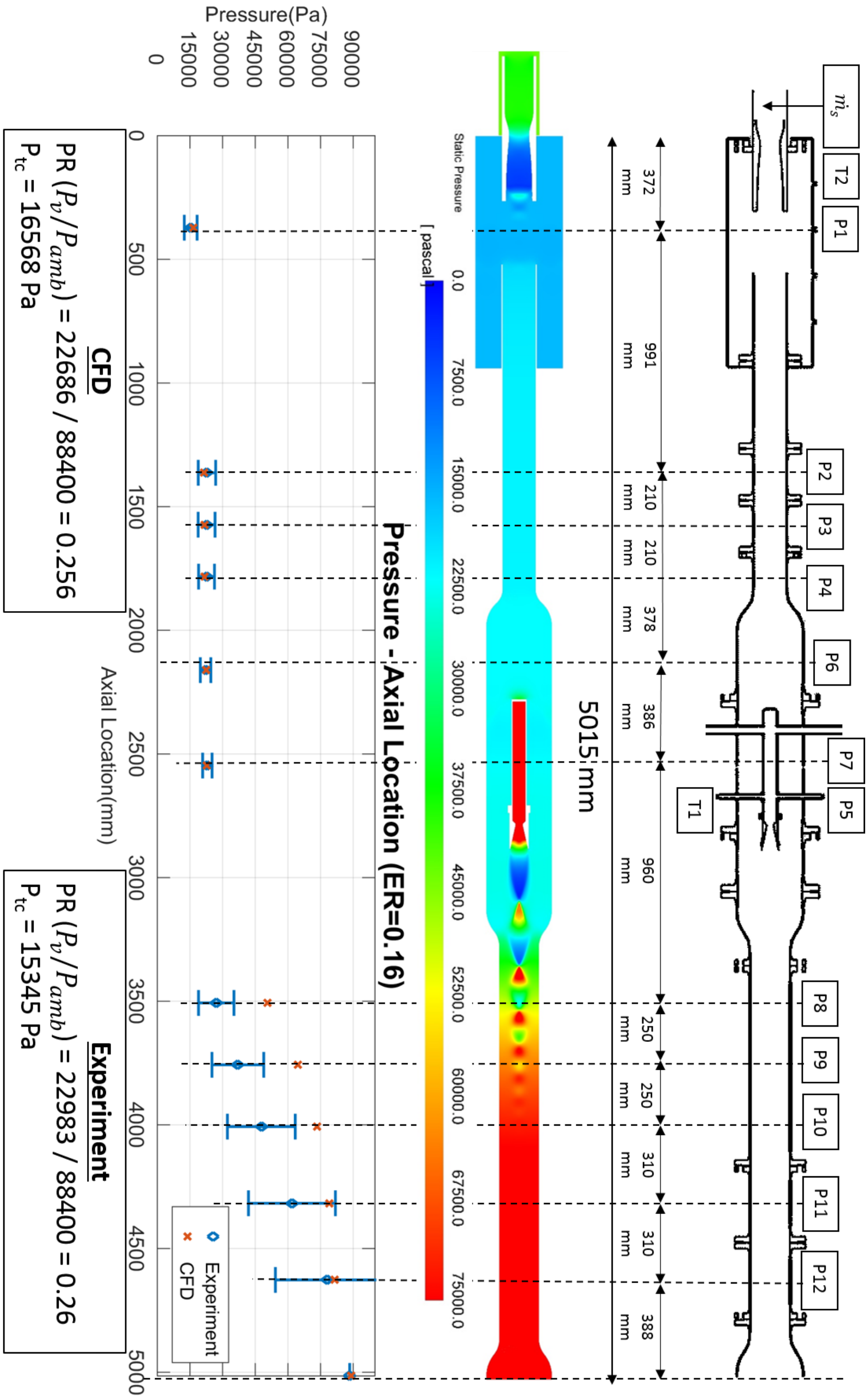

Figure 5-34. Numerical and Experimental Results Comparison for ER = 0.16.

5.5.2. Results Comparison for Case 8 ER = 0.25

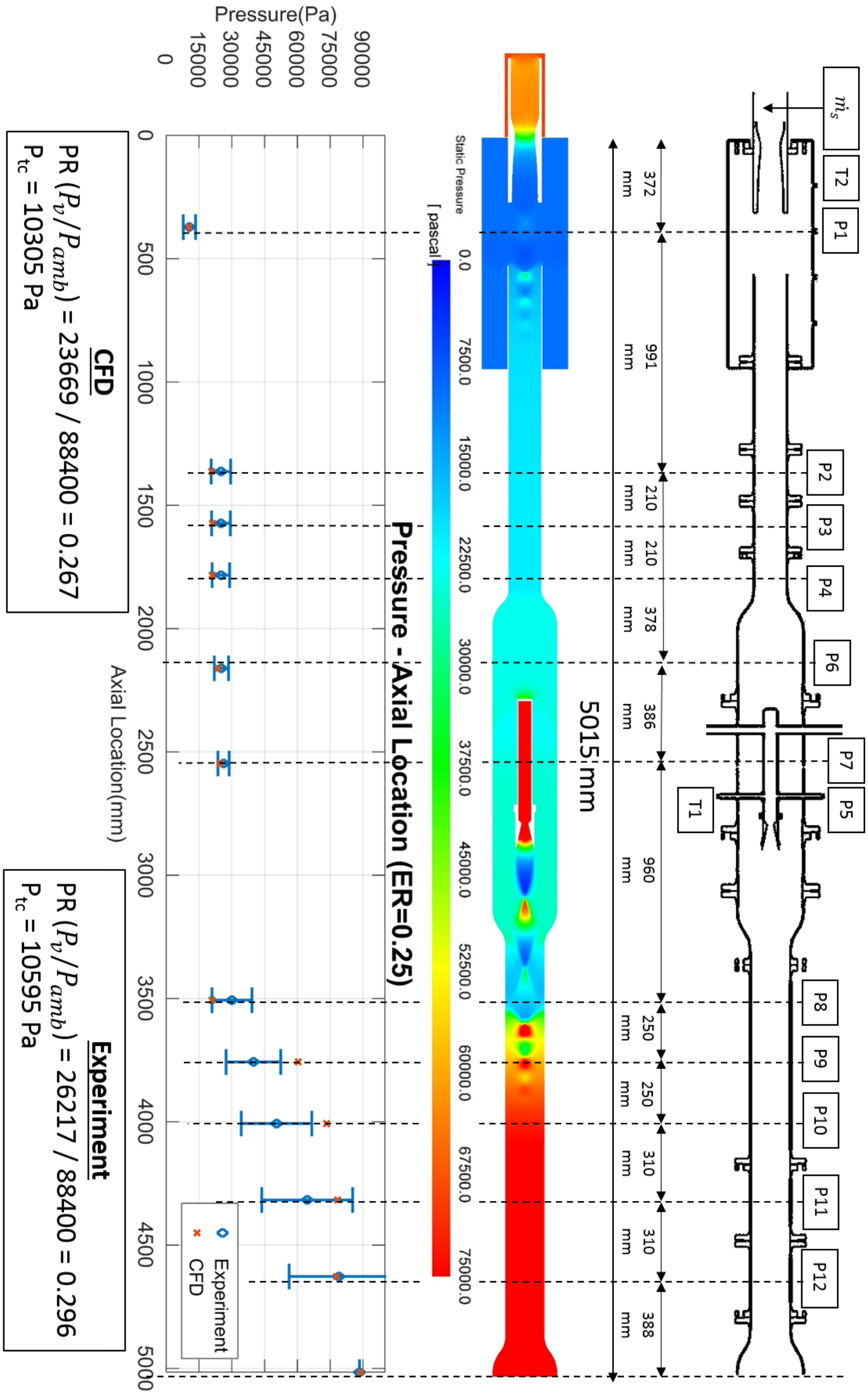

Figure 5-35. Numerical and Experimental Results Comparison for ER = 0.25.

5.5.3. Results Comparison for Case 9 ER = 0.33

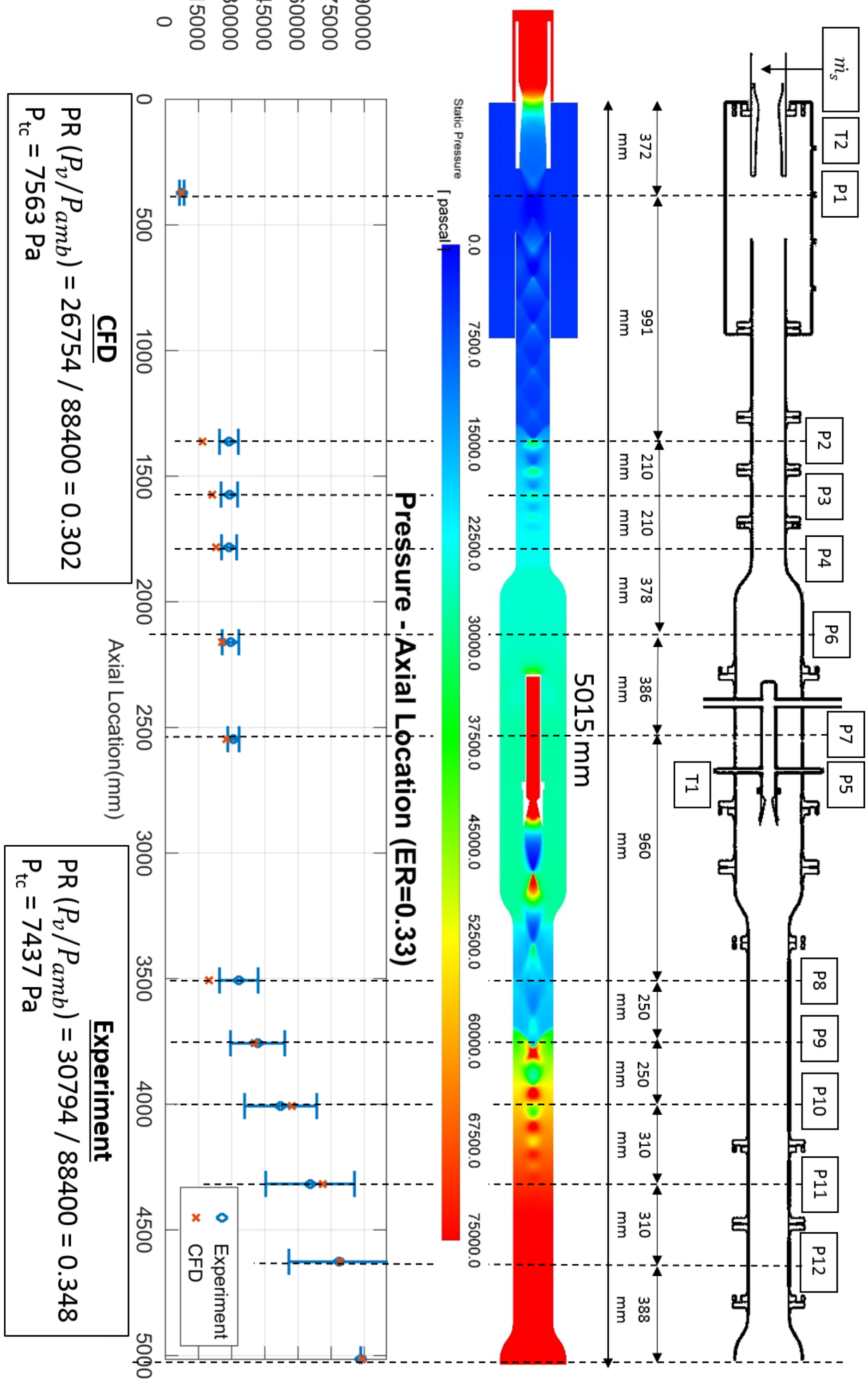

Figure 5-36. Numerical and Experimental Results Comparison for ER = 0.33.

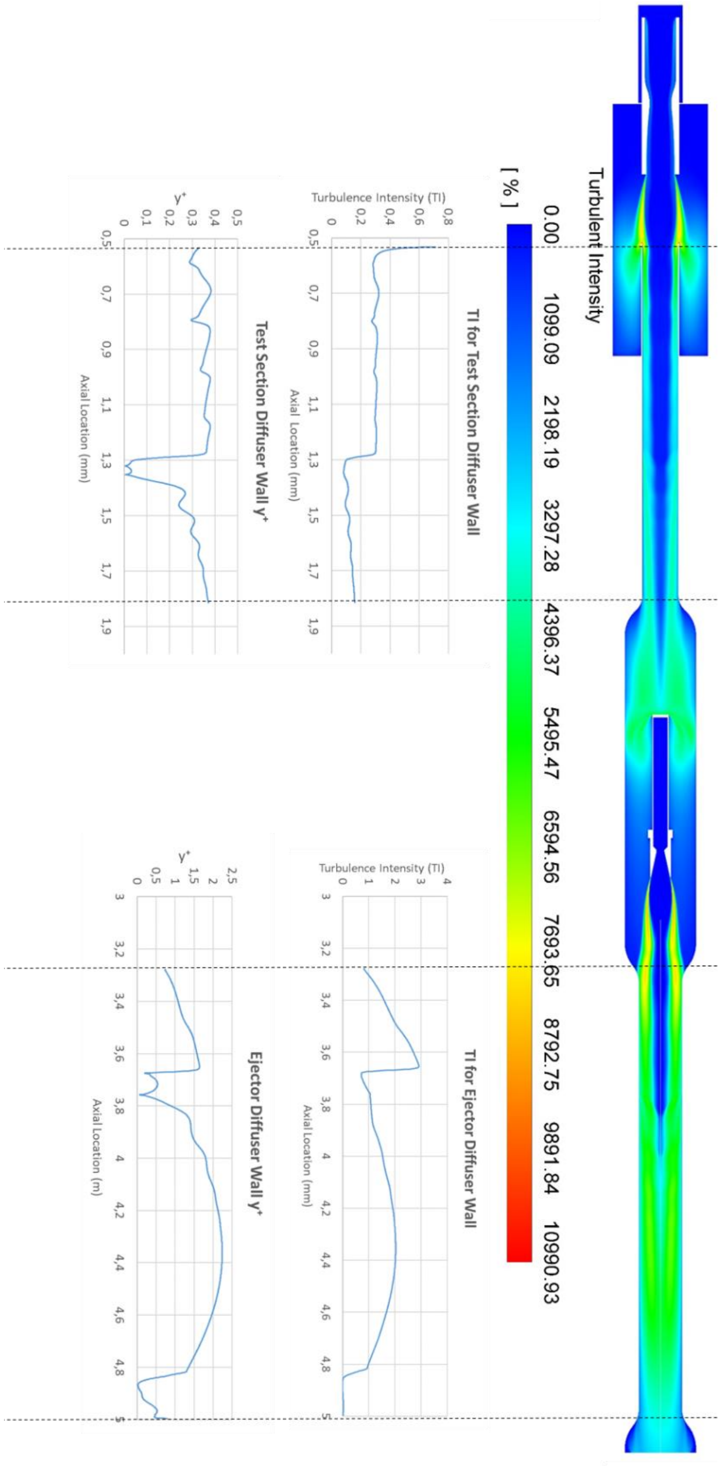

Figure 5-37. Turbulent Intensity and y⁺ Distributions on Ejector Diffuser Wall and Test Section Diffuser Wall for ER = 0.33.

5.5.4. Results Comparison for Case 10 ER = 0.36

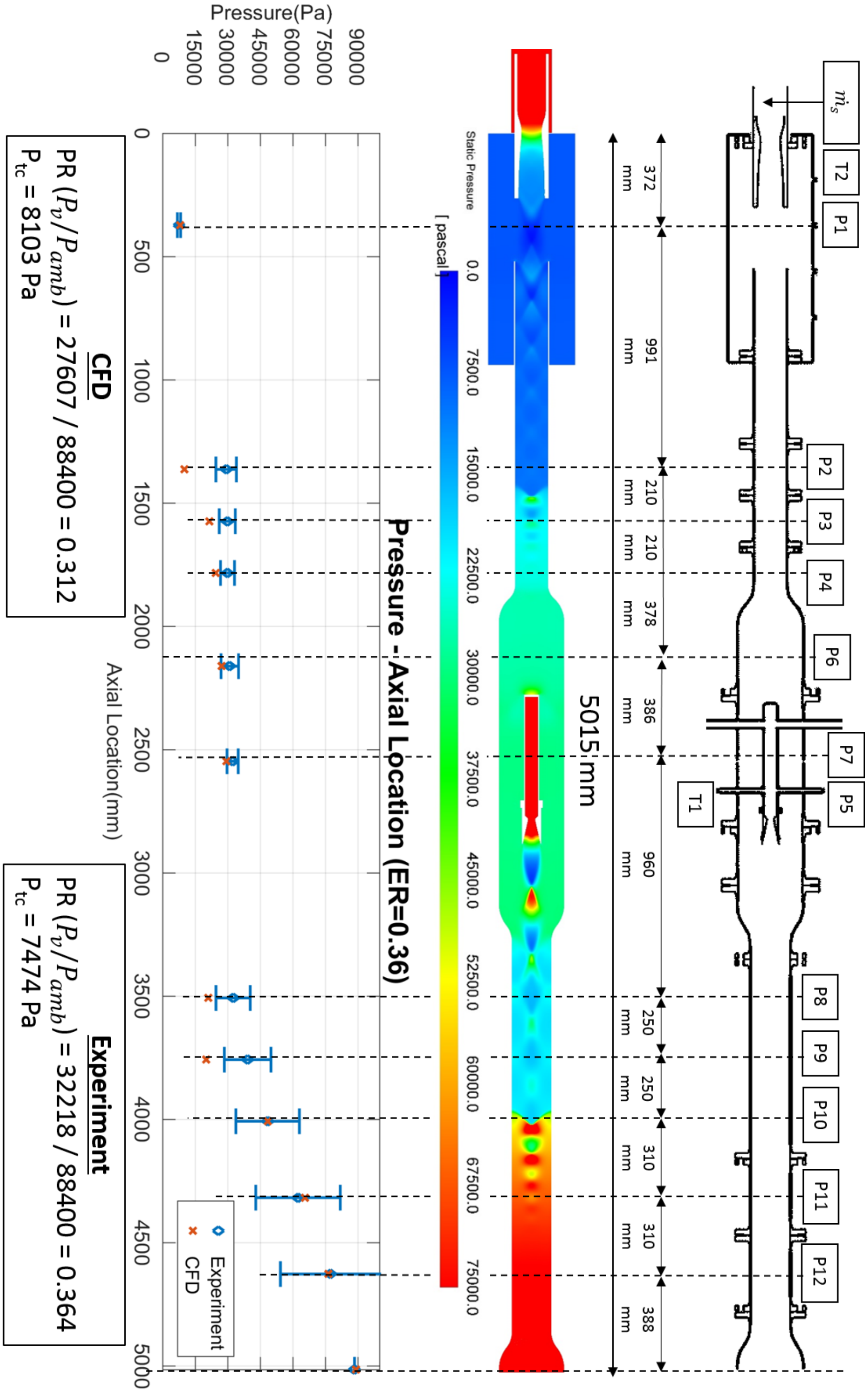

Figure 5-38. Numerical and Experimental Results Comparison for ER = 0.36.

5.5.5. Results Comparison for Case 11 ER = 0.44

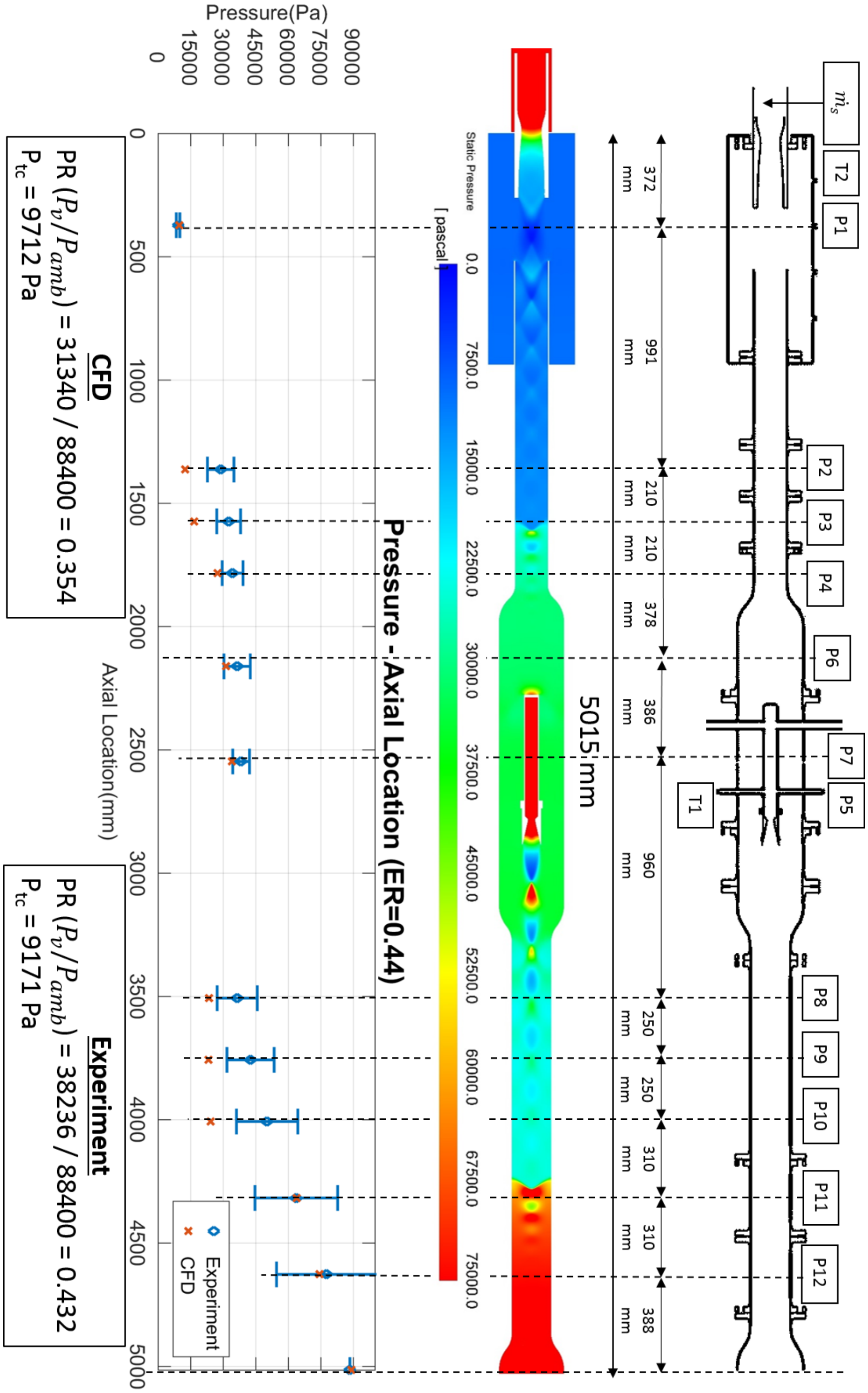

Figure 5-39. Numerical and Experimental Results Comparison for ER = 0.44.

5.5.6. Results Comparison for Case 12 ER = 0.47

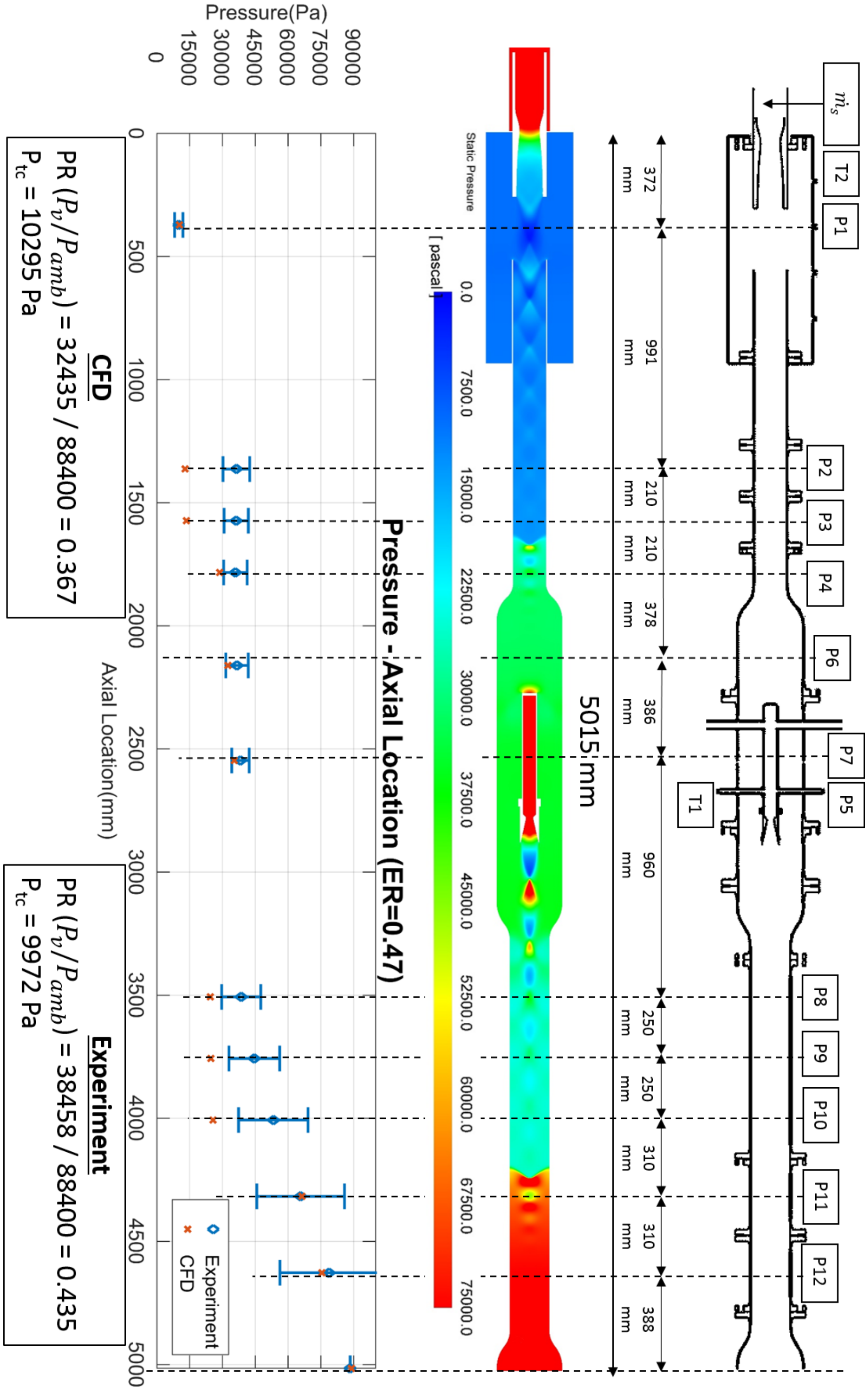

Figure 5-40. Numerical and Experimental Results Comparison for ER = 0.47.

5.5.7. Results Comparison for Case 13 ER = 0.57

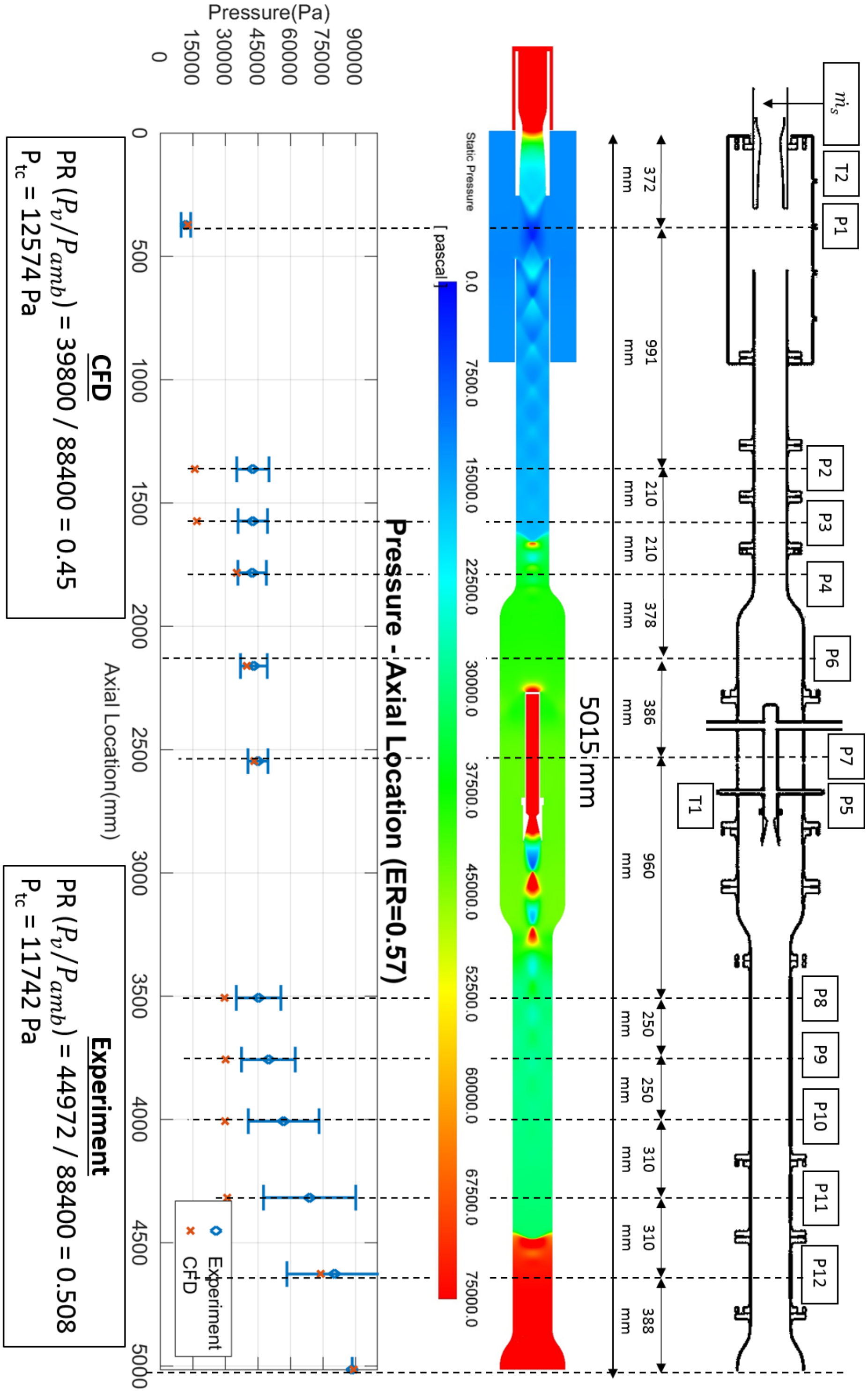

Figure 5-41. Numerical and Experimental Results Comparison for ER = 0.57.

5.5.8. Summary of the Results

The Vacuum Pressure (P_v) and Pressure Ratio of experimental and CFD results for each entrainment ratio are given in Figure 5-42, Figure 5-43 and Table 5-10. Results show the similar trend of change, however, the performance of the ejector system in experimental setup is at most 18% lower than the CFD analyses for each case, that means The Vacuum Pressure (P_v) value is that much higher. Although this 18% error is not bad, the possible reasons of that error are,

- Ejector nozzle feed manifold details are not solved in CFD analyses. There are supports and pipes, which have blockage effects on the secondary flow,
- CFD analyses are carried for axisymmetric geometry, nonetheless, experimental setup may have a symmetry problem,
- Pressure transmitter mounting location may not be modeled correctly in CFD analyses,
- Flow solver may not solve correctly the shock wave formation, the turbulent mixing and multiple shock systems due to complex flow phenomena.

Table 5-10. Vacuum Pressure and Pressure Ratio Values of Experimental and CFD Results For Different Entrainment Ratios.

	P_v (Pa)		**PR**		
ER	**Experiment**	**CFD**	**Experiment**	**CFD**	**Error%**
0.16	22983	22686	0.26	0.256	-1.2
0.25	26217	23669	0.296	0.267	-9.7
0.33	30794	26574	0.348	0.302	-13.7
0.36	32218	27607	0.364	0.312	-14.3
0.44	38236	31340	0.432	0.354	-18
0,47	38458	32435	0,435	0,367	-15,6
0,57	44972	39800	0,508	0,45	-11,5

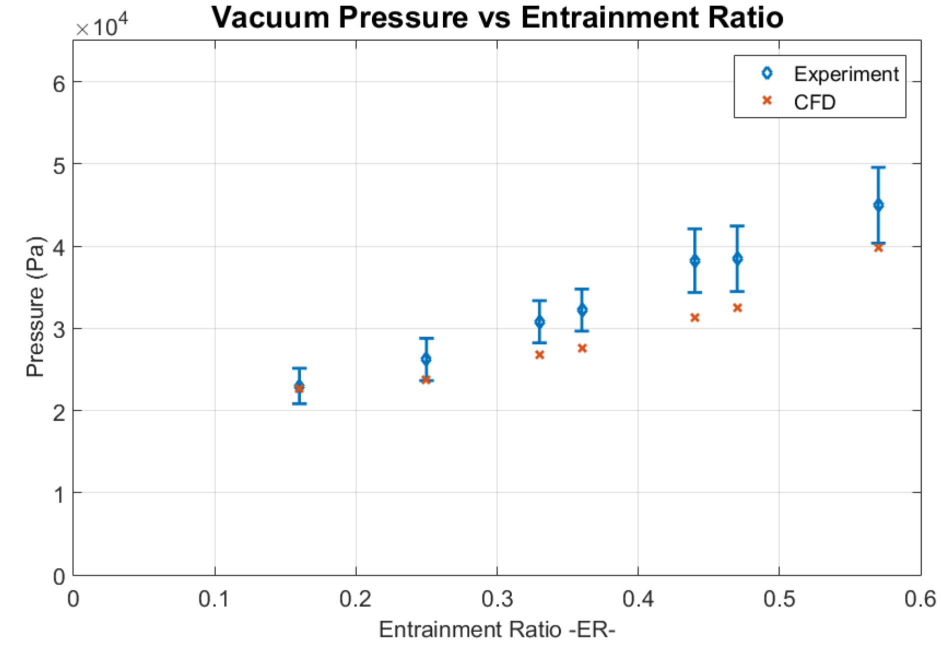

Figure 5-42. Vacuum Pressure vs. Entrainment Ratio of Experimental and CFD Results.

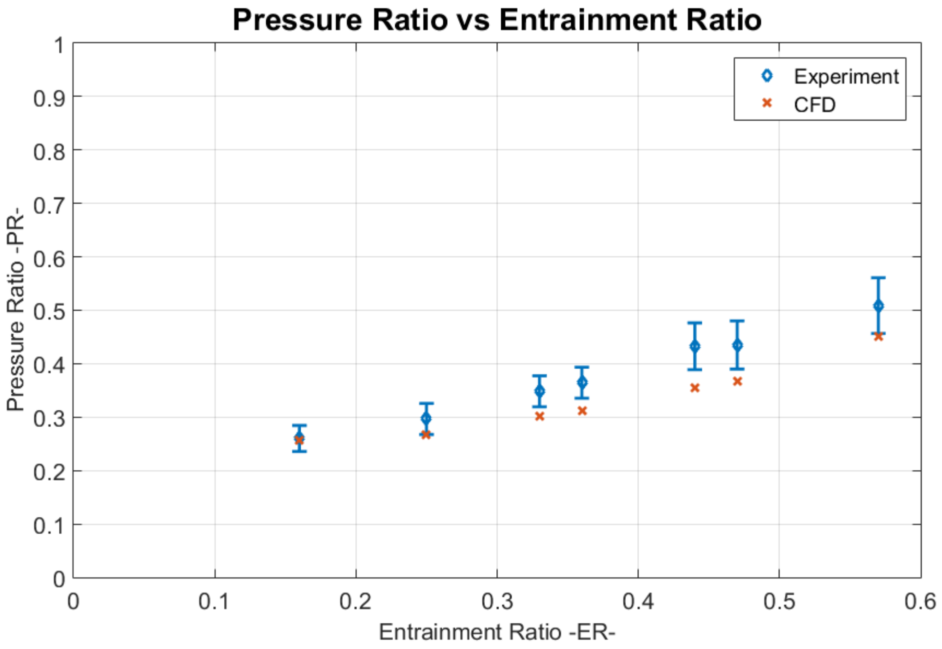

Figure 5-43. Pressure Ratio vs. Entrainment Ratio of Experimental and CFD Results.

The test chamber pressure (P_{tc}) of experimental and CFD results for each entrainment ratio are given in Figure 5-44 and Table 5-11. Results seems to be quite consistent. Nevertheless, the difference between P_{tc} values is expexted to be more, since in CFD analysis, test chamber pressure is calculated by using the Vacuum Pressure given in Table 5-10. It can be stated that; after ejector and test section diffuser started, the change in P_v does not effect the P_{tc} proportionally.

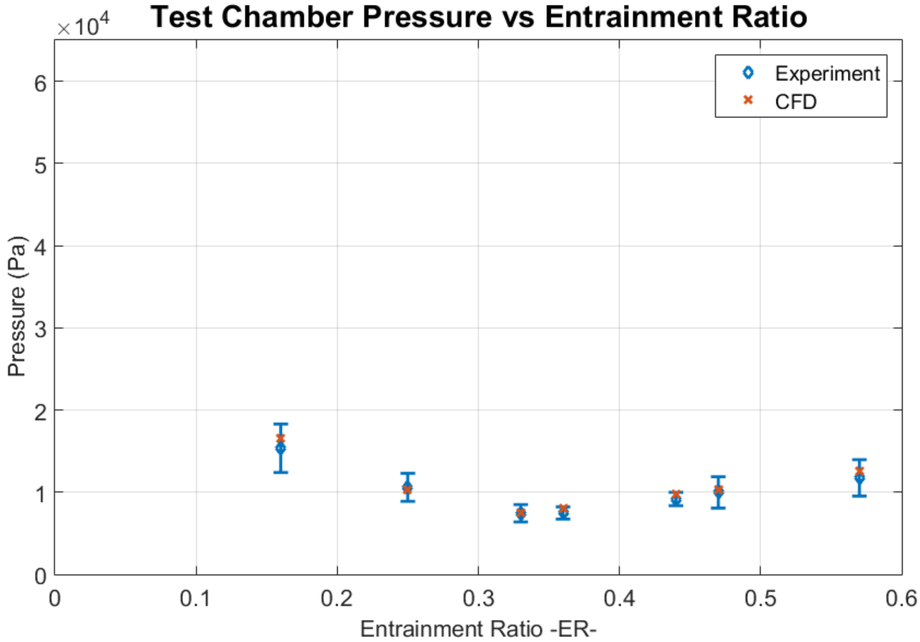

Figure 5-44. Test Chamber Pressure vs. Entrainment Ratio of Experiment and CFD Results.

Table 5-11. Test Chamber Pressure Values of Experimental and CFD Results For Different Entrainment Ratios.

	P_{tc} (Pa)		
ER	**Experiment**	**CFD Analysis**	**% Error**
0.16	15345	16568	7.9
0.25	10595	10305	2.7
0.33	7437	7563	1.7
0.36	7474	8103	8.4
0.44	9171	9712	5.8
0.47	9972	10295	3.2
0.57	12574	11742	-6.6

Besides the vacuum pressure (P_v) and test chamber pressure (P_{tc}), pressure data are measured at different locations of the experimental setup and these measured data are compared with the CFD results for each case.

In Case 7 (ER = 0.16), it is seen in both experimental and CFD results that free-jet nozzle and diffuser are not started due to the lower nozzle exit pressure and test section diffuser diameter is too big for that secondary mass flow rate. That means, with the same mass flow rates -same ER value-, if the free-jet nozzle exit diameter is lowered, nozzle exit pressure will increase due to the decrease in Mach number of the free-jet nozzle and free-jet nozzle can be started.

In Case 8 (ER = 0.25), free-jet nozzle is started but test section diffuser is partially started. When the secondary mass flow rate continues to increase, the free-jet nozzle and test section diffuser reach the starting condition. For ER > 0.33 cases, both test section diffuser and ejector diffuser are choked and started. In Figure 5-37 for design condition (ER=0.33) Turbulence intensity and y^+ distributions on the ejector diffuser wall and test section diffuser wall are given. It is seen that the TI on the test section diffuser wall changes between 0.1 to 0.4 (10% to 40%), however the TI on the ejector diffuser wall changes between 1 to 3 (100% to 300%). A turbulence Intensity of 1% or less is evaluated as low and turbulence intensity higher than 10% is considered as high [34]. It is seen in results for ER > 0,33 cases, the pressure data in supersonic region of both test section diffuser and ejector diffuser are not consistent with CFD results. After the normal shock in diffusers, the measured pressure data suddenly increase. Then, in subsonic region of diffusers pressure transmitters measure the similar pressure data with CFD results. The possible reasons of that error are,

- Flow solver may not solve correctly the shock wave formation, the turbulent mixing and boundary layer separation in analysis model.
- Due to the high turbulence pressure transmitters may not measure the data correctly.

CHAPTER 6

CONCLUSION AND FUTURE WORK

6.1. Conclusion

In this work, high altitude test system is investigated numerically and experimentally. Some of the important parameters for the system performance like ejector diffuser dimensions, test section diffuser dimensions, nozzle exit plane (NXP) location and entrainment ratio (ER) are investigated also.

Primarily, numerical methodology which includes flow solver theory and grid sensitivity was given. By evaluating the vacuum pressure P_v and the axial variation of Mach number, static pressure and static temperature data, medium grid properties were chosen to use in numerical simulations. Series of CFD analysis have been conducted for different geometries by using optimization method in MODE FRONTIER software and mesh has been generated in grid generation program by using an automated meshing script. For this reason, uniform grid was used in this study and the control on the grid spacing is performed on the cell dimensions of the geometry.

Secondly, design methodology was presented. Design methodology separates the design problem into two parts. In the first step, the design and optimization of the Ejector System were accomplished and optimum ejector geometry for given boundary conditions was determined nondimensionally by using ‘Design by Analysis’ method based on Computational Fluid Dynamics analysis and MOGA-2 (Multi-objective genetic algorithm). Then, numerical simulations of the Ejector System were repeated for the different secondary flow total temperatures using the geometry obtained from DOE analysis to calculate the vacuum pressure for different free-jet nozzles. As a third step, the numerical investigations of the Test Section were accomplished. The vacuum pressures calculated in Step 2 for different secondary flow total temperatures were used as an ‘outlet pressure’ boundary condition at the exit of the constant area diffuser. Optimum diameter for test section diffuser starting condition has been found for different free-jet nozzle geometries operating at different secondary flow total temperatures. For the same ejector system geometry, by choosing the optimum diameter for the constant area diffuser, it was guaranteed that the HATS can start regardless of the free-jet nozzle used in the test. The main goal of these analyses was to find a minimum constant area diffuser length which does not promote unstart of the test section diffuser. Then, both ejector system and test section numerical simulation results were compared with combined numerical analyses of the HATS analysis model which were performed with 2, 2.5 and 3 Mach free-jet nozzles. The numerical results of the combined HATS analyses were in good agreement with the numerical results’ of ejector system and test section analyses. However, combined numerical analysis takes fifteen times the computational time of a single Test Section numerical simulation, which is comparable with a single Ejector System numerical simulation. In addition, the convergence problem was detected while performing combined numerical analysis in several operating points.

Thirdly, experimental setup design and manufacturing steps by using the dimensions calculated in design methodology were presented in detail. Dimensioning of all parts were mentioned and all mechanical components used in the experimental setup were selected from catalogues to make the experimental setup cost-effective. It has been observed that the ejector nozzle feed manifold is the most critical component in both design and manufacturing process.

In the fourth part, results obtained from the experiments and the numerical simulations of the high altitude test system model were given. At the beginning, experimental matrix was constructed. Then, numerical analysis and experimental results were presented both separately and in combined figures. As a performance parameter, Vacuum pressure (P_v) is used and Pressure Ratio of each case is given. It is seen that ejector performance strongly depends on the geometry of the system. When the Length to Diameter Ratio of Ejector Diffuser decreases, ejector performance significantly drops until 50% (P_v value increases 50%) because, secondary flow and primary flow are not perfectly mixed. The effect of NXP length on the ejector performance was investigated by adding and removing NXP extension to the system. Ejector performance drops approximately 20% (P_v value increases 20%) in NXP extension removed cases. It is observed that there should be a constant area section between Nozzle exit plane and the transition cone for primary and secondary flow mixing. Entrainment Ratio is another parameter whose effects on the ejector performance were investigated. For seven different entrainment ratio value, both numerical and experimental results were compared with each others. It has been seen that, although vacuum pressure increases with the increase in the entrainment ratio, test chamber pressure is governed by the free-jet nozzle used in experimental setup. Numerical and experimental results show the similar trend of change, but the performance of the ejector system in experimental setup is at most 18% lower than the CFD results. The possible reasons of that error are given as flow solver ability, measurement difficulties in high turbulent flow and the difference between experimental setup and HATS analysis model.

In ejector-diffuser system design, the important design parameters are,

- The free-jet nozzle exit pressure P_{ex2}. Test chamber pressure should be lower than or equal with the P_{ex2} value for successful testing. So, desired P_{ex2} value should be determined before numerical analysis.
- Test article blockage area. Test article blockage ratio is critical for the free-jet nozzle exit area. Because, increasing the blockage ratio decreases the test section diffuser and consequently free-jet nozzle performance. For constant Mach number and defined test article geometry, free-jet nozzle geometry and mass flow rate $\dot{m}_s$ should be determined.
- Primary mass flow rate $\dot{m}_p$ should be determined and system is dimensioned by numerical simulations.

6.2. Future Work

For the future improvements of the present study, followings can be proposed,

- Tests can be performed with heated air and the effect of increase in free-jet nozzle total temperature can be observed.
- Free-jet nozzles with different Mach number can be tested.
- Test article can be mounted in the test chamber and blockage effect can be analyzed.
- To observe free-jet nozzle starting phenomena, Schlieren imaging can be used.
- To solve the shock wave formation, turbulent mixing and boundary layer separation in supersonic diffusers correctly, FLUENT analyses can be repeated with higher mesh quality cases.

REFERENCES

[1] V. Lijo, H. D. Kim, S. Matsuo, and T. Setoguchi, “A study of the supersonic ejector-diffuser system with an inlet orifice,” *Aerosp. Sci. Technol.*, vol. 59, no. 1–2, pp. 21–29, 2012.

[2] R. Manikanda Kumaran, P. K. Vivekanand, and T. Sundararajan, “Analysis of Diffuser and Ejector Performance in a High Altitude Test Facility, AIAA 2009-5008,” in *45th AIAA Joint Propulsion Conference*, 2009.

[3] J. B. R. Rose, G. R. Jinu, and C. J. Brindha, “A numerical optimization of high altitude testing facility for wind tunnel experiments,” *Chinese J. Aeronaut.*, vol. 28, no. 3, pp. 636–648, 2015.

[4] K. R. Holst, “A Method for Performance Analysis of a Ramjet Engine in a Free-jet Test Facility and Analysis of Performance Uncertainty Contributors,” 2012.

[5] V. Kulkarni and N. Sahoo, “NPTEL Aerospace Engineering - Hypersonic Aerodynamics,” 2012. [Online]. Available: https://nptel.ac.in/courses/101103003/32. [Accessed: 02-Aug-2019].

[6] R. Daschner, S. Binder, and M. Mocker, “Pebble bed regenerator and storage system for high temperature use,” *Appl. Energy*, vol. 109, no. 9, pp. 394–401, 2013.

[7] K. T. Berger, K. E. Hollingsworth, S. A. Wright, and S. J. Rufer, “NASA Langley Aerothermodynamics Laboratory: Hypersonic Testing Capabilities, AIAA 2015-1337,” in *53th AIAA Aerospace Sciences Meeting*, 2015.

[8] S. J. Beresh, K. M. Casper, J. L. Wagner, J. Henfling, R. Spillers, and B. O. Pruett, “Modernization of Sandia’s Hypersonic Wind Tunnel, AIAA 2015-1338,” in *53th AIAA Aerospace Sciences Meeting*, 2015.

[9] NASA, “Snow Covered Spheres,” 1969. [Online]. Available: https://www.nasa.gov/multimedia/imagegallery/image_feature_625.html. [Accessed: 02-Aug-2019].

[10] G. Park, S. Kim, and S. Kwon, “A starting procedure of supersonic ejector to minimize primary pressure load,” *J. Propuls. Power*, vol. 24, no. 3, pp. 631–634, 2008.

[11] S. Kim and S. Kwon, “Starting Pressure and Hysteresis Behavior of an Annular Injection Supersonic Ejector,” *AIAA J.*, vol. 46, no. 5, 2008.

[12] Z. Aidoun, K. Ameur, M. Falsafioon, and M. Badache, “Current Advances in Ejector Modeling, Experimentation and Applications for Refrigeration and Heat Pumps. Part 2: Two-Phase Ejectors,” *Inventions*, vol. 4, no. 1, p. 16, 2019.

[13] K. Sathiyamoorthy, V. Iyengar, and P. Manjunath, “Annular Supersonic Ejector Design and Optimization,” *ASME 2012 Gas Turbine India Conf.*, pp. 1–9, 2012.

[14] R. M. Kumaran, P. K. Vivekanand, T. Sundararajan, K. Kumaresan, and D. R. Manohar, “Optimization of second throat ejectors for high-altitude test facility,” *J. Propuls. Power*, vol. 25, no. 3, pp. 697–706, 2009.

[15] B. M. Tashtoush, M. A. Al-Nimr, and M. A. Khasawneh, “A comprehensive review of ejector design, performance, and applications,” *Appl. Energy*, vol. 240, no. May 2018, pp. 138–172, 2019.

[16] B. H. Park, J. Lim, S. Park, J. H. Lee, and W. Yoon, “Design and Analysis of a Second-Throat Exhaust Diffuser for Altitude Simulation,” *J. Propuls. Power*, vol. 28, no. 5, 2012.

[17] D. Daniel, “A General Simulation of an Air Ejector Diffuser System, MS Thesis,” University of Tennessee, Knoxville, 2012.

[18] G. Besagni, R. Mereu, and F. Inzoli, “Ejector refrigeration: A comprehensive review,” *Renew. Sustain. Energy Rev.*, vol. 53, pp. 373–407, 2016.

[19] R. C. Bauer, W. W. Muse, and C. R. Tinsley, “Simulation of Flow Approaching The Chin Inlet of a Ramjet Missile, Arnold Engineering Development Center, Technical Report No: AEDC-TR-74-5,” 1974.

[20] R. C. German, R. C. Bauer, and J. H. Panesci, “Methods for Determining the Performance of Ejector-Diffuser Systems Used in Rocket Altitude Simulation, AIAA 1964-1428,” in *1964 Space Simulation Testing Conference*, 1964.

[21] P. Desevaux and F. Lanzetta, “Computational Fluid Dynamic Modeling of Pseudoshock Inside a Zero-Secondary Flow Ejector,” *AIAA J.*, vol. 42, no. 7, pp. 7–10, 2004.

[22] J. H. Hart, “Supersonic Ejector Simulation and Optimization, PhD Thesis in Mechanical Engineering,” The University of Sheffield, 2002.

[23] B. J. Huang, J. M. Chang, C. P. Wang, and V. A. Petrenko, “1-D analysis of ejector performance,” *Int. J. Refrig.*, vol. 22, no. 5, pp. 354–364, 1999.

[24] J. C. Dutton and B. F. Carroll, “Optimal Supersonic Ejector Designs, ASME Paper,” in *ASME International*, 1986, pp. 414–420.

[25] R. C. German, R C; Bauer, “Effects of Diffuser Length on the Performance of Ejectors Without Induced Flow, Technical Report No: AEDC-TN-61-89, Arnold Engineering Development Center,” 1961.

[26] B. R. C German, H. Panesci, and H. K. Clark, “Zero Secondary Flow Ejector Diffuser Performance Using Annular Nozzles, Technical Report No: AEDC-TDR-62-196, Arnold Engineering Development Center,” 1963.

[27] C. Shi, H. Chen, W. Chen, S. Zhang, D. Chong, and J. Yan, “1D Model to Predict Ejector Performance at Critical and Sub-critical Operation in the Refrigeration System,” *Energy Procedia*, vol. 75, pp. 1477–1483, 2015.

[28] Z. Jian-Jun, Z. Jin, L. Hui-Qiang, and H. Yong, “Experimental investigation on starting process of supersonic single-stage air ejector,” *J. Therm. Sci.*, vol. 21, no. 4, pp. 348–353, 2012.

[29] F. Chen, C. F. Liu, J. Y. Yangj, and I. Introduction, “Supersonic Flow in the Second-Throat Ejector-Diffuser System,” *J. Spacecr. Rockets*, vol. 31, no. 1, pp. 123–129, 1994.

[30] J. Kracik and V. Dvorak, “Preliminary study of the primary nozzle position of a supersonic air ejector with a constant-area mixing chamber,” in *EPJ Web of Conferences*, 2016.

[31] R. Ashokkumar, S. Sankaran, T. Sundararajan, and K. Srinivasan, “Supersonic Exhaust Diffuser for Starting Higher Area Ratio, AIAA 2012-3294,” in *28th Aerodynamic Measurement Technology, Ground Testing and Flight Testing Conference*, 2012.

[32] J. D. Anderson, “Governing Equations of Fluid Dynamics,” in *In: Wendt J.F. Governing Equations of Fluid Dynamics: An Introduction, Springer, Berlin,* 2009, pp. 15–51.

[33] M. P. Bulat and P. V. Bulat, “Comparison of Turbulence Models in the Calculation of Supersonic Separated Flows,” *World Appl. Sci. J.*, vol. 27, no. 10, pp. 1263–1266, 2013.

[34] Ansys, “ANSYS 18.0 Fluent Tutorial Guide,” 2016.

[35] Y. Bartosiewicz, “Numerical and experimental investigations on supersonic ejectors,” *Int. J. Heat Fluid Flow*, vol. 26, pp. 56–70, 2005.

[36] J. Kolar and V. Dvorak, “Verification of K- ω SST Turbulence Model for Supersonic Internal Flows,” *Int. J. Mech. Aerospace, Ind. Mechatron. Manuf. Eng.*, vol. 5, no. 9, pp. 1715–1719, 2011.

[37] A. Mosavi, “Reviewing the Multiobjective Optimization Package of modeFrontier in Energy Sector,” in *International CAE Conference and Exhibition*, 2017.

[38] S. Poles, “An Improved Multi-Objective Genetic Algorithm, Technical Report No: 2003-006, Esteco,” 2003.

[39] G. Matsumoto, F. K. Lu, and D. R. Wilson, “Development of a Subscale Supersonic Aeropropulsion Wind Tunnel, AIAA Paper 1998-2868,” in *20th AIAA Advanced Measurement and Ground Testing Conference,* 1998.